

MAGNETIZING ROAST OF CHALCOPYRITE
FOR COPPER-LEAD SEPARATION

Thomas I. Agrafiotis

A Thesis Submitted to the
Faculty of Graduate Studies and Research
in Partial Fulfillment of the Requirements for the
Degree of Master of Engineering

Department of Mining and Metallurgical Engineering

McGill University

Montreal, Canada

January, 1983 ©

Dedicated to my parents, wife and children.

Αφιερωμένο στους γονείς μου, στη γυναίκα
μου και στα παιδιά μου.

ABSTRACT

Roasting of chalcopyrite to produce magnetic phases suitable for magnetic separation was investigated.

Roasting was conducted on samples of chalcopyrite, chalcopyrite-galena synthetic mixtures and Cu-Pb separation circuit tailings from Brunswick Mining and Smelting (B.M.S.). All samples were -400 Mesh.

The calcines were studied by separation on the Frantz Isodynamic Magnetic Separator and by X-ray diffraction, optical microscopy and electron microprobe analysis.

The best conditions were 10 minutes of roasting in a muffle furnace at 320°C. There was no agglomeration and 53% of the copper was trapped in a Davis tube. The magnetic phase was copper ferrite ($\text{CuO} \cdot \text{Fe}_2\text{O}_3$). Also identified were hematite and an unreacted chalcopyrite core.

Magnetic separation was performed using the Davis tube and a High Gradient Magnetic Separator (HGMS). On synthetic

mixtures the Davis tube yielded good separation but the HGMS separation was limited by magnetic flocculation. Separation of the B.M.S. sample was unsuccessful because of locking.

ABSTRAIT

Le grillage de la chalcoppyrite pour produire des phases magnétiques offrant des possibilités pour la séparation magnétique fut étudié. Des grillages furent effectués sur des échantillons de chalcoppyrite, des mélanges synthétiques chalcoppyrite-galène et des rejets du circuit de séparation Cu-Pb de "Brunswick Mining and Smelting" (B.M.S.). Tous les échantillons étaient de -400 mailles.

Les produits grillés furent étudiés en utilisant le séparateur magnétique "Frantz Isodynamic" et en utilisant la diffraction rayons X, l'examen microscopique et la microsonde.

Les meilleures conditions furent de 10 minutes de grillage dans un four à moufle à 320°C. On ne nota aucune agglomération et 53% du cuivre fut récupéré à l'aide du tube Davis. La phase magnétique était de la ferrite de cuivre ($\text{CuO} \cdot \text{Fe}_2\text{O}_3$). Aussi identifiées furent de l'hématite et un noyau de chalcoppyrite n'ayant point réagi.

La séparation magnétique fut exécutée avec un tube Davis et un Séparateur Magnétique à Haut Gradient (SMHG).

Avec les mélanges synthétiques, le tube Davis donna une bonne séparation mais la séparation par SMHG fut limitée dû à la flocculation magnétique. La séparation de l'échantillon de B.M.S. fut infructueuse à cause du degré de libération.

ACKNOWLEDGEMENTS

The author would like to express his appreciation to his research director, Professor James A. Finch for his guidance and encouragement received throughout this investigation and for his orientation and critical comments in the preparation of this thesis.

Thanks are also extended to M. Leroux and to fellow graduate students of the Department of Mining and Metallurgical Engineering for their help on many occasions.

This work was supported by research grants from Quebec Ministry of Education (FCAC) to whom the author is very grateful.

TABLE OF CONTENTS

ABSTRACT.....	i
ABSTRAIT.....	iii
ACKNOWLEDGEMENTS.....	v
TABLE OF CONTENTS.....	vi
LIST OF TABLES.....	xii
LIST OF FIGURES.....	xiv
1. INTRODUCTION.....	1
1.1 Principles of Magnetism.....	1
1.1.1 Magnetic Field.....	1
1.1.2 Magnetic moment and magnetization...	1
1.1.3 The inverse square law and magnetic flux density.....	3
1.1.4 Magnetic field strength.....	4
1.1.5 Effect of a magnetizable medium: Susceptibility and Permeability.....	5
1.2 Magnetic behavior of matter.....	6
1.2.1 Ferromagnetic group.....	6

1.2.2 Ferrimagnetic group.....	8
1.2.3 Paramagnetic group.....	9
1.2.4 Diamagnetic group.....	9
1.2.5 Magnetism and the periodic table.....	9
1.2.6 Magnetic susceptibility of minerals.....	11
2. LIMITATIONS ON THE PERFORMANCE OF A MAGNETIC SEPARATOR.....	14
2.1 Forces on a particle in a magnetic separator.....	14
2.2 Size limitation on the performance of a magnetic separator.....	16
2.3 Susceptibility difference limitation.....	19
2.4 Dimensionless groups.....	21
2.4.1 Watson's model.....	21
2.4.2 Nessel and Finch's model.....	23
3. METHODS OF OVERCOMING THE LIMITATIONS ON THE PERFORMANCE OF A MAGNETIC SEPARATOR.....	25
3.1 Chemical change by heating.....	25
3.2 Adsorption of iron.....	26
3.3 Temperature change.....	27
3.4 Selective seeding.....	29
3.5 Magnetizing leach.....	29
Magnetic separation of first and second kind.....	30

3.6	Changing medium susceptibility.....	31
3.7	Magnetogravimetric separation.....	32
3.7.1	Paramagnetic fluids.....	32
3.7.2	Ferromagnetic fluids or ferrofluids.	34
4.	STATEMENT OF PROBLEM.....	38
4.1	Need for beneficiation of mineral fines...	38
4.2	Magnetic separation of chalcopyrite and galena.....	39
5.	ROASTING OF CHALCOPYRITE.....	41
5.1	Background.....	41
5.2	Mechanism of Oxidation.....	43
5.3	Thermodynamic analysis using F.A.C.T. System.....	45
5.4	Magnetic separation of roasted chalcopy- rite. Literature Survey.....	46
6.	FERRITES.....	49
6.1	Chemical composition.....	49
6.2	Crystal structure.....	50
6.3	Chemistry of ferrites.....	52
7.	ROASTING OF CHALCOPYRITE IN A MUFFLE FURNACE..	57
7.1	Roasting of chalcopyrite in a muffle furnace for 6 hours.....	57
7.1.1	Experimental procedure.....	57

7.1.2 Results.....	58
7.1.3 Thermodynamic analysis of the results.....	58
7.2 Roasting of chalcopyrite in a muffle furnace for short time periods.....	60
7.2.1 Roasting of the synthetic mixture..	62
7.2.1.1 Experimental procedure.....	62
7.2.1.2 Results.....	62
7.2.1.3 Identification of the roasted product.....	65
7.2.2 Roasting of the B.M.S. sample.....	71
7.2.2.1 Effect of temperature.....	71
7.2.2.2 Effect of method of heating	71
7.2.2.3 Effect of retention time...	76
8. ROASTING OF CHALCOPYRITE IN A TUBE FURNACE...	85
8.1 Experimental procedure.....	85
8.2 Results.....	86
8.2.1 Roasting with oxygen.....	86
8.2.2 Roasting with air.....	89
8.3 Identification of the roasted products...	92
8.4 Attempt at separation between chalcopyrite and galena.....	96
9. HIGH GRADIENT MAGNETIC SEPARATION STUDY.....	102
9.1 Background.....	102

9.2 Equipment..... 102

9.3 Experimental procedure..... 104

9.4 The Recovery model for HGMS..... 104

9.5 Conditions of the tests..... 110

9.6 Results of test series 1 and 2..... 111

9.7 Magnetic flocculation or agglomeration?.. 116

9.8 Results of test series 3..... 117

9.9 HGMS of the B.M.S. sample..... 119

10. DISCUSSION..... 121

10.1 Roasting of chalcopyrite..... 121

10.2 Magnetic separation of chalcopyrite-galena mixtures..... 124

11. CONCLUSIONS..... 128

11.1 Roasting of chalcopyrite for 6 hours in a muffle furnace..... 128

11.2 Roasting of chalcopyrite-galena mixtures for 10 min. in a muffle furnace..... 128

11.3 Roasting of chalcopyrite in a tube furnace..... 129

11.4 HGMS Results..... 130

11.5 Davis tube Results..... 130

APPENDIX A - F.A.C.T. SYSTEM RESULTS..... 132

APPENDIX B - DAVIS TUBE CONCENTRATOR..... 135

APPENDIX C - X-RAY DIFFRACTION RESULTS.....	136
APPENDIX D - ESTIMATION OF DEGREE OF LIBERATION.....	143
APPENDIX E - FRANTZ ISODYNAMIC MAGNETIC SEPARATOR.....	149
APPENDIX F - ELECTRON MICROPROBE RESULTS.....	153
APPENDIX G - F.A.C.T. SYSTEM RESULTS.....	154
REFERENCES.....	157

LIST OF TABLES

TABLE 1 - Magnetic susceptibilities of elements...	12
TABLE 2 - Relative magnetic susceptibility for selected mineral pairs.....	22
TABLE 3 - Ignition temperature of pure sulfide minerals.....	41
TABLE 4 - Effect of heat treatment on magnetic properties of mineral powders.....	48
TABLE 5 - The saturation magnetization M_s in Tesla and σ in Tesla m^3/Kg together with the Curie points T_c of some simple ferrites with spinel structure.....	56
TABLE 6 - Summary of x-ray diffraction results....	59
TABLE 7 - Comparison of products predicted by F.A.C.T. and obtained by x-ray diffraction.....	59
TABLE 8. Separation of synthetic mixture at 250 mA.....	65
TABLE 9. Separation of B.M. β sample at 25mA.....	82
TABLE 10. Separation of B.M.S. sample on Davis tube	82
TABLE 11. Summary of calculations to estimate the required magnetic field. Unroasted synthetic mixture.....	108
TABLE 12. Summary of calculations to estimate the required magnetic field. Roasted synthetic mixture.....	109
TABLE 13. Conditions of the HGMS tests.....	110
TABLE 14. HGMS results of series 1.....	113

TABLE 15. HGSM Results of series 2.....	114
TABLE 16. HGMS separation of roasted chalcopyrite and roasted galena.....	117
TABLE 18. HGMS Results of series 3.....	118
TABLE 19. Conditions of HGMS tests.....	120
TABLE A-1 - F.A.C.T. printout for heating of chalcopyrite at 685°C.....	133
TABLE A-2 - F.A.C.T. printout for heating of chalcopyrite at 550°C.....	134
TABLE C-1 - Unheated chalcopyrite sample.....	136
TABLE C-2 - Chalcopyrite heated at 300°C.....	137
TABLE C-3 - Chalcopyrite heated at 320°C.....	138
TABLE C-4 - Chalcopyrite heated at 450°C.....	139
TABLE C-5 - Chalcopyrite heated at 500°C.....	140
TABLE C-6 - Chalcopyrite heated at 550°C.....	141
TABLE C-7 - Chalcopyrite heated at 685°C.....	142
TABLE D-1 - Record Sheet to measure degree of liberation "L" of the chalcopyrite..	145
TABLE D-2 - Record Sheet to measure degree of liberation "L" of galena.....	147
TABLE G-1 - F.A.C.T. printout for roasting of chalcopyrite with oxygen.....	155
TABLE G-2 - F.A.C.T. printout for roasting of chalcopyrite with air.....	156

LIST OF FIGURES

Figure 1 - Magnetic lines of force.....	2
Figure 2 - Magnetic behavior of matter.....	7
Figure 3 - The magnetization curve (solid line) and hysteresis loop (broken curve) for a ferromagnet.....	7
Figure 4 - Magnetic characteristics of the elements.....	10
Figure 5 - Magnetic Separation.....	15
Figure 6 - Magnetic drag and gravitational force vs. particle size.....	18
Figure 7 - Relative recovery R_A/R_B vs relative susceptibility $(k_A/k_B)^B$ for two particle sizes.....	20
Figure 8 - The four step Magnex process.....	28
Figure 9 - Effect of temperature on susceptibility of a paramagnetic.....	28
Figure 10- General Pole Design for Magnetogravimetric Separation.....	33
Figure 11- (a) Channel separator: A, feed hopper; B, 'lights' outlet; C, 'heavies' outlet (b) detail on discharge to show splitter plate (shaded).....	33
Figure 12 - Hysterisless magnetization curve typical of ferrofluids.....	36
Figure 13 - Magnetogravimetric particle separator.....	37

Figure 14 - The cube represents symbolically the elementary cell of the spinel lattice. The four shaded and the four non-shaded octants are occupied by the metal ions in the same way as indicated in Fig. 15..... 51

Figure 15 - Two octants of the spinel structure. The large spheres represent the oxygen ions. The small black and white spheres represent the metal ions on tetrahedral and octahedral sites respectively..... 51

Figure 16 - Oxygen equilibrium pressures of different iron oxides as a function of temperature. Oxygen pressure in terms of $\log P_{CO_2}/P_{CO}$ for hematite Fe_2O_3 , magnetite Fe_3O_4 , and wüstite FeO 54

Figure 17 - Magnetic profile of the synthetic mixture. Size $-37+15\mu m$ 63

Figure 18 - Magnetic profile of the synthetic mixture after roasting at $320^\circ C$, by slow heating for 10 min. Size $-37+15\mu m$ 64

Figure 19 - X-ray diffraction pattern of the synthetic mixture after roasting at $320^\circ C$ for 10 min. by slow heating..... 66

Figure 20 - Microphotograph of $-37+15\mu m$ particles of the roasted synthetic mixture at 600 magnification with reflected light, under polarized conditions. C = chalcopryite, P = pyrite, F = ferrite, H = hematite..... 68

Figure 21 - Microphotograph of $-37+15\mu m$ particles of the mags fraction up to 15mA on Frantz of the roasted synthetic mixture. Magnification of 600 with reflected light, under polarized conditions. F = ferrite, P = pyrite, H = hematite..... 68

- Figure 22 - An oxidized particle of chalcopyrite on which microprobe examination was performed..... 69
- Figure 23 - Fe:Cu and S:Cu ratios as beam scans from the edge (position 1) towards the center (position 8) of the particle shown in figure 22. Fe:Cu ratio for ferrite 1.76. Fe:Cu, S:Cu ratios for chalcopyrite 0.88 and 1.01 respectively..... 70
- Figure 24 - Microphotograph of a $-37+15\mu\text{m}$ locked particle of chalcopyrite with galena, of B.M.S. sample. Magnification 600, reflected light under polarized conditions. C = chalcopyrite, G = galena..... 72
- Figure 25 - Microphotograph of a $-25+15\mu\text{m}$ locked particle of galena with chalcopyrite of B.M.S. sample. Magnification 600, reflected light under polarized conditions. C = chalcopyrite, G = galena..... 72
- Figure 26 - Magnetic profile of B.M.S. sample. Size $-37+15\mu\text{m}$ 73
- Figure 27 - Magnetic profile of B.M.S. sample after roasting at 320°C , by slow heating for 10 min. Size $-37+15\mu\text{m}$ 74
- Figure 28 - Magnetic profile of B.M.S. sample after roasting at 350°C , by slow heating for 10 min. Size $-37+15\mu\text{m}$ 75
- Figure 29 - Magnetic profile of B.M.S. sample after roasting at 350°C , by direct heating for 10 min. Size $-37+15\mu\text{m}$ 77
- Figure 30 - Magnetic profile of B.M.S. sample after preheating at 150°C , then roasting at 350°C for 10 min. Size $-37+15\mu\text{m}$ 78

- Figure 31 - Magnetic profile of B.M.S. sample after roasting at 320°C, by direct heating for 10 min. Size -37+15µm..... 79
- Figure 32 - Magnetic profile of B.M.S. sample after preheating at 150°C, then roasting at 320°C for 10 min. Size -37+15µm..... 80
- Figure 33 - Magnetic profile of B.M.S. sample after roasting at 320°C, by slow heating for 5 min. Size -37+15µm..... 81
- Figure 34 - Microphotograph of -37+15µm particles of the mags up to 10 mA on Frantz, of the roasted B.M.S. sample at 320°C, by slow heating for 10 min. Magnification 600, reflected light, under polarized conditions. C = chalcopryrite, P = pyrite, F = ferrite, H = hematite..... 84
- Figure 35 - Microphotograph of a -37+15µm particle of the mags on Davis tube, of the roasted B.M.S. sample at 320°C, by slow heating for 10 min. Magnification 600, reflected light, under polarized conditions. C = chalcopryrite, G = Galena, F = ferrite..... 84
- Figure 36 - Roasting of CuFeS_2 in tube, furnace. The "agglomeration index" vs. temperature..... 87
- Figure 37 - Roasting of CuFeS_2 in tube furnace. The conversion of CuFeS_2 vs. temperature..... 88
- Figure 38 - Roasting of CuFeS_2 in tube furnace. The conversion of CuFeS_2 vs. retention time..... 90
- Figure 39 - Roasting of CuFeS_2 in tube furnace. The conversion of CuFeS_2 vs. O_2 flow rate..... 91
- Figure 40 - Roasting of CuFeS_2 in tube furnace. The conversion of CuFeS_2 vs. temperature..... 93

Figure 41 - Roasting of CuFeS_2 , in tube furnace. Conversion of CuFeS_2 vs. time.....	84
Figure 42 - X-ray diffraction pattern of chalcopyrite after roasting at 320°C , for 45 sec. with an oxygen flow rate of 0.25 lt/s.....	95
Figure 43 - Microphotograph of $-37\mu\text{m}$ particles of roasted CuFeS_2 at 320°C , for 45s at O_2 flow rate 0.33 lt/s. Magnification 440, reflected light under polarized conditions. C = chalcopyrite, P = pyrite, F = ferrite.	97
Figure 44 - Microphotograph of $-37\mu\text{m}$ particles of Davis tube mags of roasted CuFeS_2 under the same conditions. Magnification 440 reflected light under polarized conditions. C = chalcopyrite, F = ferrite.....	97
Figure 45 - Microphotograph of $-37\mu\text{m}$ particles of roasted CuFeS_2 at 700°C , for 30s at air flow rate 0.33 lt/s. Magnification 440, reflected light under polarized conditions. C = chalcopyrite, F = ferrite, H = hematite.....	98
Figure 46 - Microphotograph of $-37\mu\text{m}$ particles of Davis tube mags of roasted CuFeS_2 under the same conditions. Magnification 440, reflected light, polarized conditions. C = chalcopyrite, P = pyrite, F = ferrite, H = hematite.....	98
Figure 47 - Roasting of PbS in tube furnace. "The agglomeration index" vs. temperature.....	100
Figure 48 - Microphotograph of $-37\mu\text{m}$ particles of sintered product of roasting of synthetic mixture at 320°C for 45s at O_2 flow rate 0.33 lt/s. Magnification 440, reflected light, polarized conditions C = chalcopyrite, G = galena, H = hematite.....	101

Figure 49 - Microphotograph of -37 μ m particles of sintered product of roasting of synthetic mixture under the same conditions. Magnification 440, reflected light, polarized conditions. C = chalcopryrite, G = galena, H = hematite, P = pyrite, F = ferrite.....	101
Figure 50 - Schematic diagram of HGMS.	
Figure 51 - Size distribution of the synthetic mixture before and after roasting at 320°C, by slow heating, for 10 min.....	106
Figure 52 - Copper Recovery in the magnetics vs. magnetic field, after HGMS on unroasted and roasted synthetic mixture.....	112
Figure 53 - Copper grade in the magnetics and non-magnetics vs. magnetic field, after HGMS on unroasted and roasted synthetic mixture.....	115
Figure 54 - Photograph of the Frantz Isodynamic Magnetic Separator.....	150
Figure 55 - A force balance of a paramagnetic particle between the pole pieces of the Frantz separator.....	151

1. INTRODUCTION

1.1 Principles of Magnetism (1)

1.1.1 Magnetic Field

Every magnet is surrounded by a magnetic field and any other magnet placed in this field experiences a magnetic force which is produced by the field.

The magnetic field is well defined by its lines. These lines emerge from one pole (north pole) and terminate at the other pole (south pole). Figure 1 shows the magnetic field of a bar magnet (1) and also the magnetic field around two unlike and like charges.

1.1.2 Magnetic moment and magnetization

Two unlike but equal pole strengths q_m and $-q_m$ with a distance ℓ between them comprise a dipole. The dipole is characterized by the magnetic moment.

$$m = q_m \cdot \ell \quad \text{Eq.1}$$

Intensity of magnetization is the magnetic moment per unit volume ie.

$$M = m/V \quad \text{Eq.2}$$

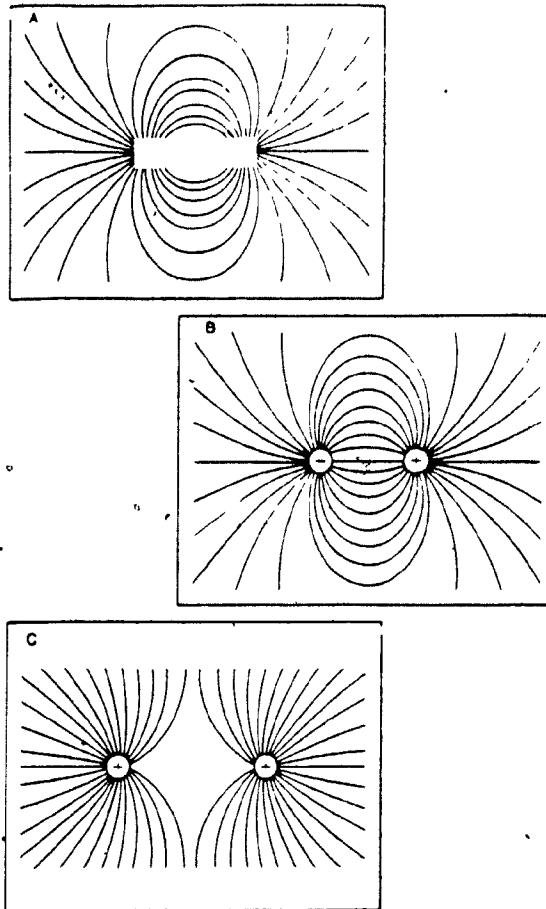


Figure 1: Magnetic lines of force

(A) Lines of force of a bar magnet. (B) the attraction between two unlike magnetic charges can be attributed to tension along the lines of force. (C) The repulsion between like charges is attributed to repulsion between adjacent lines of force. (1).

Magnetic moment acts along ℓ and it is a vector and consequently magnetization is a vector so

$$\hat{m} = q_m \cdot \hat{\ell} \quad \text{Eq. 3}$$

$$\hat{M} = \hat{m}/V \quad \text{Eq. 4}$$

1.1.3 The inverse square law and magnetic flux density

The force which acts between two separated magnetic poles is proportional to the magnitude of each of the two poles and inversely proportional to the square of the distance between them. Mathematically in a vacuum:

$$F = \frac{\mu_0 q_m q_m'}{4\pi r^2} \quad \text{Eq. 5}$$

where F = force, newtons (N)

μ_0 = constant of proportionality (permeability of free space)

= $4\pi \times 10^{-7}$ newton/ampere² (N/A²) or henrys/metre (H/m)

r = distance, metre (m)

q_m, q_m' = pole strengths, amperes-metres (A.m)

As the force on a pole is proportional to its magnitude

q'_m we could define

$$F = q'_m \cdot B \quad \text{Eq.6}$$

Combining eqs 5 and 6 we get that at a distance r from a magnetic pole the magnetic quantity B is

$$B = \mu_0 \frac{q_m}{4\pi r^2} \quad \text{Eq.7}$$

The lines of magnetic force around a pole spread out radially. If a sphere with radius r is drawn with its centre on the pole then the number of lines of force crossing this sphere is independent of its radius. This number is the magnetic flux Q where

$$Q = \mu_0 \cdot q_m \quad \text{Eq.8}$$

Combining eqs. 7 and 8, B is the magnetic flux density and equals $Q/4\pi r^2$ the flux per unit area of the sphere. The unit of flux is the weber and that of flux density the tesla. Therefore B can be expressed as

B : newtons/ampere-metre or
weber/metre² or
tesla.

1.1.4 Magnetic field strength

Recalling eq. 7 we can define

$$B = \mu_0 \cdot H$$

Eq. 9

5

where

$$H = \frac{q_m}{4\pi r^2}$$

Eq. 10

H is the pole strength per unit area or magnetic field strength with units A/m.

1.1.5 Effect of a magnetizable medium; Susceptibility and Permeability

When the magnetic force acts through a medium magnetic flux density is the sum of that in the vacuum ($\mu_0 \cdot H$) plus that due to the magnetizable medium.

$$B_{total} = \mu_0 H + \mu_0 M = \mu_0 (H + M) \quad \text{Eq. 11}$$

In many magnetic media the magnetization is proportional to the field strength ie.

$$M = k \cdot H$$

Eq. 12

where k is the magnetic susceptibility. k is a pure number, ie. it has no dimensions. So eq. 11 becomes:

$$B_{total} = \mu_0 (H + kH) = \mu_0 H (1 + k) \quad \text{Eq. 13}$$

The terms $(1+k)$ can be replaced by the symbol μ known as magnetic permeability.

In the absence of magnetic medium $k=0$ hence $\mu=1$. The quantity μ_0 sometimes is called permeability of free space and μ becomes the relative permeability of the magnetizable medium .

k is the volume susceptibility whereas x is the mass susceptibility defined as

$$x = k/\rho$$

Eq. 14

where ρ is the density (Kg/m^3).

1.2 Magnetic behavior of matter (2)

Matter does not behave the same when exposed to increasingly strong magnetic fields. Three main groups of materials are formed as shown in figure 2 (2).

1.2.1 Ferromagnetic group (1,2)

These are the strongly magnetic materials which means that they can be magnetized by a very weak magnetic field. Therefore the ferromagnetic's curve in figure 2 is out of scale when compared to the other curves and it is only an indication of the way that magnetization varies with the applied magnetic field.

Inside a ferromagnetic material when the field is applied all regions with paired north and south poles

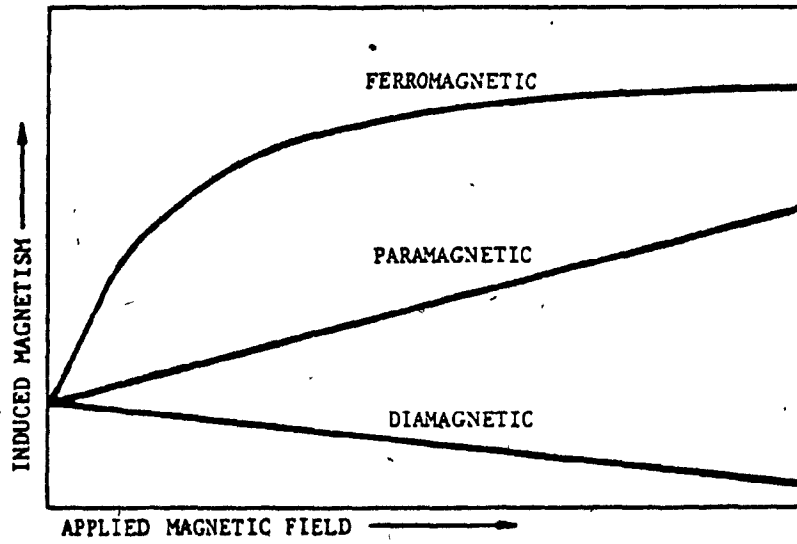


Figure 2. Magnetic behavior of matter. (2).

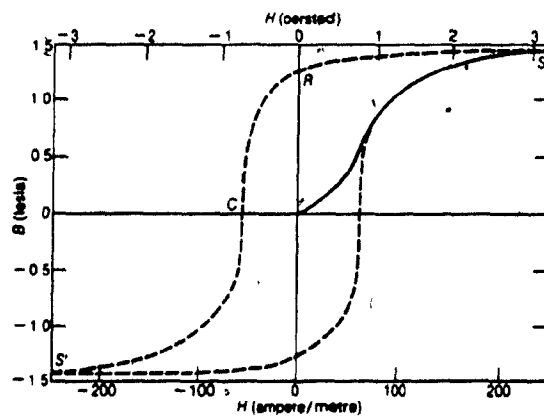


Figure 3. The magnetization curve (solid line) and hysteresis loop (broken curve) for a ferromagnet. (1)

become aligned.

8

A typical example of this group is iron whose magnetization curve is shown in figure 3(1). This plot of flux density B versus an applied external field H shows that B reaches its saturation value S in quite small fields. By reducing the external field H and reversing the direction of it, the plot becomes a closed loop known as hysteresis loop. (broken curve). The value of B at the point R is known as residual flux density and the retention of magnetization in zero field is called remanence. The value of B at point C is known as the coercive force. When saturation of the material in both directions is not reached then this results in a curve of smaller size. Therefore the hysteresis loop is not unique unless saturation is reached in both dimensions.

1.2.2 Ferrimagnetic group (1)

These materials exhibit the same magnetization curve as the ferromagnetics. However, they differ from ferromagnetics in the way that the magnetic susceptibility varies with temperature. Ferromagnetics magnetic susceptibility decreases above a certain temperature known as Curie temperature. For ferrimagnetics a decrease in temperature first causes an increase in k , then a decrease. The temperature at which this change in direction occurs is the Néel

temperature.

9

Minerals of the general formula $MO.Fe_2O_3$, where M is a metal (e.g. Cu, Ni, Fe, etc.) are known as ferrites and display ferrimagnetism. Some rare earth iron oxides are also ferrimagnetic.

1.2.3 Paramagnetic group (1,2)

This group of materials show a much lower response to applied magnetic fields. However, they can be strongly magnetized in a high magnetic field. The magnetic susceptibility (slope of curve in figure 2) is constant over a small range of temperature.

1.2.4 Diamagnetic group (2)

This group shows a slight response to applied magnetic fields which is opposite to that of paramagnetics. The magnetic susceptibility is negative but constant over a wide range of temperature.

1.2.5 Magnetism and the periodic table (2)

Figure 4(2) shows Mendeleev's periodic table of the elements showing to which of the above groups the elements belong. Three (3) elements are ferromagnetic (Fe,

GROUP		PERIOD																	
I A	II A	VIII										IB	IIB	IIIA	IVA	VA	VIA	VIIA	VIIIA
1	2	3	4	5	6	7	8	9	10	11	12	13	14	15	16	17	18		
H	He													B	C	N	O	F	Ne
Li	Be													Al	Si	P	S	Cl	Ar
Na	Mg	III B	IV B	V B	VI B	VII B	VIII				IB	IIB	Al	Si	P	S	Cl	Ar	
K	Ca	Sc	Ti	V	Cr	Mn	Fe	Co	Ni	Cu	Zn	Ga	Ge	As	Se	Br	Kr		
Rb	Sr	Y	Zr	Nb	Mo	Tc	Ru	Rh	Pd	Ag	Cd	In	Sn	Sb	Te	I	Xe		
Cs	Ba	La	Hf	Ta	W	Re	Os	Ir	Pt	Au	Hg	Tl	Pb	Bi	Po	At	Rn		
Fr	Ra	Ac	?	Ha															

TRANSITION ELEMENTS

58	59	60	61	62	63	64	65	66	67	68	69	70	71
Ce	Pr	Nd	Pm	Sm	Eu	Gd	Tb	Dy	Ho	Er	Tm	Yb	Lu
90	91	92	93	94	95	96	97	98	99	100	101	102	103
Th	Pa	U	Np	Pu	Am	Cm	Bk	Cf	Es	Fm	Md	No	Lr





FERROMAGNETIC  3
PARAMAGNETIC
 IN PURE FORM  16
 FORMS PARAMAGNETIC COMPOUNDS  32
 BECOMES PARAMAGNETIC IN COMPOUNDS  7

Figure 4. Magnetic characteristics of the elements. (2).

Co, Ni) and fifty-five (55) paramagnetic, the rest are diamagnetic. Of the 55 paramagnetic elements

- 32 form compounds that are paramagnetic.
- 16 are paramagnetic in pure form but form diamagnetic compounds.
- 7 become paramagnetic when one or more elements are present in a compound.

Table 1(2) gives the magnetic susceptibility of the elements in their pure form.

1.2.6 Magnetic susceptibility of minerals

It is not possible to form a table with the magnetic susceptibility of the minerals because they vary in chemical and mineralogical composition. Only experiment can provide reliable data for the magnetic susceptibility of minerals.

Table 1. Magnetic Susceptibilities of Elements (2)

Element	Formula	Magnetic Susceptibility $\times 10^6$
Aluminum	Al _{99.99}	+ 0.61
Americium	Am	+ 4.00
Antimony	Sb _{99.99}	- 0.75
Arsenic (amorphous crystalline)	As	- 0.037
Barium	Ba	+ 0.15
Beryllium	Be	- 1.00
Bismuth	Bi	- 1.34
Boron	B	- 0.62
Bromine	Br	- 0.46
Cadmium	Cd _{99.99}	- 0.176 (-0.310)
Calcium	Ca	+ 1.00
Carbon	C	+ 0.49
Cerium	Ce	+ 17.5
Cesium	Cs	+ 0.22
Chlorine	Cl	- 0.57
Chromium	Cr	+ 3.5
Cobalt	Co	Ferromagnetic
Copper	Cu	- 0.086
Dysprosium	Dy	+ 637.0
Erbium	Er	+ 265.0
Europium	Eu	+ 224.0
Gadolinium	Gd	+ 4800.0
Gallium	Ga	- 0.33
Germanium	Ge	- 0.105
Gold	Au	- 0.15
Hafnium	Hf	+ 0.5
Helium	He	- 0.47
Hydrogen	H	- 1.99
Indium	In	- 0.56
Iodine	I	- 0.35
Iridium	Ir	+ 0.16
Iron	Fe	Ferromagnetic
Krypton	Kr	- 0.344
Lanthanum	La	+ 0.85
Lead	Pb	- 0.132
Lithium	Li	0.50
Lutecium	Lu	0.00
Magnesium	Mg	+ 0.54
Manganese	Mn	+ 9.63
Mercury	Hg	- 0.1667
Molybdenum	Mo	+ 0.93
Neodymium	Nd	+ 39.01
Neon	Ne	- 0.33
Nickel	Ni	Ferromagnetic
Niobium	Nb	+ 2.20

Table 1. continued

Element	Formula	Magnetic Susceptibility $\times 10^6$
Nitrogen	N ₂	- 0.43
Osmium	Os	+ 0.064
Oxygen	O	+ 107.8
Palladium	Pd	+ 5.33
Phosphorus	P	- 0.86 white - 0.67 red
Platinum	Pt	+ 1.035
Plutonium	Pu	+ 2.52
Potassium	K	+ 0.53
Praseodymium	Pr	+ 35.6
Rhenium	Re	+ 0.363
Rhodium	Rh	+ 1.08
Rubidium	Rb	+ 0.198
Ruthenium	Ru	+ 0.427
Samarium	Sm	+ 12.1
Scandium	Sc	+ 7.0
Selenium	Se	- 0.32
Silicon	Si	- 0.13
Silver	Ag	- 0.22
Sodium	Na	+ 0.70
Strontium	Sr	+ 1.05
Sulfur	S	- 0.485
Tantalum	Ta	+ 0.849
Technetium	Tc	+ 2.7
Tellurium	Te	- 0.31
Terbium	Tb	+ 917.0
Thallium	Tl	- 0.249
Thorium	Th	+ 0.57
Thulium	Tm	+ 291.0
Tin	Sn	+ 0.026
Titanium	Ti	+ 3.19
Tungsten	W	+ 0.32
Uranium	U	+ 2.6
Vanadium	V	+ 5.00
Xenon	Xe	- 0.334
Ytterbium	Yb	+ 1.44
Yttrium	Y	+ 2.15
Zinc	Zn	- 0.175
Zirconium	Zr	+ 1.34

2. LIMITATIONS ON THE PERFORMANCE OF A MAGNETIC SEPARATOR

2.1 Forces on a particle in a magnetic separator (2,3)

What happens in a magnetic separator is best illustrated in figure 5(3). Every particle of the feed experiences forces and its motion is designated from the force which predominates. In a magnetic separator usually there are four types of forces;

- the magnetic force which pulls the magnetic material towards the collecting surface
- the gravitational force which pulls all the particles out of the separator
- the frictional force tending to pull out the magnetic particles from the collecting surface
- the interparticle forces

When the magnetic force on a particle predominates, this particle reports to the magnetic outlet (mags portion). When the other three forces predominate the particle reports to the non-magnetic outlet (non-mags portion). However, some particles due to interaction of competing forces do not come out as mags or non-mags. These particles are the middlings of the separation.

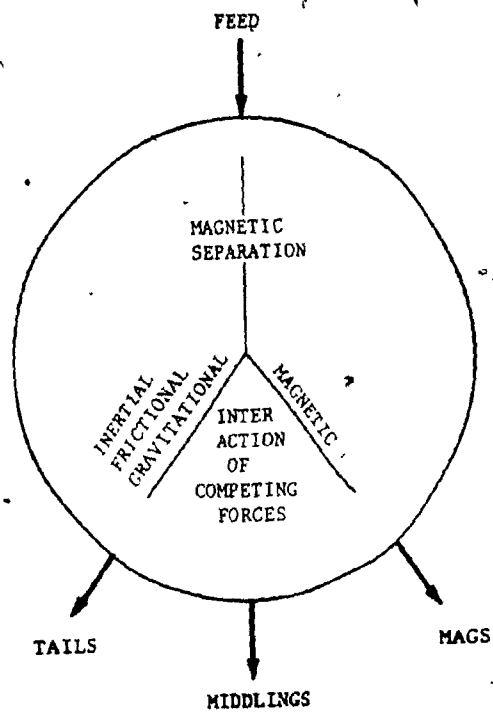


Figure 5. Magnetic Separation (3).

2.2 Size limitation on the performance of a magnetic separator (2,3)

In a magnetic separator a particle experiences a magnetic force and competitive forces due to gravity friction and inertia.

The magnetic force is given by the equation

$$F_m = \frac{4}{3} \cdot \mu \cdot \mu_0 \cdot \pi \cdot (k_p - k_m) \cdot b^3 \cdot H \cdot \frac{dH}{dx} \quad \text{Eq. 15}$$

where: μ_0 : permeability of free space

μ : relative permeability of magnetizable medium

k_p : magnetic susceptibility of the particle

k_m : magnetic susceptibility of the medium

b : particle radius

H : intensity of magnetic field

dH/dx : intensity gradient

The hydrodynamic drag force for a spherical particle is given by the following equation according to Stoke's law.

$$F_d = 6 \cdot \pi \cdot v \cdot u \cdot b \quad \text{Eq. 16}$$

where: v : viscosity of the fluid medium

u : velocity of particle relative to stream.

The gravitational or buoyant force is given by the following equation

$$F_g = \frac{4}{3} \cdot \pi \cdot b^3 (d_p - d_m) \cdot g \quad \text{Eq.17}$$

where: d_p : density of particle
 d_m : density of medium
 g : acceleration of gravity.

Oberteuffer (3) plotted those competing forces as a function of particle size as shown in figure 6(3). The forces have been computed for a CuO particle attracted by a ferromagnetic wire of radius $3b$ and magnetized by a field of $10kOe$ with a slurry velocity of $5cm/sec$. When the separator treats large particles then the gravitational force will predominate. When the particles are fine the drag force will predominate. The magnetic force F_m will predominate only if the particles are within the size range of $5\mu m$ to approximately $1mm$ for CuO case. This is a particle size limitation on the performance of a magnetic separator.

High gradient magnetic separation (HGMS) has achieved successful application in the case of separation between a paramagnetic and a diamagnetic mineral. In kaolin

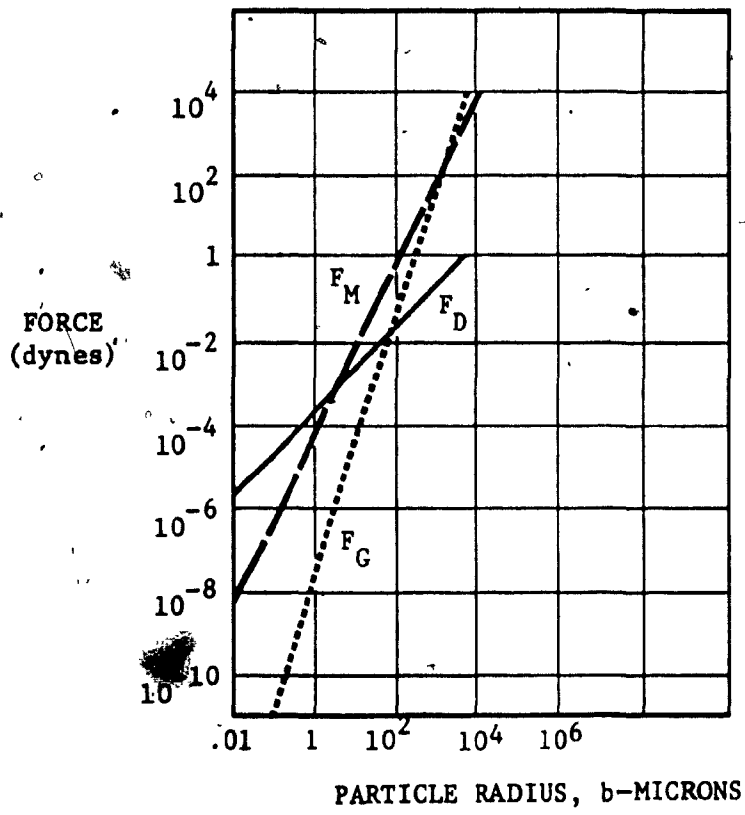


Figure 6. Magnetic drag and gravitational force vs. particle size. (2).

beneficiation iron and titanium compounds are removed as paramagnetic impurities from the bulk diamagnetic kaolin concentrate. The particle size is less than 200 Mesh and preferably, below 20 microns. In coal desulfurization and ash removal, paramagnetic pyrite is removed from the diamagnetic coal. Studies of water slurries of pulverized coal (4,5) proved to be successful and the particle size was below 42 and below 33 microns respectively.

2.3 Susceptibility difference limitation

Oberteuffer (3) showed that the optimum size for separation is the same for all minerals and concluded that separation of weakly magnetic substances would be possible only within a restricted size range.

Dobby et al (6) studied the same problem and presented their result in a graph which is shown in figure 7(6). This is a plot of the relative recovery versus relative susceptibility for different particle sizes. Assuming that a relative recovery of 5:1 is acceptable then the minimum relative susceptibility must be 20:1 for single-sized particles and 50:1 for a wide range (0-37 μ m) of particle size. Large particles of the weakly magnetic mineral will experience the same magnetic force as smaller particles of the more magnetic mineral. This plot was developed from work in HGMS but the result

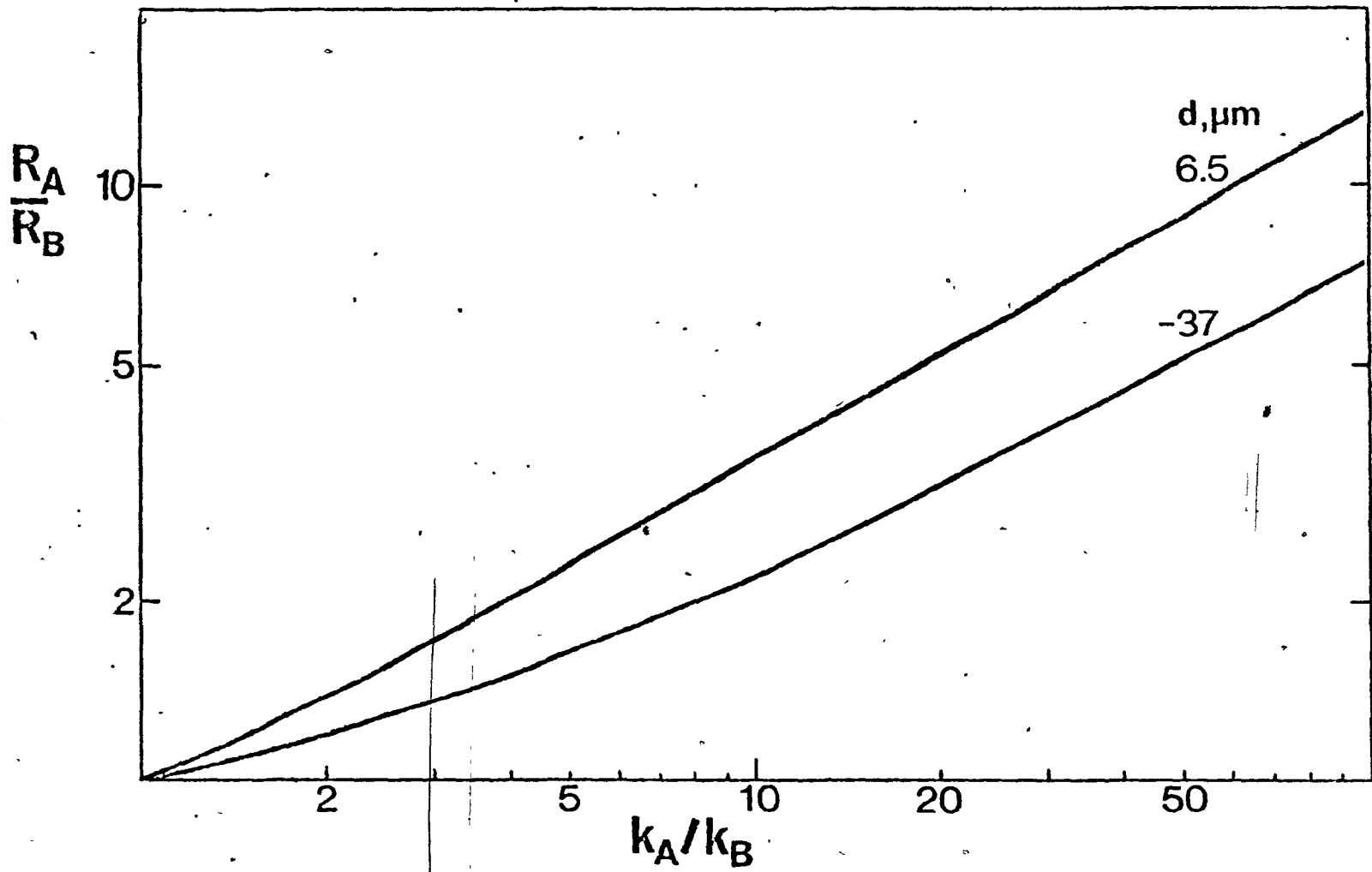


Figure 7. Relative recovery R_A/R_B vs relative susceptibility (k_A/k_B) for two particle sizes (6).

is the same for any magnetic separator. Table 2(6) shows the relative susceptibility for selected mineral pairs. Only the pairs on the right above the double line are offered for potential magnetic separation.

The results were obtained for water slurries and would be different if the water was replaced by salt solutions bearing a substantial k_m . This is considered later.

2.4 Dimensionless groups

High Gradient Magnetic Separation has been studied extensively and this has resulted in two quite useful dimensionless groups which are used for preliminary estimation purposes.

2.4.1 Watson's model (7)

Watson uses the concept of the "magnetic velocity V_m " which is the velocity that a particle would obtain in a uniform field gradient, when the competitive force is the hydrodynamic drag force and the flow is Stokesian. V_m is given by the following equation:

$$V_m = \frac{2}{9} \frac{b^2 \cdot k \cdot \mu_0 \cdot H \cdot M_w}{\eta \cdot \alpha} \quad \text{Eq. 18}$$

where M_w : wire magnetization

n : dynamic viscosity (Kg/m.s)

α : radius of the wire (m)

For magnetic capture to occur:

$$V_o < V_m \quad \text{Eq. 19}$$

where V_o is the fluid flow velocity. Therefore for a given system the operating variable V_o can be selected.

2.4.2 Nesset and Finch's model (8)

Nesset and Finch related recovery to a dimensionless group, the loading number N_L . This group represents the ratio of magnetic to fluid shear forces at full load on the upstream side of the wire. Full load means the maximum amount of material that the matrix can hold for a particular set of conditions. The loading number is given by the following equation:

$$N_L = \frac{b.k.\mu_o.H.M_w}{V_o^{3/2} \cdot (\rho_f \cdot n \cdot \alpha)^{1/2}} \quad \text{Eq.20}$$

where ρ_f is the fluid density. $N_L > 25$ corresponded to acceptable recovery.

Assuming build-up is over the front 90° of the matrix wire, the mass loading γ_m (mass of mags per unit mass of matrix) can be predicted by the equation.

$$\gamma_m = \frac{\epsilon}{4} \left[\left(\frac{N_L}{2.5} \right)^{0.8} - 1 \right] \frac{\rho_p}{\rho_w} \quad \text{Eq. 21}$$

where ϵ : packing density (≈ 0.7)

ρ_p : particle density (Kg/m^3)

ρ_w : wire density (Kg/m^3)

Eventually recovery can be estimated by assuming the matrix loads to about 75% of full capacity

$$R(\%) = \left(0.75 \frac{\gamma_m}{L} \right) \times 100 \quad \text{Eq. 22}$$

where $R(\%)$: recovery in percent

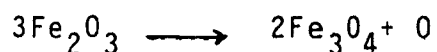
L : the mass of magnetics in the feed
per unit of matrix mass.

3. METHODS OF OVERCOMING THE LIMITATIONS ON THE PERFORMANCE OF A MAGNETIC SEPARATOR

In the previous chapter the two limitations (particle size limitation and magnetic susceptibility difference limitation) on the performance of a magnetic separator were discussed. In this chapter some methods for overcoming these limitations will be examined.

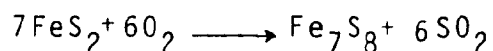
3.1 Chemical change by heating (9)

The products of heating of some substances may have a different magnetic susceptibility. The classic example is the magnetizing roast of hematite to magnetite according to the reaction.



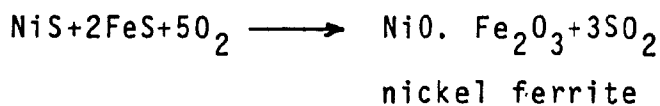
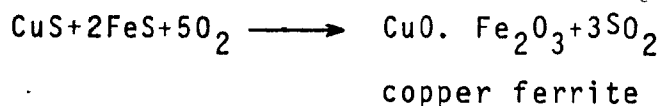
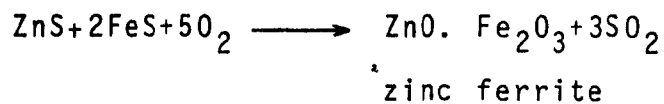
between 400-600°C.

Another example is the roasting of pyrite to the more magnetic form of pyrrhotite at about 400°C



Another important class in the sense that the product is very magnetic are the reactions which produce ferrites from roasted

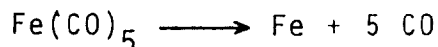
sulfides. At 300-600°C the following can occur.



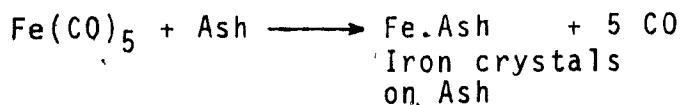
3.2 Adsorption of iron

The basis of this method is to selectively coat mineral particles with a thin layer of iron. This will enhance the overall particle susceptibility.

The Magnex process (10) applies this concept in the desulfurization and ash removal from coal. It is a four step process shown in figure 8 (10). Coal is crushed to minus 14-mesh and is heated to 170°C. Then it is exposed to iron pentacarbonyl vapour which at that temperature decomposes according to the following reaction.



The reaction is not this simple and intermediate products are formed. The iron is preferentially adsorbed on the surface of the ash and pyrite according to the reactions



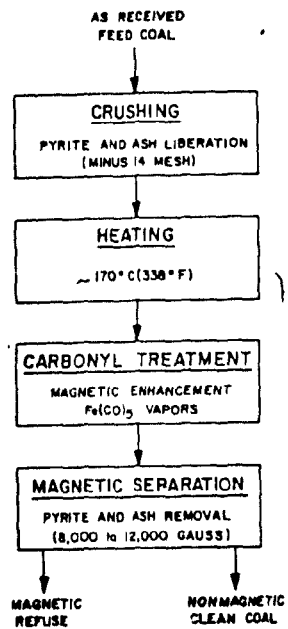


Figure 8. The four step Magnex process. (10).

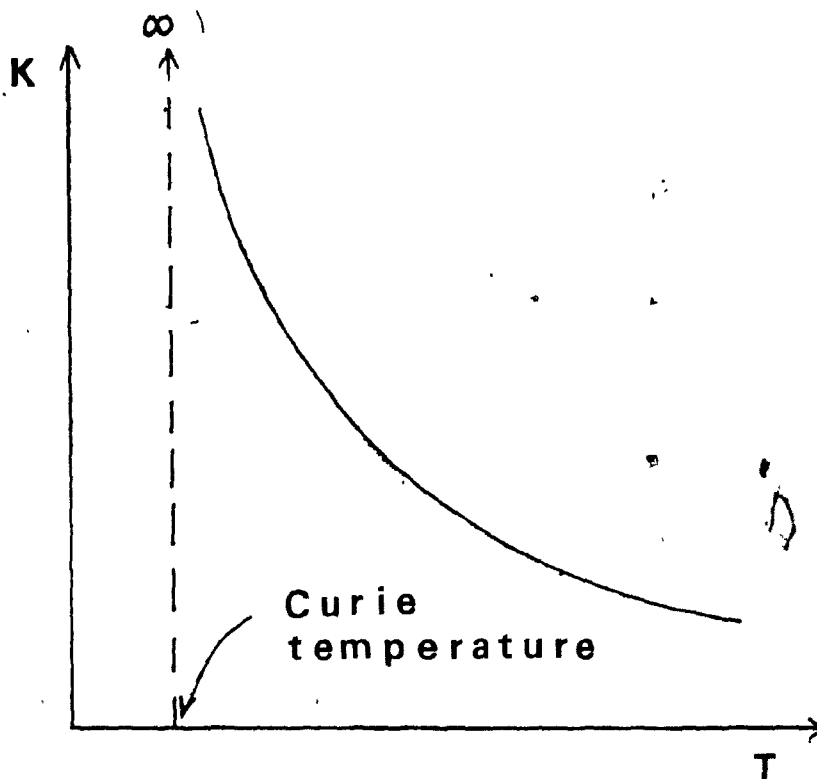


Figure 9. Effect of temperature on susceptibility of a paramagnetic.

possibility.

Cryogenic HGMS uses this principle, the low temperatures being achieved using liquid nitrogen, helium or natural gas. These media also exhibit a low viscosity and decrease the drag force. Cryogenic HGMS has been applied to beneficiation of fine (-200 Mesh) coals on a laboratory scale.

3.4 Selective seeding

Selective seeding is a technique designed to flocculate desired mineral(s) with introduced magnetite seeds. The flocs are readily separable at low magnetic field. After separation magnetite can be recovered for reuse by dispersion of the flocs.

Experiments (12) were performed using $Al(OH)_3$ (gibbsite), SiO_2 (quartz) and magnetite. After flocculation the flocs were captured by HGMS at 1 kilogauss. Upgrading of $Al(OH)_3$ was from 40 to 69% with 93% recovery.

3.5 Magnetizing leach

The basis of this method is to increase the magnetic properties of processed minerals by leaching.

Krukiewicz and Laskowski (13) used an alkali leach

to produce a magnetite coating on siderite. The reaction proceeds in two steps: decomposition of FeCO_3 with formation of $\text{Fe}(\text{OH})_2$ and oxidation to α, δ and $\gamma\text{-Fe}_2\text{O}_3$ oxides and Fe_3O_4 .

The oxidation step is the most important because it determines the constitution and the magnetic susceptibility of the leached product.

The above researchers carried out experiments on different decomposition rates of siderite and on different oxidation rates. They found that the product was more magnetic when the siderite was completely decomposed and the oxidation conditions were: temperature of 90°C , oxidation time of 30 min. and air flow rate of 40 lt/hr. The resulted magnetic susceptibility was 41.4×10^{-3} emu/cm³-0e and the oxides formed were $\gamma\text{-Fe}_2\text{O}_3$ and Fe_3O_4 .

Magnetic separation of first and second kind

The methods described in paragraphs 3.1-3.5 depend on the inherent or changed susceptibility of the partic(es). This can be called "magnetic separation of the first kind." (14) A second approach can be based on changing the magnetization of the medium. This separation is called "magnetic separation of the second kind".

3.6. Changing medium susceptibility

Considering the expression of the magnetic force (Eq.15) k_m is the medium susceptibility. For water $k_m=0$ but for other liquids k_m has a certain value. For example a solution of $MnCl_2$ is paramagnetic, a saturated solution (72gr $MnCl_2$ in $100cm^3$ water) has a susceptibility of 0.87×10^{-3} .

Consider two minerals A and B with susceptibilities k_A and k_B . As discussed the magnetic susceptibility limitation implies that for a reasonable separation the ratio of the two susceptibilities be greater than 20. If the medium selected has a susceptibility k_m so that $k_A > k_m > k_B$ then relative to the medium, A is paramagnetic whereas B is diamagnetic. This results in a decrease in the 20:1 ratio of susceptibilities required for separation.

This method has been applied to the separation of wolframite from cassiterite (15) where cassiterite carried enough iron to be paramagnetic. As medium $MnCl_2$ solution was used and the particle size was 60% minus $45 \mu m$. This method does not depend on the density of paramagnetic particles.

Paramagnetic or diamagnetic minerals with different

densities can be separated with the magnetogravimetric method which uses either paramagnetic fluids or ferrofluids.

3.7 Magnetogravimetric separation (14)

3.7.1 Paramagnetic fluids

When a paramagnetic fluid is exposed to a non-homogeneous magnetic field it experiences a force that acts in the direction of the field gradient and produces an apparent density gradient. In a mixture of feebly magnetic and diamagnetic particles with a strongly paramagnetic fluid such as $MnCl_2$ solution if that force acts in the direction of gravity, levitation and separation of particles can be achieved.

The apparent density of the medium at any point in the field is given by the following equation.

$$\rho_a = \rho_m + \frac{k_m}{g} \cdot \frac{H}{\mu_0} \cdot \frac{dH}{dx} \quad \text{Eq.23}$$

where ρ_a and ρ_m are the apparent and the real densities of the medium respectively. In figure 10 the design of the electromagnets and the distribution of density are shown. In figure 11 the channel assembly for the feed and the two

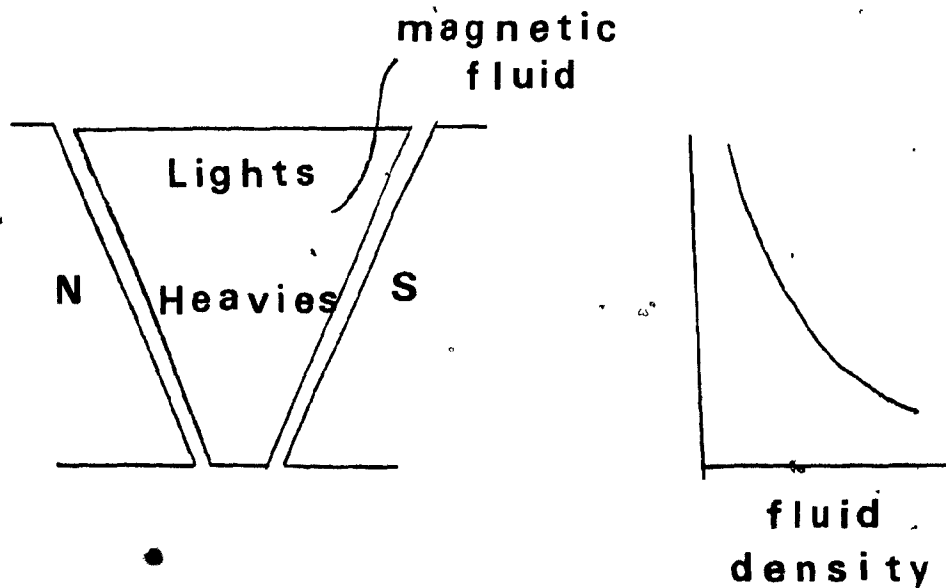


Figure 10. General Pole Design for Magnetogravimetric Separation. (9).

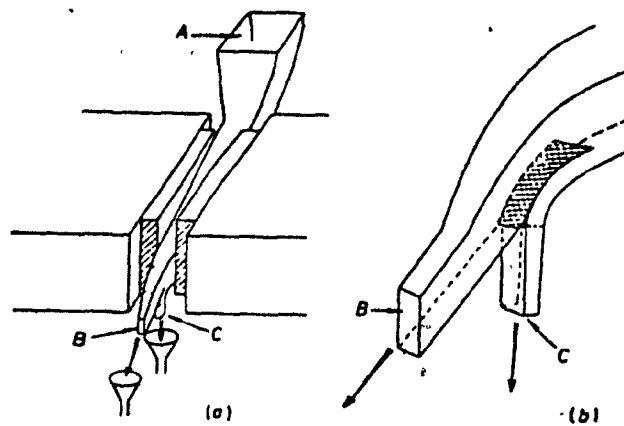


Figure 11. (a) Channel separator: A, feed hopper; B, 'lights' outlet; C, 'heavies' outlet (b) detail on discharge to show splitter plate (shaded). (9).

different outlets for the heavy particles and the light ones are shown.

The method is best suited to the separation of non-magnetic materials. At equilibrium particles are levitated to a position in the field, which depends on the magnetic force, the magnetic susceptibility of the liquid and of the particle and on the particle density. So for particles with insignificant magnetic susceptibility the equilibrium height depends only on their density. The method could be used for mineralogical work. It has been used for the separation of barite from galena (particle size $-1.7+.85\text{mm}$) and celestite from galena in a pilot scale (14).

3.7.2 Ferromagnetic fluids or ferrofluids

In 1960 NASA developed a technique to prepare stable suspensions of metallic particles of less than 150 \AA in a hydrocarbon carrier fluid. The United States Bureau of Mines later perfected this technique. According to this technique magnetic particles are formed by precipitation of ferrous and ferric salts with an excess of ammonium hydroxide in an aqueous medium. Kerosene and oleic acid are added and the mixture is heated. During heating the magnetic particles are coated by oleic acid and transferred into the

kerosene phase, resulting in the formation of the magnetic fluid.

These fluids when in a non-homogeneous magnetic field exhibit an apparent density and density gradient. The principle is the same as before in the paramagnetic fluid case and ferrofluids behave as heavy media. However, in comparison with conventional heavy media they are not limited to the range of 4-4.5 g/cm³ but can be extended over the entire density spectrum up to 21g/cm³ or more (platinum and gold have been levitated in ferrofluids).

Ferrofluids exhibit a hysteresisless magnetization curve as shown in figure 12(14) and reach their saturation level at reasonable fields. Figure 13(2) shows a magneto-gravimetric separator and the balance of the forces which act on a particle. The United States Bureau of Mines has a large scale separator. This unit has been used for the recovery of aluminum from a shredded automobile scrap. (particle size: -2+1/4 inch).

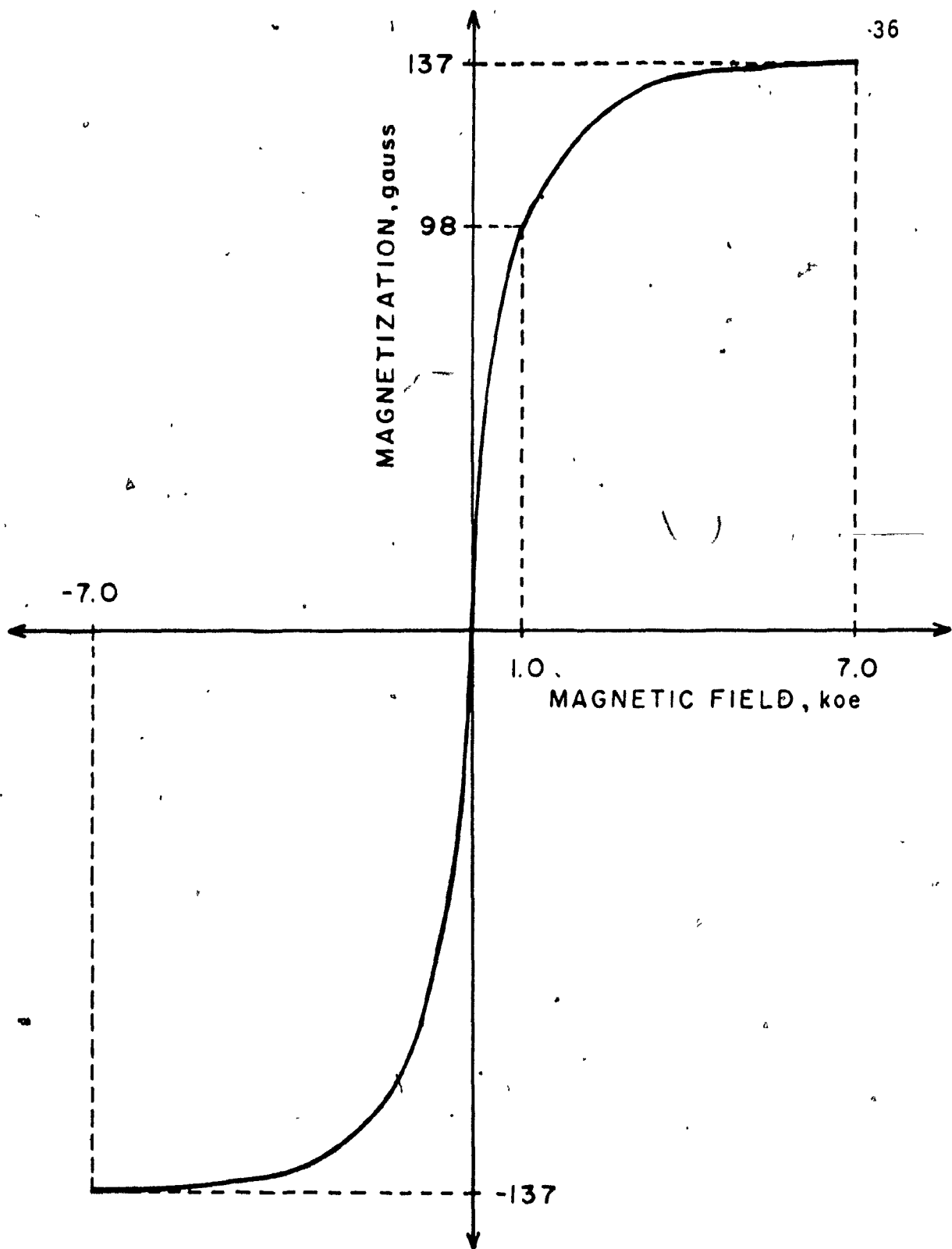


Figure 12. Hysteresisless magnetization curve typical of ferrofluids. (14).

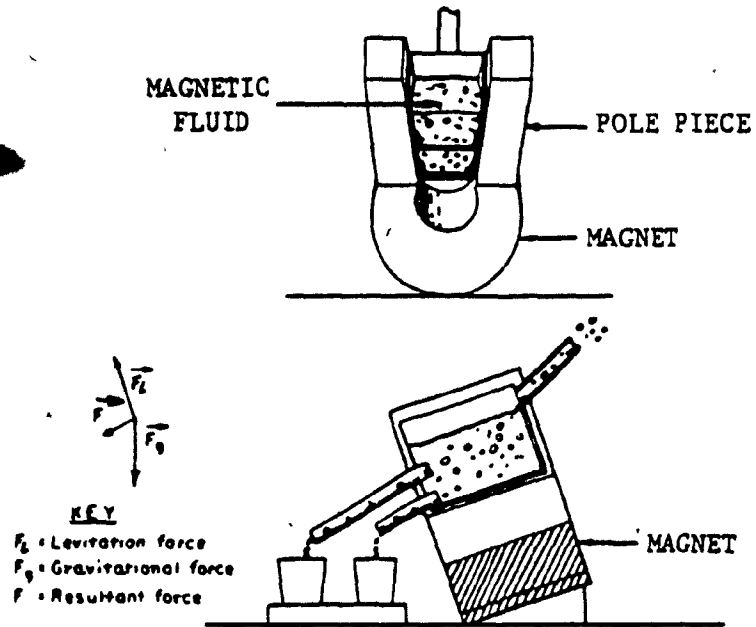


Figure 13. Magnetogravimetric particle separator. (2).

4. STATEMENT OF PROBLEM

4.1 Need for beneficiation of mineral fines

Many ores contain valuable minerals in finely disseminated form. The recovery of these fine mineral particles is generally very difficult. This poses a significant problem as diminishing raw materials sources necessitates the recovery of these fine particles. In many systems the efficiency of recovering fine particles is still extremely low and often fine particles must be discarded as slimes. Shortage of minerals does not always mean lack of resources but rather lack of adequate technology to treat available ores.

In recent years, various advances have taken place in the recovery of mineral particles in the very fine size range. HGMS is the most recent development in wet magnetic separation processes aimed at fine particles. The technique has been investigated, for removal of iron impurities from industrial minerals such as barite, calcite, kyanite (16) and from coal (17). HGMS is now being applied industrially for the purification of kaolin. Because of its applicability to fine particles the HGMS process has large potential

in development of mineral separation processes.

This thesis is concerned with chalcopyrite-galena separation in the treatment of complex sulfides. These minerals are often initially floated together and subsequently separated. This separation often proves difficult.

4.2 Magnetic separation of chalcopyrite and galena

The relative susceptibility of chalcopyrite to galena is 330 (6) which exceeds the magnetic susceptibility limitation mentioned before. However, this separation is still unattractive when the minerals to be separated are extremely fine ($-37\mu\text{m}$), due to the very high magnetic fields required. However, there is evidence that chalcopyrite can be converted by heating to a more magnetic form (i.e. copper ferrite) and then can be more easily separated from diamagnetic galena. In other words a chemical change during the roasting of chalcopyrite can overcome the particle size limitation imposed by the low susceptibility.

The object of this work is to study the roasting of chalcopyrite under various conditions with respect to the magnetic character of the calcine. The calcines will be identified and their magnetic profile will be determined

on the Frantz Isodynamic Separator. Synthetic and "real" mixtures of chalcopyrite and galena will be tested to illustrate the separation potential.

5. ROASTING OF CHALCOPYRITE

5.1 Background (18)

Chalcopyrite ignites when heated in air and the ignition temperature is lower from the ignition temperature of other sulfides of the same particle size. Table 3 gives the ignition temperatures of pure sulfide minerals as measured by Volsky and Sergievskaya (19). From table 3 it can be seen that the ignition temperature increases as the sulfur content decreases if chalcopyrite is considered as an exception. No reason was given for this anomaly.

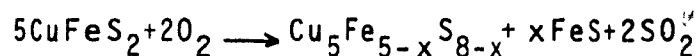
Table 3. Ignition temperature of pure sulfide minerals (19)

Particle size mm	Ignition temperature °C				
	Pyrite 53.4% S	Pyrrhotite 36.4% S	Chalcopyrite 34.5% S	Sphalerite 32.9% S	Galena 13.4% S
0.10-0.15	422	460	364	637	720
0.15-0.20	423	465	375	644	730
0.20-0.30	424	471	380	646	730
0.30-0.50	426	475	385	646	735
0.50-1.00	426	480	395	646	740
1.00-2.00	428	482	410	646	750

Industrial scale oxidation of chalcopyrite has been conducted in three ways.

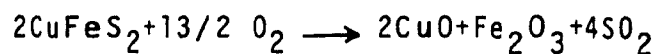
A. Partial oxidation

During this process a certain percentage of sulfur is removed so that the calcine can be subsequently melted to a matte. The reaction which takes place is the following:

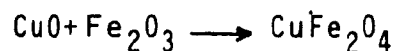


B. Complete oxidation (dead-roasting)

This oxidation conducted by air or oxygen forms oxides according to the following reaction



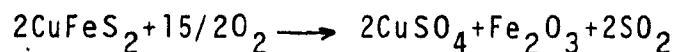
Ferrites are also formed due to the reaction



C. Sulfation roasting

This roasting is carried out usually in a fluidized

bed reactor in the presence of air. The following reaction takes place:



5.2 Mechanism of Oxidation

The mechanism of oxidation has been studied by many investigators. Habashi (18) summarizes the work of some of them. Tafel and Greylich (20) determined the temperatures at which there was maximum water solubility and acid solubility which suggests formation of sulfates. They found that cupric sulfate was formed at 350°C up to the temperature of 550°C. Above this temperature decomposition to copper oxysulfate ($\text{CuO} \cdot \text{CuSO}_4$) occurred and was complete at 700°C. Water soluble iron was mainly ferrous-sulfate with negligible amounts of ferric sulfate. Above 650°C copper oxysulfate started to decompose to cuprous oxide and/or ferrite. Ferrous sulfate was also completely decomposed at 600°C.

Mennier and Vanderpoorten (21) studied the progress of oxidation on chalcopyrite cubes between 300-900°C. At the end of each test, the cube was cut into halves and the layered structure was examined microscopically and by means of X-ray diffraction. They found that the reaction starts

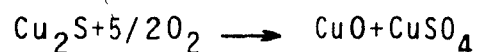
at 330°C when chalcopyrite is covered by a thin layer of different colors. At 500°C the layer was of appreciable thickness and identified as ferric oxide and bornite, with some small amounts of cupric sulfate, cupric oxide and magnetite. Near to the bornite layer cuprous oxide and cuprous ferrite $\text{Cu}_2\text{Fe}_2\text{O}_4$ were identified. At 800°C oxidation of chalcopyrite resulted in the formation of the ferrite CuFe_2O_4 .

Margulis and Ponomarev (22) and Lenchev and Bumazhnov (23) confirmed that oxidation of chalcopyrite taken place via bornite formation.

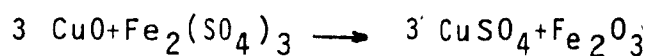
Maurel (24) studied the oxidation of chalcopyrite by differential thermal analysis and x-ray diffraction. He found that at 530°C bornite, cupric sulfate and ferric oxide were formed and at 600°C cupric oxide, cuprous oxide, ferric oxide and cupric sulfate were formed.

Razouk et al (25) studied the oxidation of chalcopyrite by thermogravimetric analysis and proposed the following mechanism which seems to contradict those proposed by the previous workers:

Between 350 and 400°C



Between 450 and 600°C



Above 600°C the sulfates decompose and at 900°C copper ferrite is formed.

There is some confusion over the mechanisms of oxidation of chalcopyrite which possibly could be explained by the different conditions by which oxidation was carried out.

5.3 Thermodynamic analysis using F.A.C.T. System

Facility for the Analysis of Chemical Thermodynamics (F.A.C.T.) is an interactive computing system for thermodynamic calculations.

One of the programs incorporated in F.A.C.T., EQUILIB, determines the equilibrium concentration of chemical species when specified elements or compounds react. The user

only supplies the reactants, temperatures and pressures of reactants and indicates which species he would like to be considered in the products. The program then produces the solution by providing the products that are most stable.

The program was used for the oxidation of CuFeS_2 for the temperatures of 685, 550 and 500°C and the printouts are presented in Appendix A. At 685°C the products were ferrite, Fe_2O_3 and CuSO_4 . At 550 and 500°C only Fe_2O_3 and CuSO_4 were predicted by the program.

5.4 Magnetic separation of roasted chalcopyrite.

Literature Survey

Near the turn of the century at Ain Barbar in Algeria a method of magnetic separation of roasted chalcopyrite (26) was used. The minerals to be separated, were chalcopyrite, marmatite ($\text{Zn}(\text{Fe})\text{S}$) and galena. According to this method the mixture was heated lightly to 525°C for 15-25 minutes depending on the particle size (+3mm). The reactions were considered to be: at 440°C the sulfur of the iron constituent of chalcopyrite ($\text{Cu}_2\text{S} + \text{Fe}_2\text{S}_3$) disassociated giving:



at 525°C oxidation began following the reaction



Further heating resulted in the formation of sulfates with agglomeration of the chalcopyrite and sphalerite. With this treatment the grains of chalcopyrite obtained a net magnetic susceptibility difference from the rest of the mixture. Magnetic separation was then performed by a cross-belt separator. The first pole removed all the pyrite and some chalcopyrite, the second pole most of the chalcopyrite with some sphalerite, the third pole mixed products including some chalcopyrite and the fourth pole mixed products without pyrite and the tailing contained sphalerite, galena and gangue. Copper concentrate assayed 18% Cu and represented a recovery of 82%, zinc concentrate assayed 40% Zn with a recovery of 87%.

Dean and Davis (27) studied the effect of heat treatment on magnetic properties of mineral powders. Some of their results are presented in table 4 (27).

Table 4. Effect of heat treatment on magnetic properties of mineral powders (27)

Mineral	Heat treatment	H _c A/m	B _r Tesla	M _w A/m	H _{max} A/m
Magnetite	None	1,592	0.0137	2,846.10 ³	214,920
do	Heated in air	7,960	0.0240	1,200.10 ³	214,920
Hematite	None	(1)	(1)	(2)	159,200
do	reduced to Fe ₃ O ₄	33,830	0.0340	784,000	159,200
Lepidocrocite	None	(1)	(1)	(2)	214,920
do	heated in air to 370°	3,423	0.0085	414,000	214,920
do	reduced to Fe	7,005	0.0130	1,255.10 ³	214,920
Ilmenite	None	(1)	(1)	(2)	265,864
do	Heated in air	26,666	0.0242	59,100	265,864
Pyrite	None	(1)	(1)	(2)	214,920
do	Light roast	47,760	0.0080	180,000	214,920
Chalcopyrite	None	(1)	(1)	(2)	214,920
do	Light roast	27,860	0.0030	100,000	214,920
Arsenopyrite	None	(1)	(1)	(2)	214,920
do	Light roast	23,880	0.0085	230,000	214,920

(1) Too small to determine.

(2) Less than 12000.

H_c, B_r, coercive force and remanence respectively.

M_w is the magnetization.

H_{max} is the maximum external field applied.

6. FERRITES

6.1 Chemical composition (28)

Ferrites have the structure of the mineral spinel $MgAl_2O_4$. The general chemical formula is $MeFe_2O_4$, where Me represents a divalent metal ion with an ionic radius approximately between 0.6 and 1 Å. In the case of simple ferrites Me is one of the divalent ions of the transition elements Mn, Fe, Co, Ni, Cu, Zn, Mg and Cd. A combination of these ions is also possible forming a solid solution of two ferrites or a mixed ferrite. It is also possible for Me to represent a combination of ions which have an average valency of two.

The valency of the metal ions of ferrites can be determined by an analysis of the oxygen concentration. However this analysis does not reveal if different ions occur in more than one valency state. For example in the case of $MnFe_2O_4$ an oxygen analysis does not reveal whether the formula is $Mn^{II}Fe_2^{III}O_4$ or $Mn^{III}Fe^{II}Fe^{III}O_4$. The ferrite $Cu_{0.5}Fe_{2.5}O_4$ also poses a problem since it is not known if iron ions are trivalent and copper ions monovalent or it is a mixed crystal of $Cu^{II}Fe_2O_4$ and $Fe^{II}Fe_2O_4$. In many cases

a magnetic property, e.g. the saturation magnetization, can distinguish between the possible chemical structures.

6.2 Crystal structure (28,29,30)

The spinel structure derives its name from the mineral spinel $MgAl_2O_4$ which crystallizes in the cubic system. The smallest cell of this structure which has cubic symmetry contains eight "molecules" of $MeFe_2O_4$. Two kinds of interstitial sites occur, the tetrahedral site which is surrounded by 4 oxygen ions, and the octahedral site which is surrounded by 6 oxygen ions. Each cubic unit cell contains 64 tetrahedral sites and 32 octahedral sites. Of the 64 tetrahedral sites only 8 are occupied by metal ions (A sites). Of the 32 octahedral sites 16 are occupied by metal ions (B sites). The structure can be described by subdividing the elementary cube with edge a into eight octants with edge $1/2 a$ as shown in figure 14 (28).

The oxygen ions are positioned in the same way in all octants. Each octant contains four anions, which form the corners of a tetrahedron as shown in figure 15 (28).

The metal ions are positioned according to their valency. It might be thought at first that the eight divalent

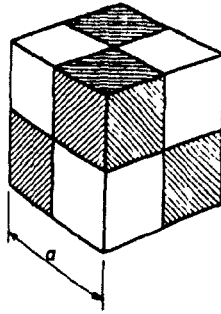


Figure 14. The cube represents symbolically the elementary cell of the spinel lattice. The four shaded and the four non-shaded octants are occupied by the metal ions in the same way as indicated in Fig. 15. (28).

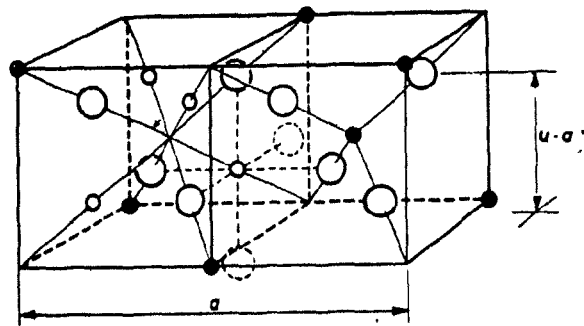


Figure 15. Two octants of the spinel structure. The large spheres represents the oxygen ions. The small black and white spheres represent the metal ions on tetrahedral and octahedral sites respectively. (28).

cations are situated on the eight occupied A sites and the 16 trivalent iron cations on the 16 occupied B sites. When this happens the spinel formed is called normal spinel. However this does not happen in all cases. Experiments show that there is a whole range of distributions represented by the chemical formula $\text{Me}_\delta^{\text{II}} \text{Fe}_{1-\delta}^{\text{III}} \left[\text{Me}_{1-\delta}^{\text{II}} \text{Fe}_{1+\delta}^{\text{III}} \right] \text{O}_4$, where the brackets indicate octahedral sites. The limiting case $\delta=1$ is the normal spinel and the limiting case $\delta=0$ is called an inverse spinel. The case $\delta=0$ is more likely because $r_B > r_A$ and $r_{\text{Me}^{\text{II}}} > r_{\text{Me}^{\text{III}}}$ where r is the ionic radius. The distribution of the metal cations on A or B sites has been examined by x-ray diffraction, neutron diffraction and magnetic measurements. For MgFe_2O_4 and CuFe_2O_4 the temperature dependence of the distribution corresponds to a Boltzmann distribution

$$\frac{\delta(1+\delta)}{(1-\delta)^2} = e^{-E/kt} \quad \text{Eq.24}$$

The activation energy E is approximately 0.14 eV. The factors which determine the distribution of the cations on A and B sites are ionic radius, electronic configuration, electrostatic energies and polarization effects.

6.3 Chemistry of ferrites (29)

Most of the ferrites of spinel structure decompose

when melted under normal conditions (in air or under 1 atm oxygen pressure). The oxygen splits off at higher temperatures reducing Fe^{II} to Fe^{III} following the reaction

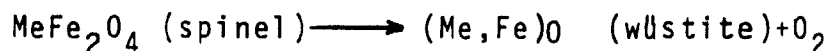


Figure 16 (29) shows the oxygen equilibrium pressures of the different iron oxides Fe_2O_3 (hematite), Fe_3O_4 (magnetite) and FeO (wüstite) as a function of temperature. Oxygen pressures are given in terms of the logarithmic ratio $P_{\text{CO}_2}/P_{\text{CO}}$ which corresponds to the oxygen partial pressure according to $P_{\text{O}_2} = K(P_{\text{CO}_2}/P_{\text{CO}})^2$.

The dissociation temperature of hematite decreases in the presence of spinels as the Fe_2O_3 dissolves into MeFe_2O_4 under formation of Fe^{II} ions and cation vacancies. This property of Fe_2O_3 is very important since it implies that ferrites cannot be processed to desired shapes by melting, as happens with metals. The technology of ferrites consequently is a ceramic technology. The starting materials, mostly oxides or compounds easily convertible to oxides by thermal decomposition, are mixed and converted into the desired products by solid-state reactions at higher temperatures between 800 and 1500°C. Then the products are pressed to desired shapes by a sintering process at this high temperature. The following reaction is taking place

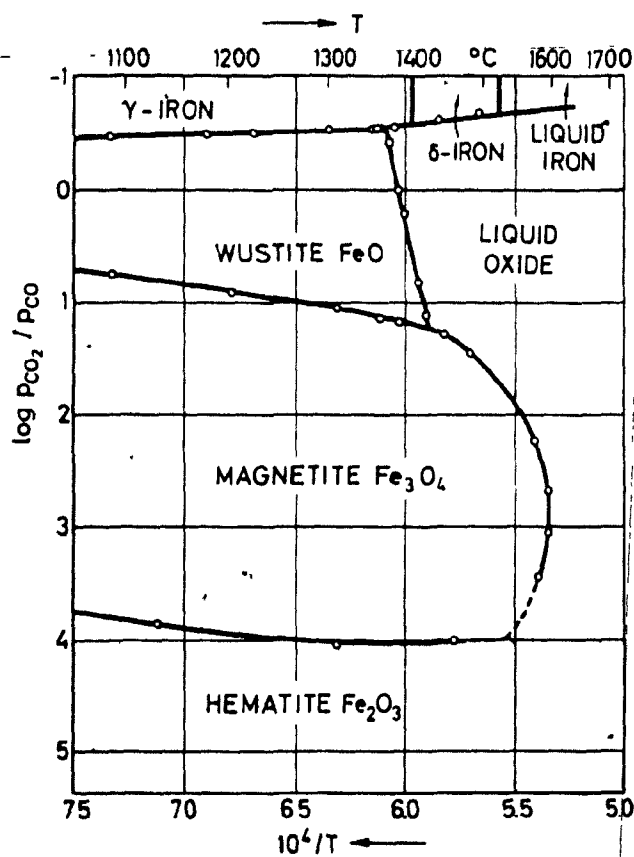


Figure 16. Oxygen equilibrium pressures of different iron oxides as a function of temperature. Oxygen pressure in terms of $\log P_{CO_2} / P_{CO}$ for hematite Fe_2O_3 , magnetite Fe_3O_4 , and wüstite FeO . (29).



The mechanism of this reaction has been studied by Wagner (31) who suggested that the spinel phase $\text{Me}^{\text{II}}\text{Me}_2^{\text{III}}\text{O}_4$ is formed at the interface of $\text{Me}^{\text{II}}\text{O}$ and $\text{Me}_2^{\text{III}}\text{O}_3$. The reaction proceeds by counterdiffusion of the metal cations Me^{II} and Me^{III} in the ratio of 3:2 through a lattice of oxygen anions. The speed of the formation is determined by the speed of the slowest diffusing ion. So far, few diffusion measurements have been performed.

Diffusion through solids is possible only by ion displacement. The reactants are dissolved into the reaction layer and produce vacancies and point defects enhancing the diffusion. According to Zener (32) the diffusion coefficient D is given by

$$D = D_0 e^{-\Delta U/RT} \quad \text{Eq. 25}$$

where $\Delta U = \Delta H_f + \Delta H_m$. Eq. 26

This means that the activation energy ΔU is the sum of the enthalpies to form (ΔH_f) and move (ΔH_m) a defect.

5.4 Magnetic properties

Table 5 summarizes the magnetic properties taken from reference 28.

Table 5. The saturation magnetization M_s together with the Curie points T_c of some simple ferrites with spinel structure (28)

Ferrite	0°C		20°C		T_c °C
	$\frac{\mu_0 M_s}{\rho}$ Am ² /kg	$\mu_0 M_s$ A/m	$\frac{\mu_0 M_s}{\rho}$ Am ² /kg	$\mu_0 M_s$ A/m	
MnFe ₂ O ₄	112.10 ⁻⁶	0.70	80.10 ⁻⁶	0.50	300
Fe ₃ O ₄	98.10 ⁻⁶	0.64	92.10 ⁻⁶	0.60	585
CoFe ₂ O ₄	90.10 ⁻⁶	0.60	80.10 ⁻⁶	0.53	520
NiFe ₂ O ₄	56.10 ⁻⁶	0.38	50.10 ⁻⁶	0.34	585
CuFe ₂ O ₄	30.10 ⁻⁶	0.20	25.10 ⁻⁶	0.17	455
MgFe ₂ O ₄	31.10 ⁻⁶	0.18	27.10 ⁻⁶	0.15	440
Li _{0.5} Fe _{2.5} O ₄	69.10 ⁻⁶	0.42	65.10 ⁻⁶	0.39	670

ρ is the density (kg/m³).

7. ROASTING OF CHALCOPYRITE IN A MUFFLE FURNACE

7.1 Roasting of chalcopryrite in a muffle furnace for 6 hours

7.1.1 Experimental procedure

For this set of experiments chalcopryrite samples from Rouyn Dist, Québec, with ~ 10% wt. impurities such as silica and pyrite, was ground (-37 μ m) and heated to different temperatures. Heating was in a Lindberg furnace with automatic control of the temperature. The sample (5g) was put in a tray and then into the furnace. The furnace was turned on and zero time was taken when the desired temperature was obtained. All heatings were for 6 hours to reach equilibrium. Every hour during heating, the sample was taken out of the furnace and was ground to -37 μ m in a mortar and pestle to increase the homogeneity of the mixture and reduce agglomeration.

The calcine after air cooling was examined by means of x-ray diffraction. In each case the conditions were: 40 kV, 20 mA, 6 hrs of exposure with a Fe tube and Mn filter. Intensities of the lines were estimated by eye. Six experiments

were carried out at the temperatures of 300, 320, 450, 500, 550 and 685°C to ascertain when copper ferrite is formed and to what extent.

The amount of the strongly magnetic material can be measured using the Davis tube which produces a relatively weak magnetic field (e.g. hematite cannot be trapped). A description of this device is given in Appendix B. Water flow rate was 0.6 cm/s in the Davis tube for all experiments.

7.1.2 Results

The full x-ray diffraction results are given in Appendix C. A summary of the results is given in table 6. The sample consisted of CuFeS_2 , FeS and Cu_2S . Reaction starts at 320°C with the formation of CuSO_4 and hematite. Copper ferrite was formed at the temperatures above 500°C. The amount of magnetic material caught in the Davis tube in these cases was very small (less than 10% wt.).

7.1.3 Thermodynamic analysis of the results

The above results were checked against those thermodynamically predicted by F.A.C.T. System (section 5.3.). The predicted results are in good agreement as shown in table 7.

Table 6. Summary of x-ray diffraction results

Temperature	Products
-	CuFeS ₂ , FeS, Cu ₂ S
300°C	CuFeS ₂ , FeS, Cu ₂ S
320	CuFeS ₂ , CuSO ₄ , α-Fe ₂ O ₃
450	CuSO ₄ , α-Fe ₂ O ₃
500	CuSO ₄ , α-Fe ₂ O ₃ , CuFe ₂ O ₄
550	Fe ₂ (SO ₄) ₃ , α-Fe ₂ O ₃ , CuFe ₂ O ₄
685.	α-Fe ₂ O ₃ , CuFe ₂ O ₄

Table 7. Comparison of products predicted by F.A.C.T. and obtained by x-ray diffraction

Temperature	F.A.C.T.*	x-ray diffraction
685°C	CuFe ₂ O ₄ , Fe ₂ O ₃ , CuSO ₄	CuFe ₂ O ₄ , Fe ₂ O ₃
550	Fe ₂ O ₃ , CuSO ₄	CuFe ₂ O ₄ , Fe ₂ O ₃ , Fe ₂ (SO ₄) ₃
500	Fe ₂ O ₃ , CuSO ₄	CuFe ₂ O ₄ , Fe ₂ O ₃ , CuSO ₄
450	Fe ₂ O ₃ , CuSO ₄	Fe ₂ O ₃ , CuSO ₄

* Assuming only CuFeS₂ as feed.

7.2 Roasting of chalcopyrite in a muffle furnace for short time periods

Six hours was felt to be sufficient to reach equilibrium. Ferrite formation was not favoured. Consequently tests were done with much shorter times. For this set of experiments samples of synthetic mixture of chalcopyrite and galena, and of material from Brunswick Mining and Smelting Co. (BMS), were roasted in the muffle furnace for short time periods not exceeding 10 minutes. The temperature of 320°C was selected from table 6 (section 7.1.2) as the temperature where some reaction takes place, and from table 3 (section 5.1).

Experimental work was done on mixtures of chalcopyrite and galena and not on chalcopyrite only, because the ignition temperature of galena is very high (table 3, paragraph 5.1) and does not affect the results. The samples tested were:

- A synthetic mixture consisting of 60% of chalcopyrite (same as before) and 40% wt. of galena (-37µm) with 8% wt. SiO₂. The synthetic mixture was used in the beginning in order to avoid any liberation problems which might interfere in the separation process.

- C
- The B.M.S. sample was a 3rd cleaner tail from the Cu-Pb separation circuit. Major phases of this sample were chalcopyrite, galena, pyrite and silica. The particle size of the sample was $-37\mu\text{m}$. The degree of liberation of chalcopyrite was found to be 88% and that of galena 55% (see Appendix D).

7.2.1 Roasting of the synthetic mixture

7.2.1.1 Experimental procedure

The synthetic mixture was roasted at 320°C in a muffle furnace. The hearth of the furnace was open so that air freely circulated the space above the sample. Five grammes of sample were put into the furnace. Then the furnace was turned on to reach the temperature of 320°C. As soon as it reached the desired temperature, it was left for 10 minutes. After air cooling the -37+15µm fraction was collected by microsieving and the magnetic profile was measured on the Frantz Isodynamic Magnetic Separator (see description in Appendix E).

7.2.1.2 Results

The magnetic profile of the unroasted material is shown in figure 17 and that after roasting is shown in figure 18.

In table 8 the results of the separation of the roasted synthetic mixture at 250 mA are presented. Lead is concentrated in the non-mags along with a very small amount of copper and

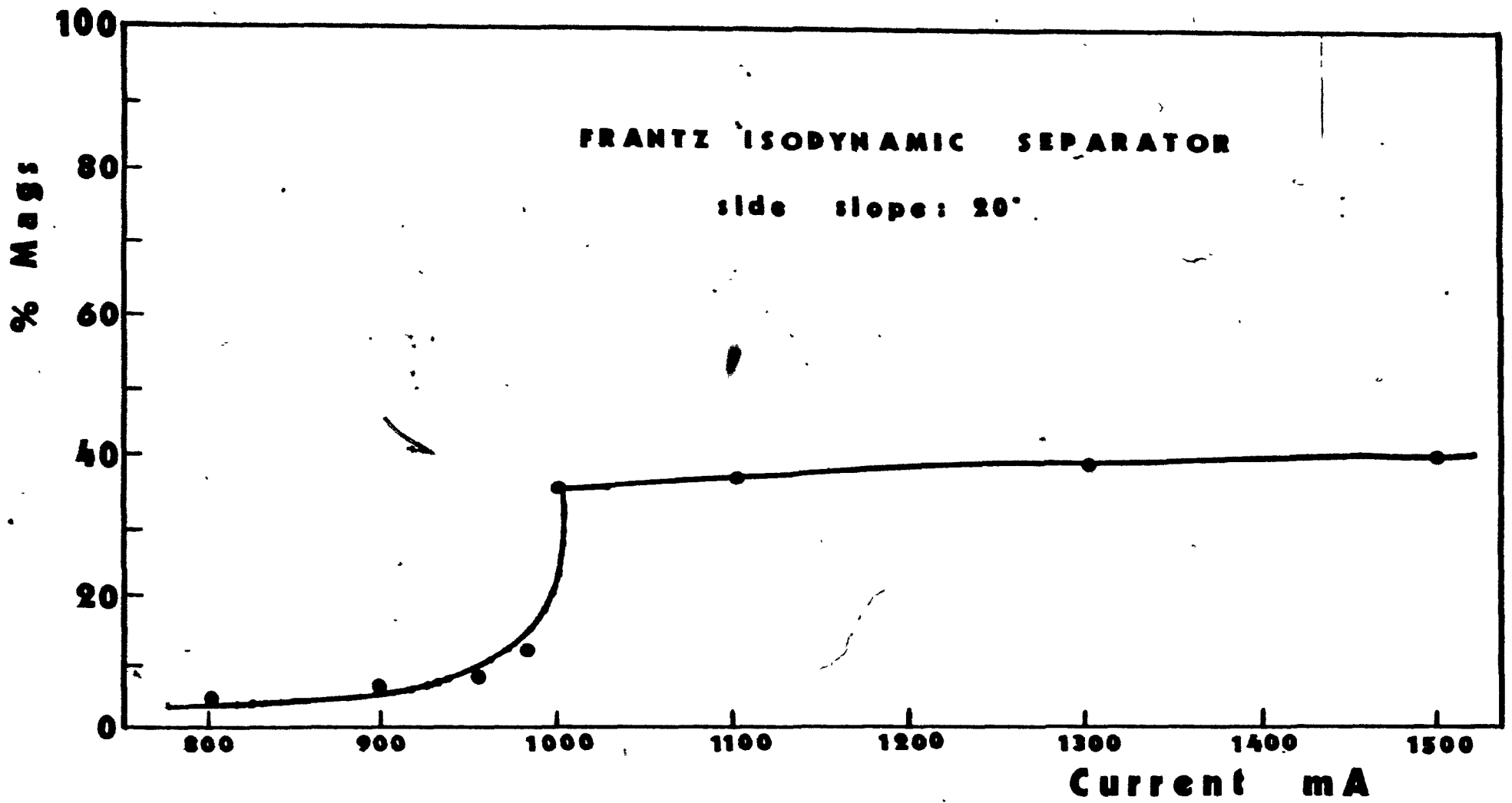


Figure 17. Magnetic profile of the synthetic mixture. Size $-37+15\mu\text{m}$.

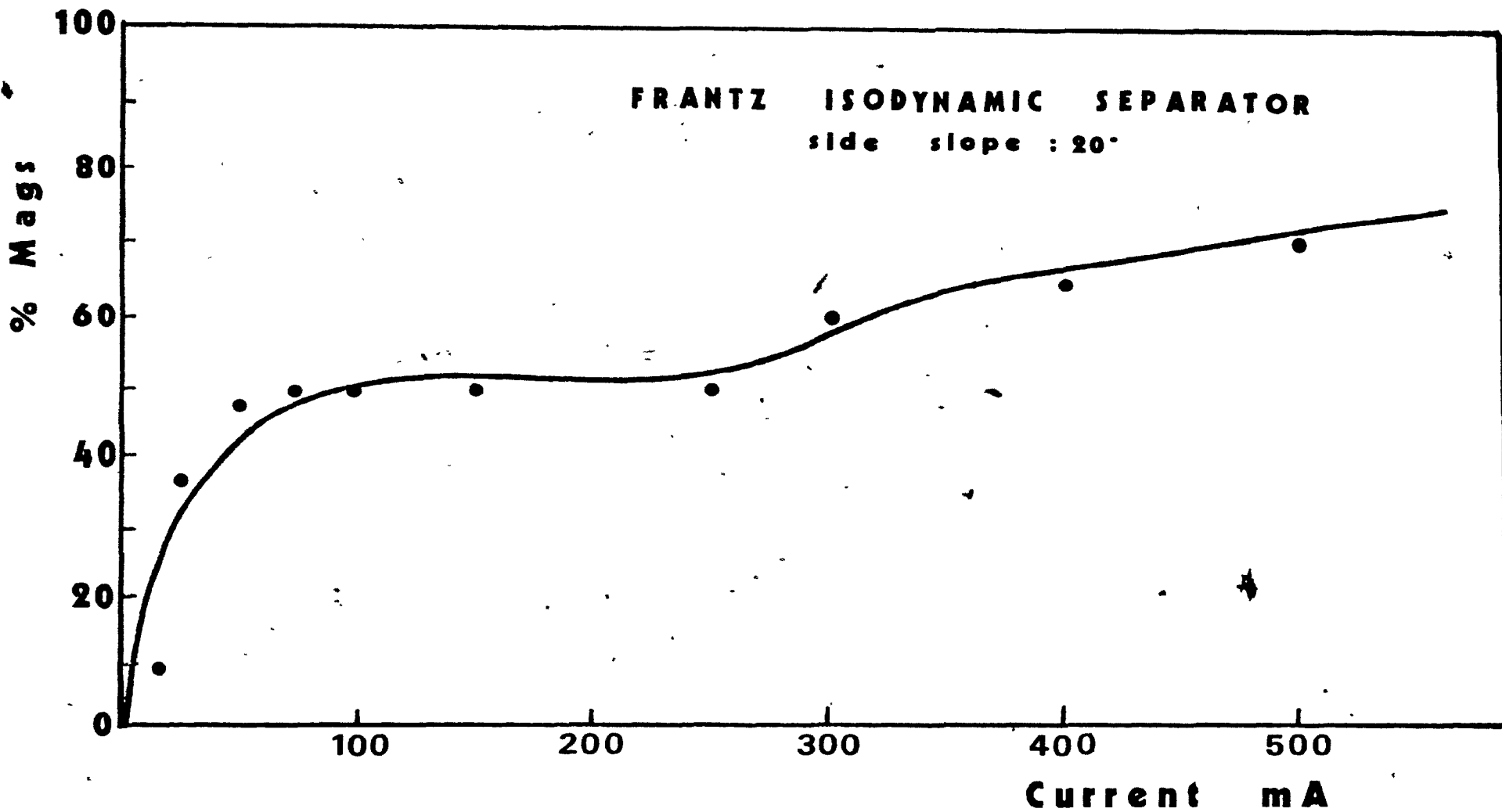


Figure 18. Magnetic profile of the synthetic mixture after roasting at 320°C, by slow heating for 10 min. Size -37+15µm.

iron. Only 74% of the lead is recovered in the non-mags, the rest of it being trapped in the mags.

Table 8. Separation of synthetic mixture at 250 mA

Size (μm)	I (mA)	Product	Wt. %	Assay (%)			Distribution (%)		
				Cu	Pb	Fe	Cu	Pb	Fe
-37+15	250	Mag	43.6	22.5	35	40	93	26	95
		Non-mag	56.4	1.2	75	1.6	7	74	5
			100.0				100.0	100.0	100.0
		Calculated feed		10.5	57.6	18.3			
		Assayed feed		11	55	16			

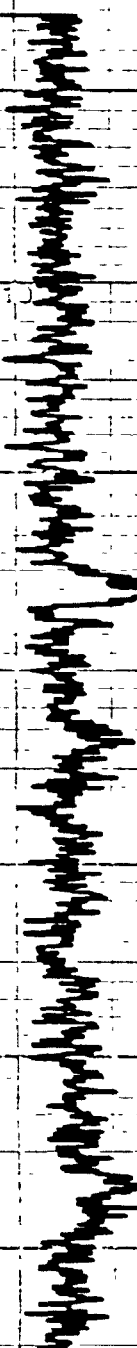
7.2.1.3 Identification of the roasted product

The product of the roasting was identified by means of x-ray diffraction, microscope examination, and electron microprobe examination.

Figure 19 shows the x-ray diffraction pattern of the roasted product with the phases identified. Copper ferrite and hematite were formed. However, galena was also oxidized which was not expected at this low temperature, giving Pb_2O_3 and PbSO_4 .

14

FIGURE 19. X-ray diffraction pattern of the synthetic mixture after roasting at 320°C for 10 min. by slow heating.



$\alpha\text{-Fe}_2\text{O}_3$

$\text{CuO} \cdot \text{Fe}_2\text{O}_3$

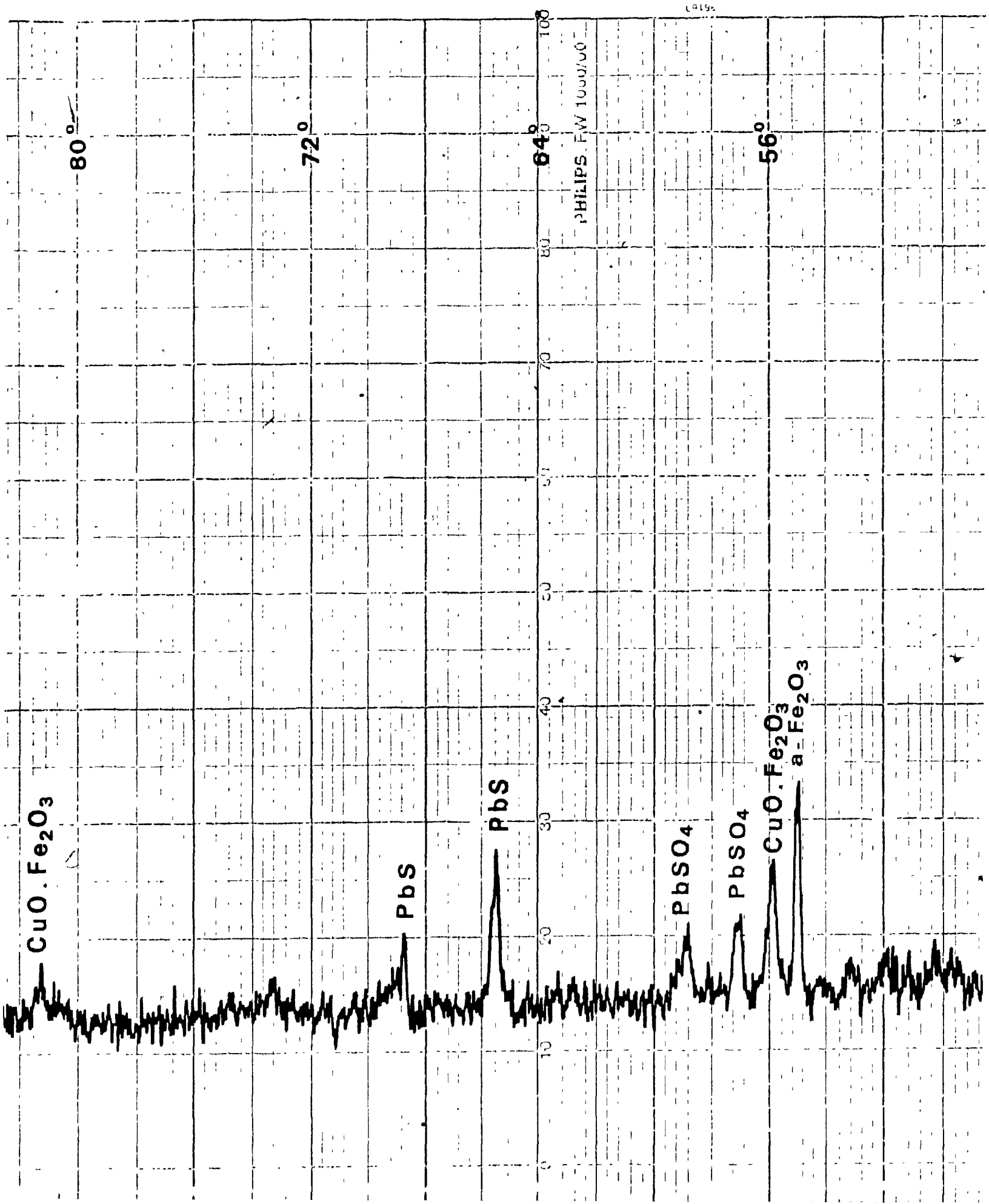
104°

96°

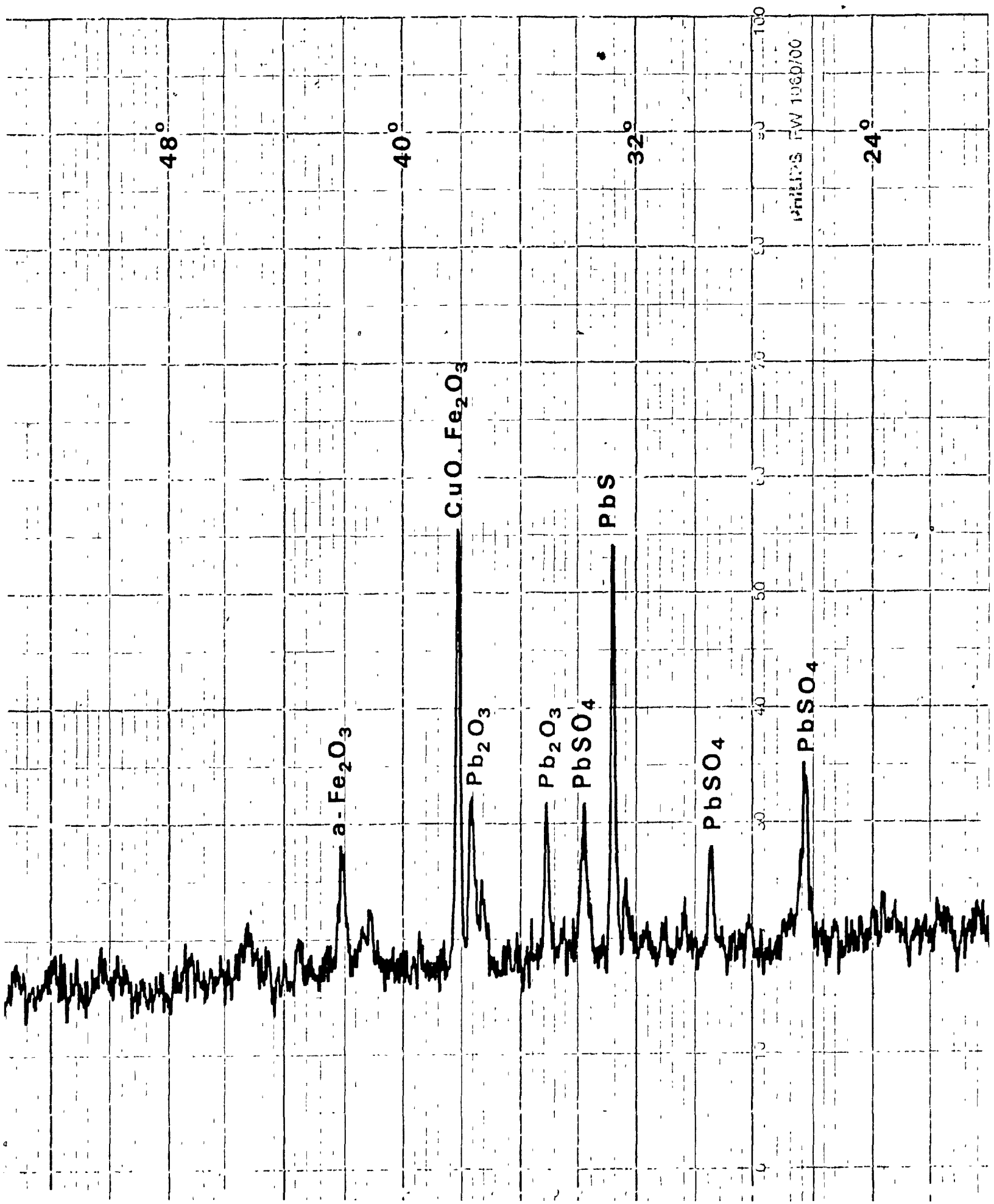
88°

80°

FIGURE 19. X-ray diffraction pattern of the synthetic mixture after roasting at 320°C for 10 min. by slow heating.



3 of 3



48°

40°

32°

24°

a-Fe₂O₃

CuO.Fe₂O₃

Pb₂O₃

Pb₂O₃

PbSO₄

PbS

PbSO₄

PbSO₄

100
50
0
0 10 20 30 40 50 60 70 80 90 100

PHILIPS FW 1060/00

For microscope examination a Carl-Zeiss microscope with reflected light was used. Figures 20 and 21 show first the roasted synthetic mixture and second the mags up to 15mA under polarized conditions.

In electron microprobe examination when the beam was scanned through oxidized chalcopyrite grains from the edge towards the center, showed a decrease of Fe concentration and an increase in S concentration. For a particular grain shown in figure 22 scanning from the edge towards the center gave Fe:Cu and S:Cu ratios of weight concentrations which are presented in figure 23 (see also Appendix F). Position no. 1 of beam corresponds to the edge of the grain and position no. 8 corresponds to the center of the grain. The distance between two consecutive positions of beam is approximately 2 μ m.



Figure 20. Microphotograph of $-37+15\mu\text{m}$ particles of the roasted synthetic mixture at 600 magnification with reflected light, under polarized conditions. C = chalcopyrite, P = pyrite, F = ferrite, H = hematite.



Figure 21. Microphotograph of $-37+15\mu\text{m}$ particles of the mags fraction up to 15mA on Frantz of the roasted synthetic mixture. Magnification of 600 with reflected light, under polarized conditions. F = ferrite, P = pyrite, H = hematite.



Figure 22. An oxidized particle of chalcopyrite on which microprobe examination was performed.

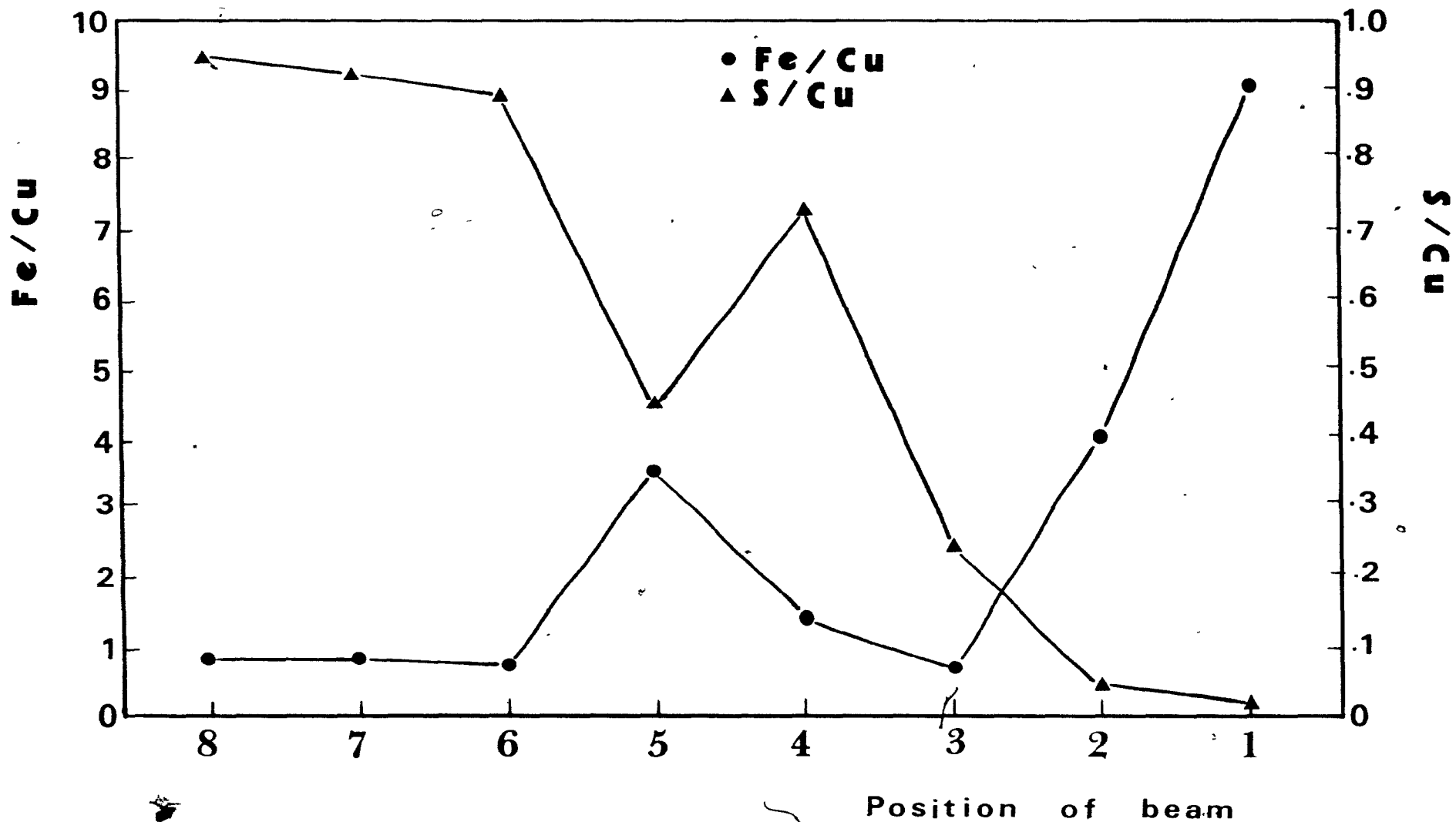


Figure 23. Fe:Cu and S:Cu ratios as beam scans from the edge (position 1) towards the center (position 8) of the particle shown in figure 22. Fe:Cu ratio for ferrite 1.76. Fe:Cu, S:Cu ratios for chalcopyrite 0.88 and 1.01 respectively.

7.2.2 Roasting of the B.M.S. sample

It was mentioned before (paragraph 7.2) that the degree of liberation of chalcopryrite for the B.M.S. sample was 88% and that of galena 55%.

Figure 24 shows a locked particle of chalcopryrite with galena (size $-37+25\mu\text{m}$) and figure 25 a particle of galena locked with chalcopryrite. (size $-25+15\mu\text{m}$) under polarized conditions. Figure 26 shows the magnetic profile of the B.M.S. sample.

Roasting of the sample was done under various conditions in order to study the effect of temperature, method of heating and retention time.

7.2.2.1 Effect of temperature

The sample was heated at the temperatures of 320 and 350^oC. It was slowly heated to the desired temperature and was held there for 10 min. Figures 27 and 28 show the magnetic profiles of the calcines. The most promising for separation is when the temperature was 320^oC.

7.2.2.2 Effect of method of heating

Since the slow heating is not practical industrially,



Figure 24. Microphotograph of a $-37+25\mu\text{m}$ locked particle of chalcopyrite with galena, of B.M.S. sample. Magnification 600, reflected light under polarized conditions. C = chalcopyrite, G = galena.

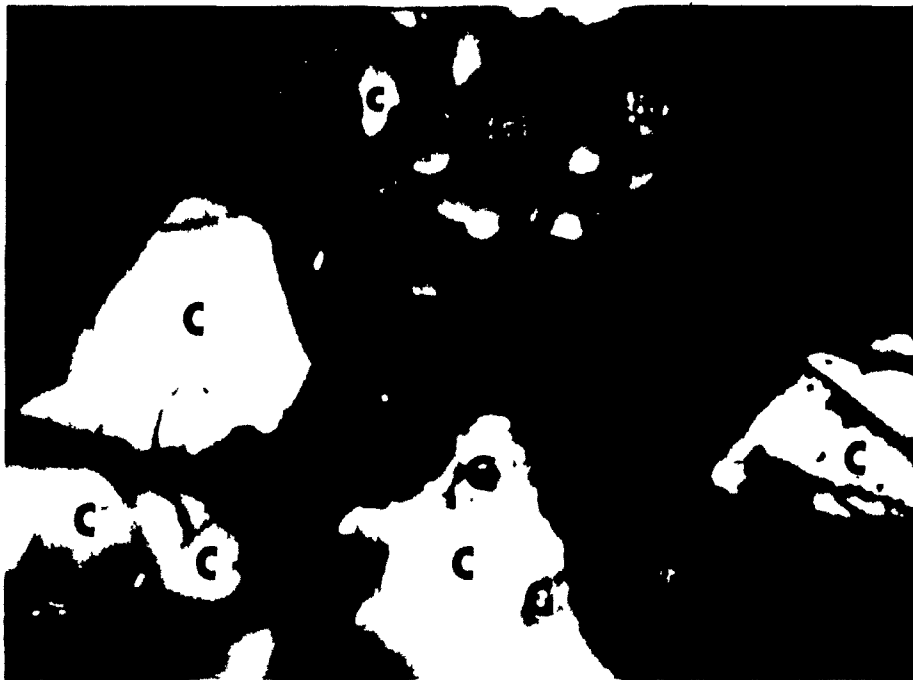


Figure 25. Microphotograph of a $-25+15\mu\text{m}$ locked particle of galena with chalcopyrite of B.M.S. sample. Magnification 600, reflected light under polarized conditions. C = chalcopyrite, G = galena.

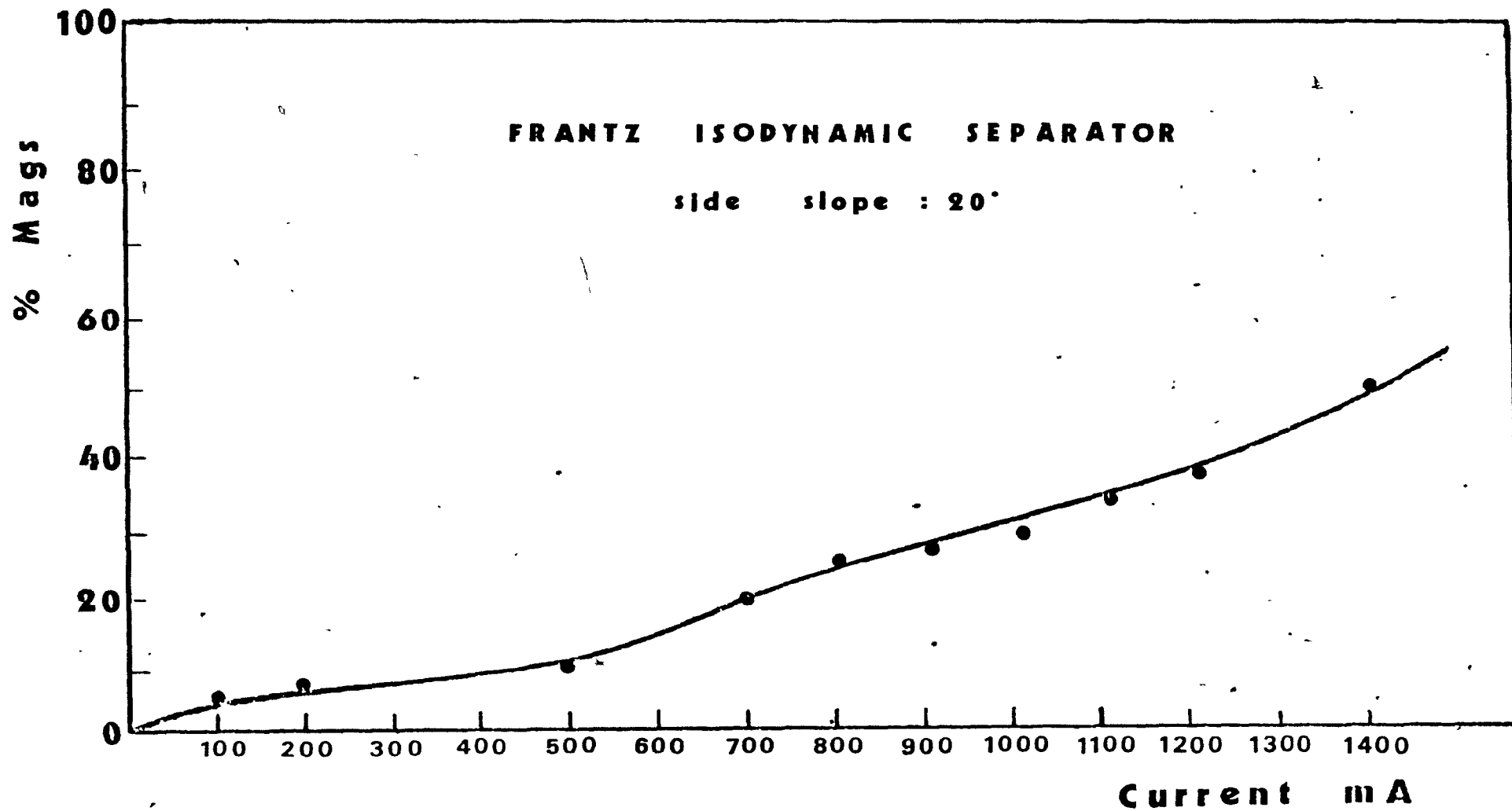


Figure 26. Magnetic profile of B.M.S. sample. Size -37+15 μ m.

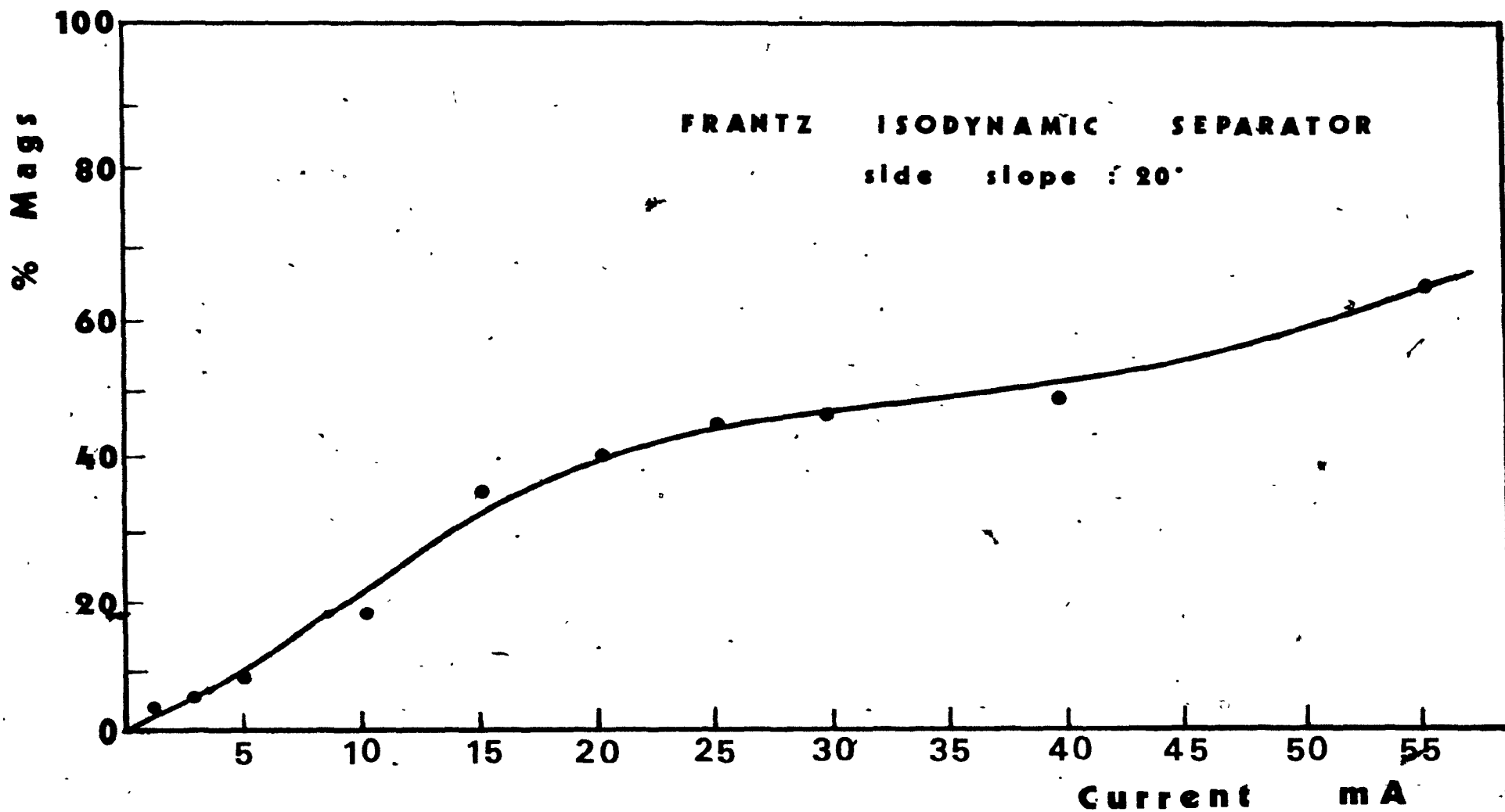


Figure 27. Magnetic profile of B.M.S. sample after roasting at 320°C, by slow heating for 10 min. Size -37+15 μ m.

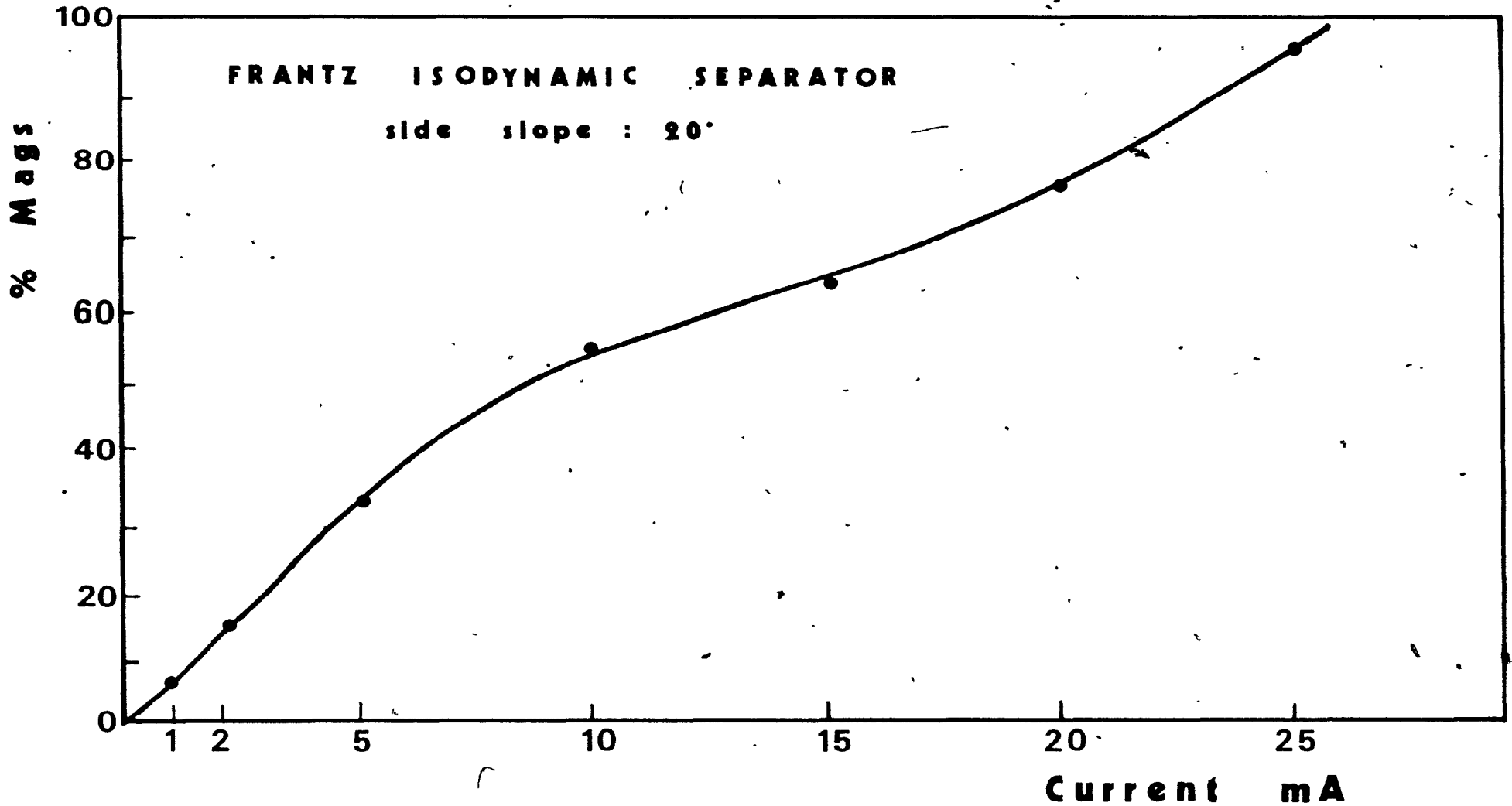


Figure 28. Magnetic profile of B.M.S. sample after roasting at 350°C, by slow heating for 10 min. Size -37+15 μ m.

two other methods of heating were examined. Direct heating when the sample is put into the furnace held at the desired temperature and also by preheating the sample at 150°C then putting it into the furnace held at the desired temperature.

Figure 29 shows the magnetic profile of the calcine after direct heating in 350°C for 10 minutes and figure 30 the magnetic profile after preheating at 150°C , then roasting at 350°C .

Figure 31 shows the magnetic profile of the calcine after direct heating in 320°C for 10 minutes and figure 32 the magnetic profile after preheating at 150°C , then roasting at 320°C .

7.2.2.3 Effect of retention time

Since the curve of slow heating at 320°C is the most promising for potential separation, it was decided to examine the effect of time by roasting with slow heating at 320°C for 5 minutes. The magnetic profile is shown in figure 33 and it seems that 5 minutes is not enough.

Table 9 gives the results of separation at 25mA of the roast at 320°C by slow heating for 10 minutes.

Table 10 gives the results of separation on the Davis tube of the calcine roasted under the same conditions as before. Water flow rate was kept constant at 0.6cm/s.

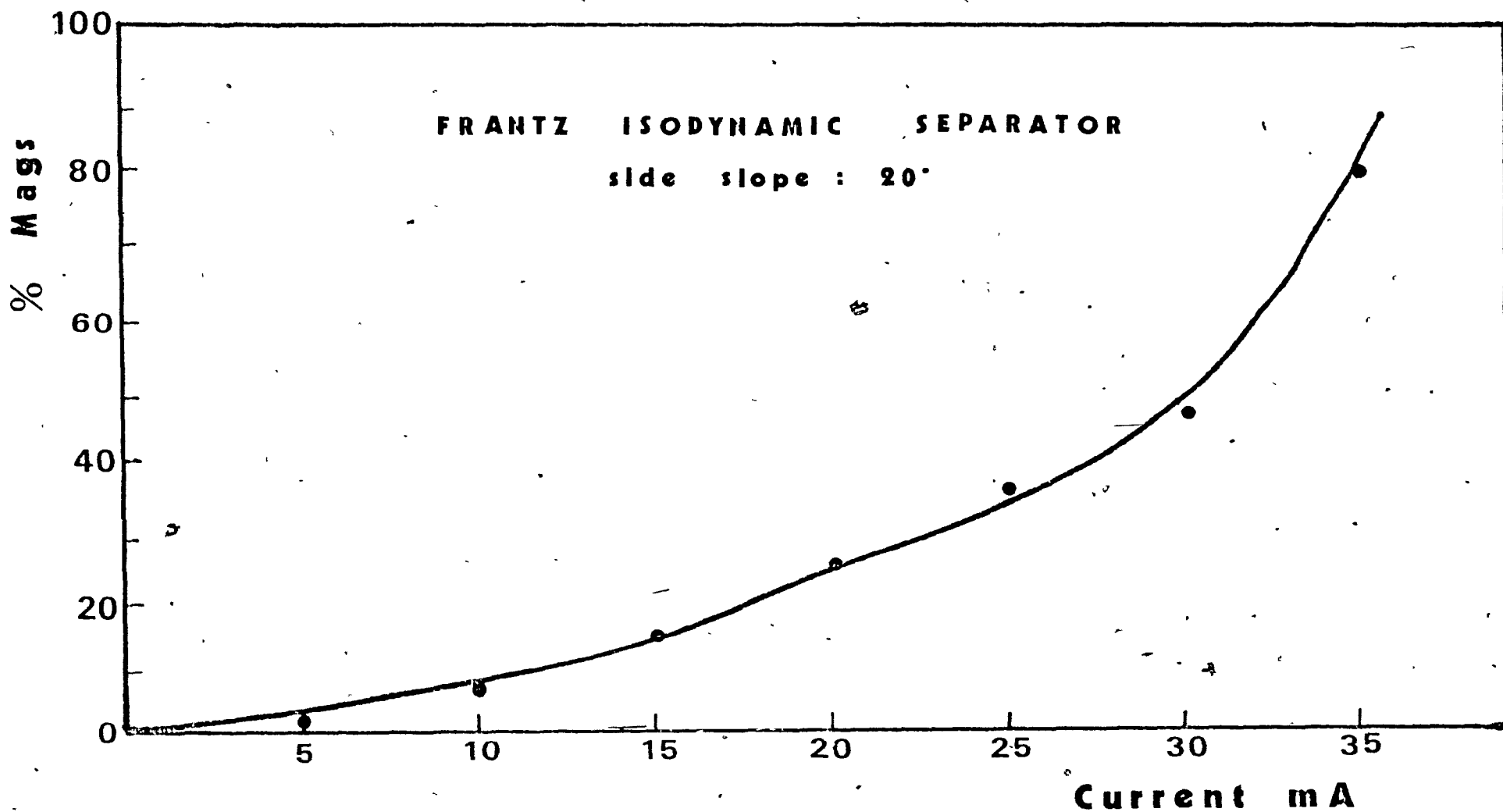


Figure 29. Magnetic profile of B.M.S. sample after roasting at 350°C, by direct heating for 10 min. Size -37+15 μ m.

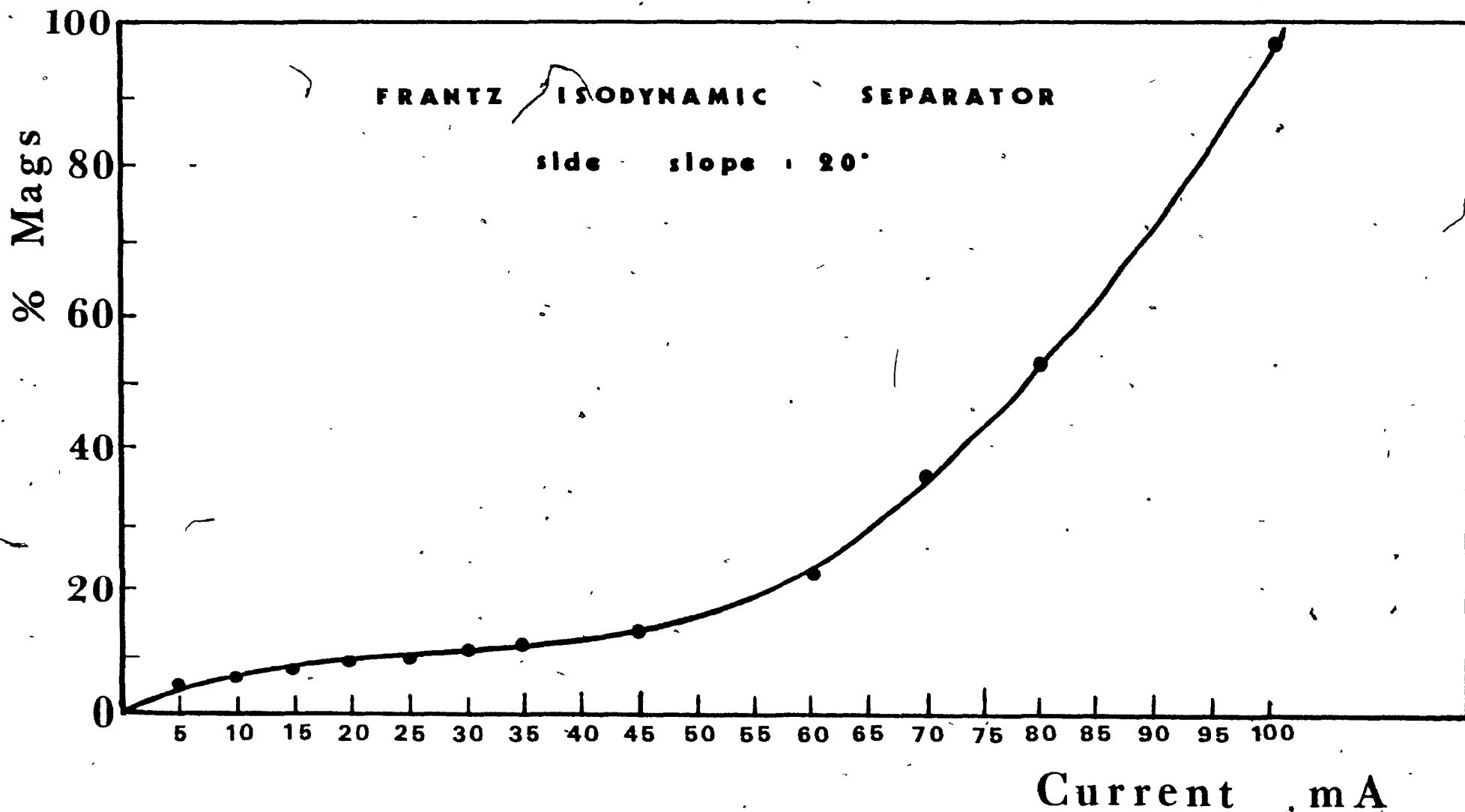


Figure 30. Magnetic profile of B.M.S. sample after preheating at 150°C, then roasting at 350°C for 10 min. Size -37+15 μ m.

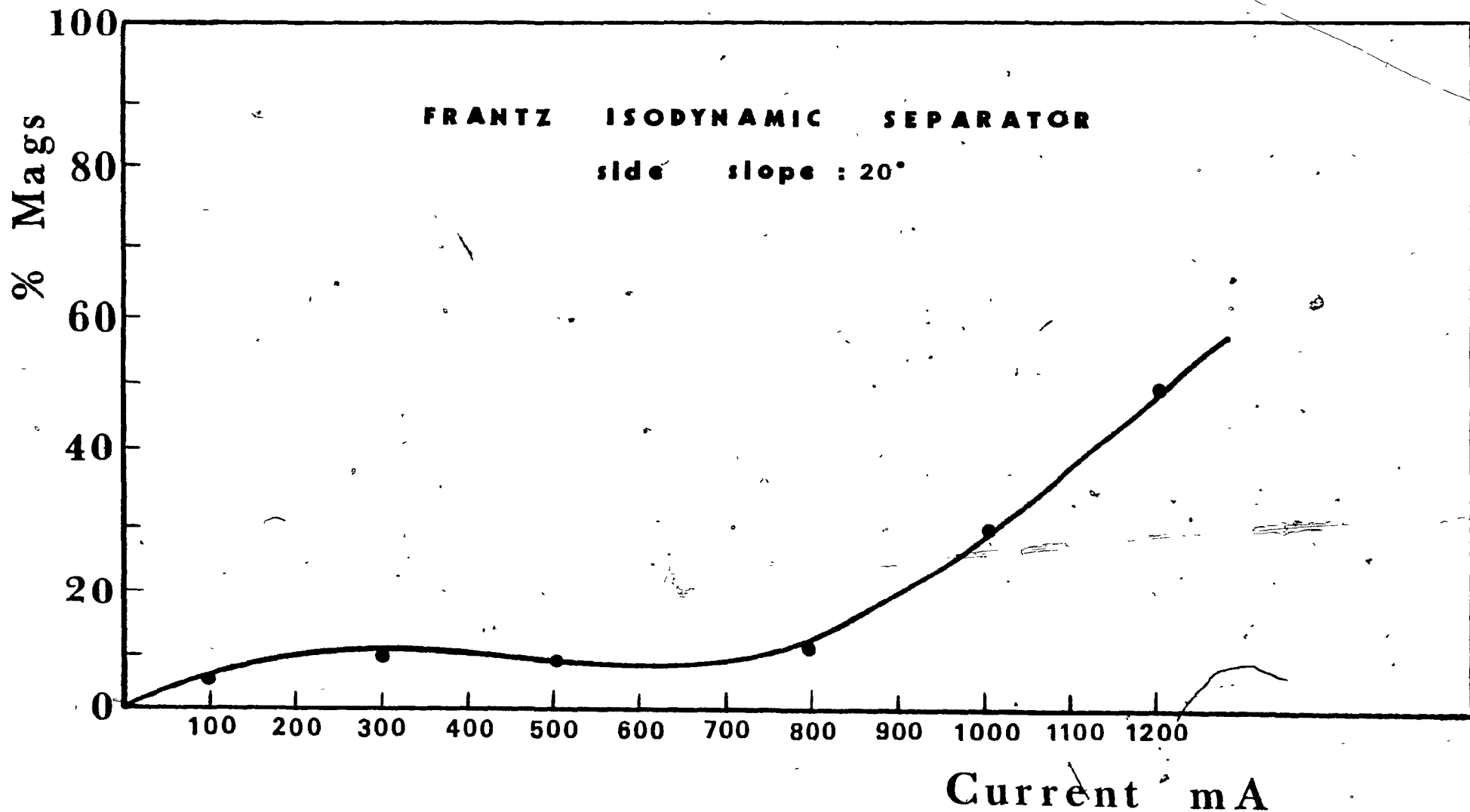


Figure 31. Magnetic profile of B.M.S. sample after roasting at 320°C, by direct heating for 10 min. Size -37+15 μ m.

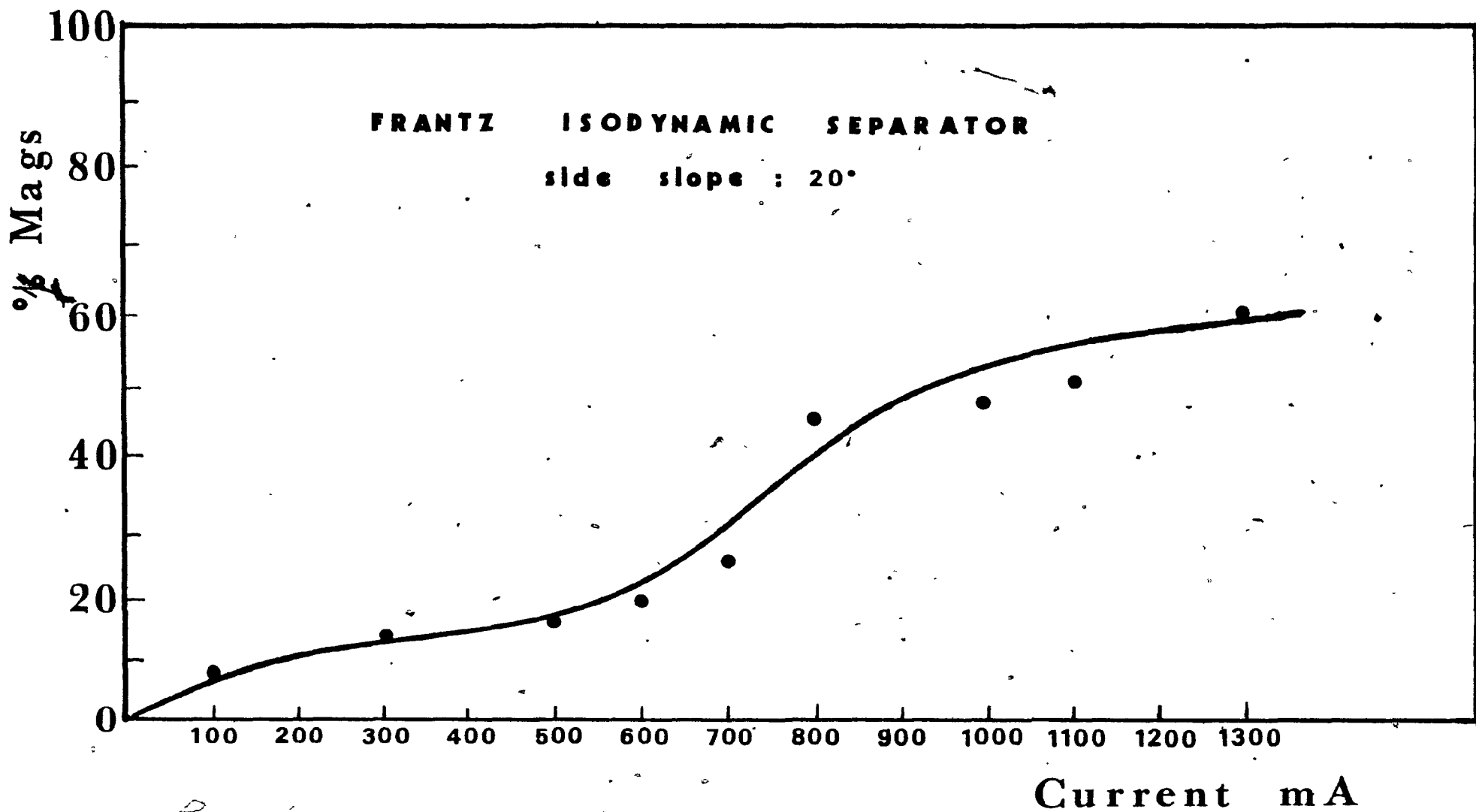


Figure 32. Magnetic profile of B.M.S. sample after preheating at 1500C, then roasting at 3200C for 10 min. Size -37+15µm.

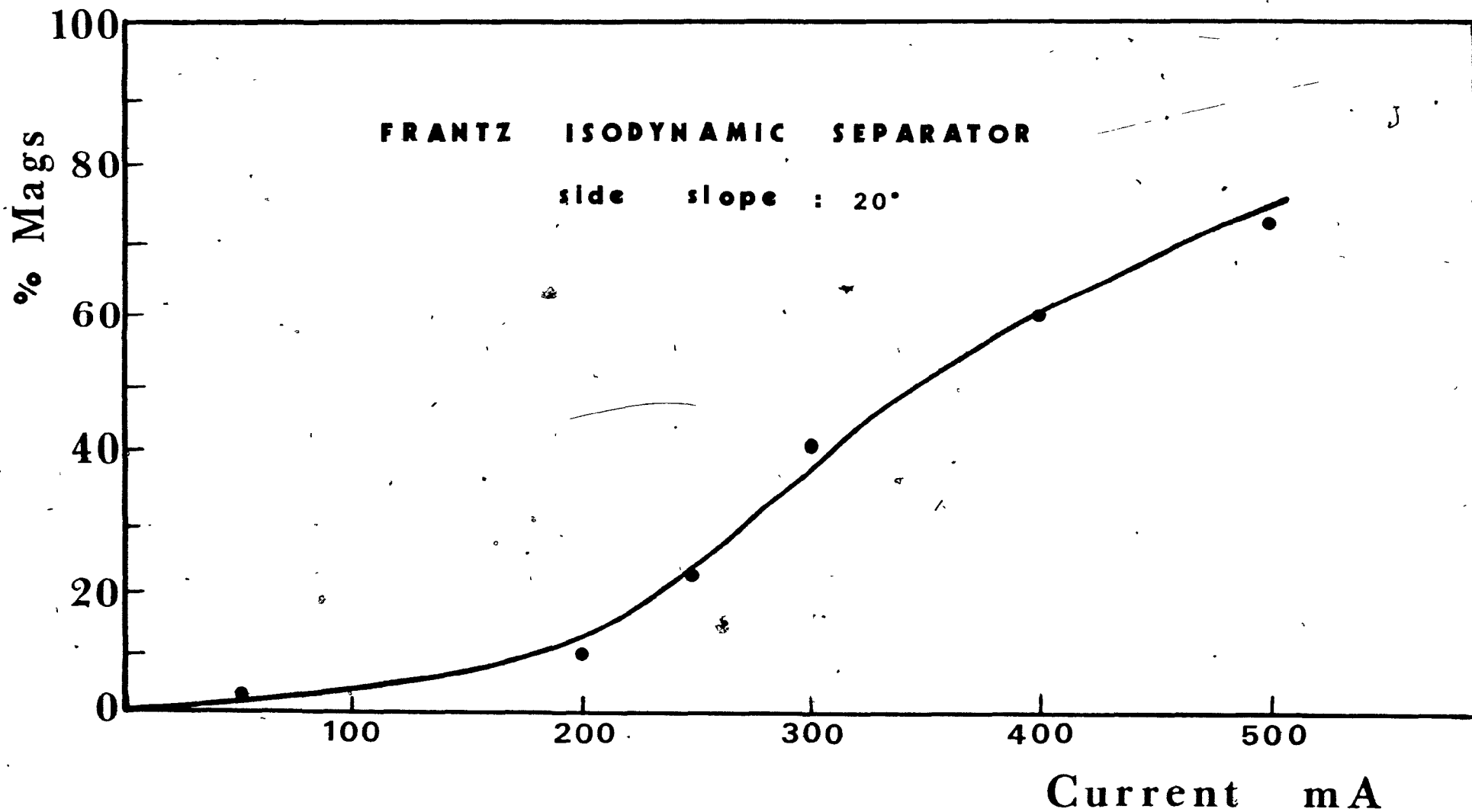


Figure 33. Magnetic profile of B.M.S. sample after roasting at 320°C, by slow heating for 5 min. Size -37+15 μ m.

Table 9. Separation of B.M.S. sample at 25mA

Size (μm)	I (mA)	Product	Wt (%)	Assay (%)			Distribution (%)		
				Cu	Pb	Fe	Cu	Pb	Fe
-37+15	25	Mags	34	15	6.5	16	42	24.6	35
		Non-mags	66	10.2	10.2	15	58	75.4	65
			100				100.0	100.0	100.0
		Calcul. feed		11.8	8.9	15.3			
		Assayed feed		13	8.8	18.7			

Table 10. Separation of B.M.S. sample on Davis tube

Size (μm)	Flow cm/s	Product	Wt (%)	Assay (%)			Distribution (%)		
				Cu	Pb	Fe	Cu	Pb	Fe
-37	0.6	Mags	14.8	9.5	7.5	36	11.5	8.7	19.4
		Non-Mags	85.2	12.8	13.7	26	88.5	91.3	80.6
			100.0				100.0	100.0	100.0
		Calcul. feed		12.3	12.5	27.4			
		Assayed feed		13.7	12.5	27.0			

Figure 34 shows the mags up to 10mA for the sample roasted by slow heating at 320°C for 10 minutes. Figure 35 shows a locked particle of chalcopyrite with galena which

reports to the mags on the Davis tube. The roasting was done under the same conditions as before. This figure shows clearly that the locking of the sample is a very serious problem and grinding is needed for further liberation.

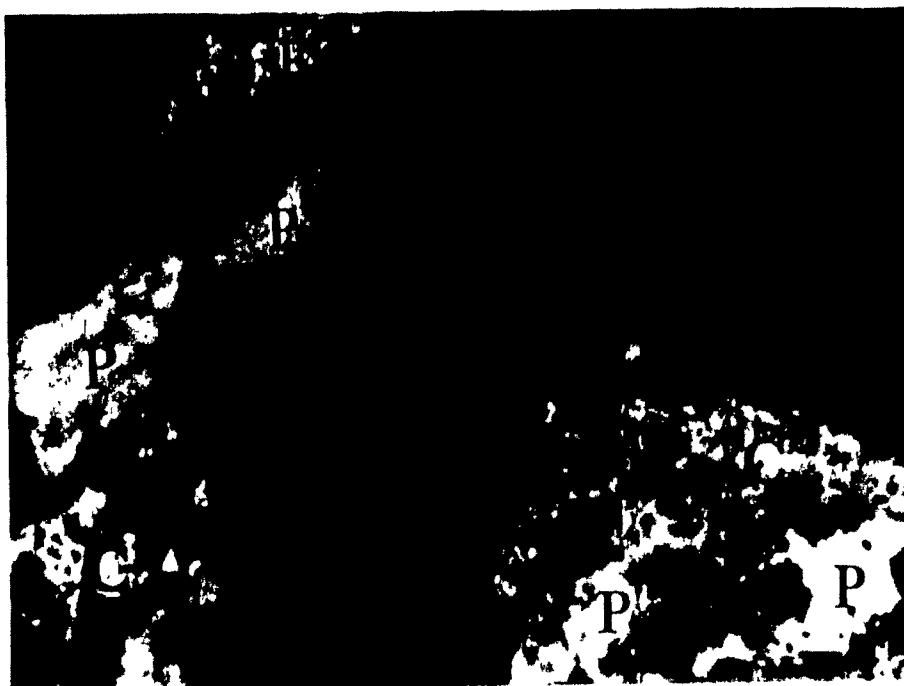


Figure 34. Microphotograph of $-37+15\mu\text{m}$ particles of the mags up to 10 mA on Frantz, of the roasted B.M.S. sample at 320°C , by slow heating for 10 min. Magnification 600, reflected light, under polarized conditions. C = chalcopryrite, P = pyrite, F = ferrite, H = hematite.

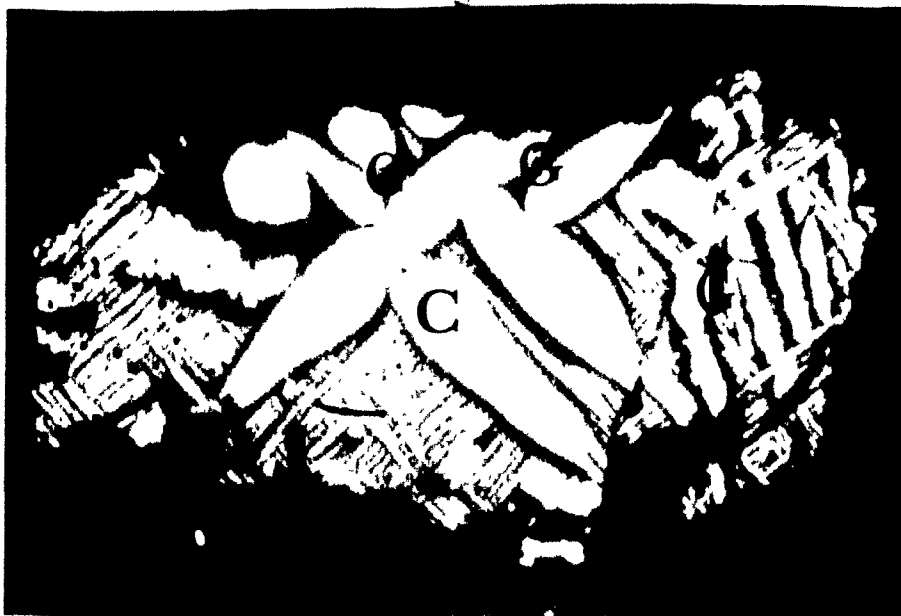


Figure 35. Microphotograph of a $-37+15\mu\text{m}$ particle of the mags on Davis tube, of the roasted B.M.S. sample at 320°C , by slow heating for 10 min. Magnification 600° , reflected light, under polarized conditions. C = chalcopryrite, G = Galena, F = ferrite.

8. ROASTING OF CHALCOPYRITE IN A TUBE FURNACE

For this set of experiments chalcopyrite powder (-37 μ m) from Rouyn Dist, Quebec, was roasted in a tube furnace. This kind of furnace was selected so that the roasting could be conducted under various controlled conditions, which more closely approximate industrial conditions.

8.1 Experimental procedure

The roasting took place in a Lindberg tube furnace. The tube was tilted at an angle of 20° so that the material could easily move through the tube assisted by a vibrator. Air or oxygen was introduced from the upper side and came out freely into the atmosphere. The tube was loaded from the upper end with 5g of material and the gas flow was turned on. By means of the vibrator the material moved into the tube and after roasting was collected from the lower end of the tube.

Three parameters were studied temperature which was automatically controlled, gas flow rate measured by a flow meter and retention time of the particles in the tube.

The roasted material after collection was ground for 1 min. with the mortar and the pestle and was then screened

through a 400 Mesh ($37\mu\text{m}$) sieve and the percentage of material over $37\mu\text{m}$ was recorded. This was an indication of the agglomeration which took place. All the material was then ground down to $-37\mu\text{m}$ and passed through the Davis tube concentrator to measure the amount of chalcopyrite converted to magnetic product (identification is discussed later). The flow rate of the washing water in the Davis tube was kept constant at 0.6 cm/s .

8.2 Results

8.2.1 Roasting with oxygen

Experiments were carried out at the temperatures of 320, 335, 350, 370, 385 and 400°C . The "agglomeration index" (material over $37\mu\text{m}$ after 1 min. grinding) and the percentage of chalcopyrite converted to magnetic product were measured and plotted against temperature. The other two parameters, retention time and oxygen flow rate were kept constant at 15 seconds and 0.35 lt/s respectively. Results are presented in figures 36 and 37.

The goal of this study was to minimize the agglomeration of the material but maintain conversion of chalcopyrite to magnetic product. Following these criteria the temperature

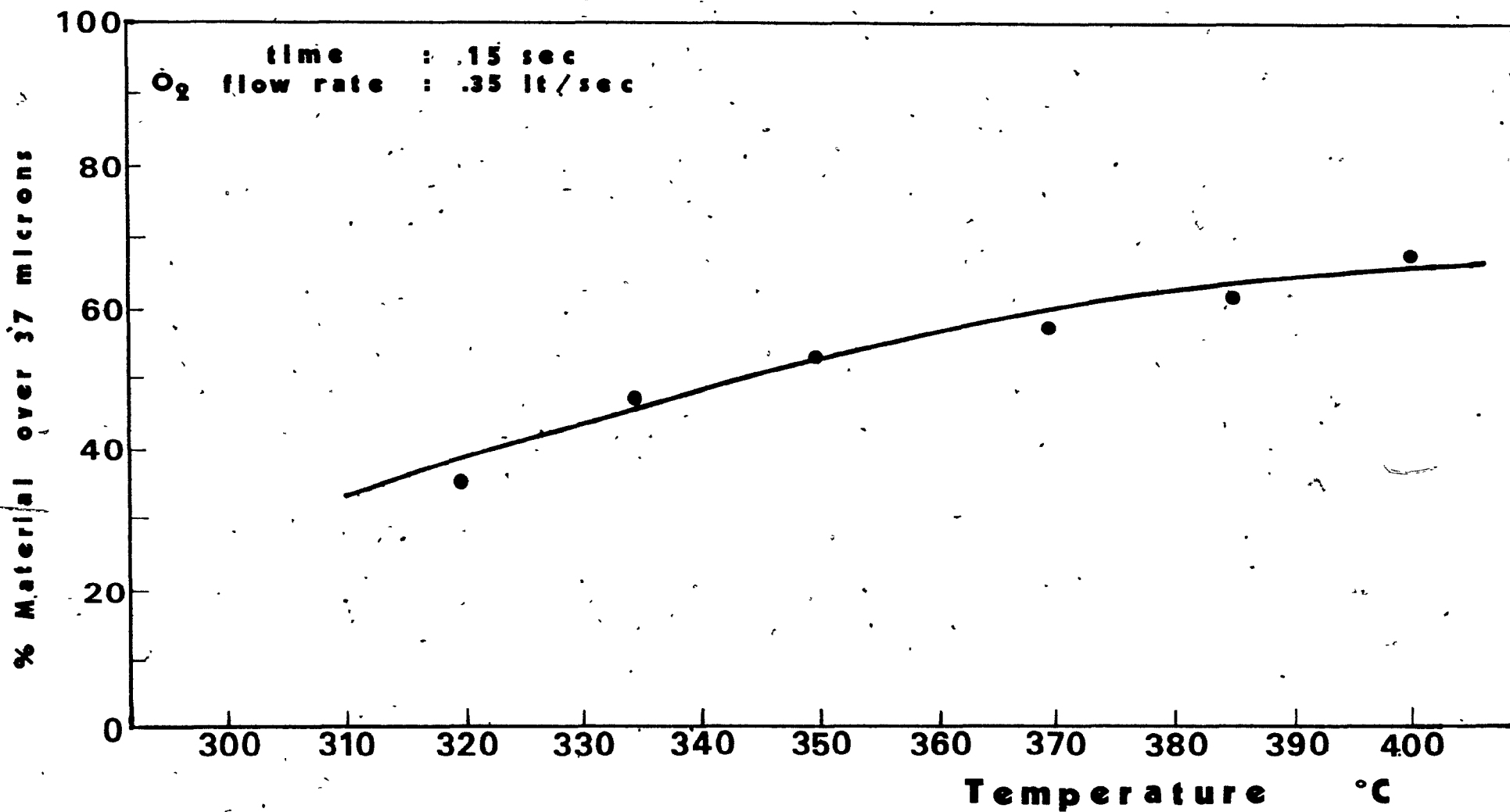


Figure 36. Roasting of CuFeS_2 in tube, furnace. The "agglomeration index" vs. temperature.

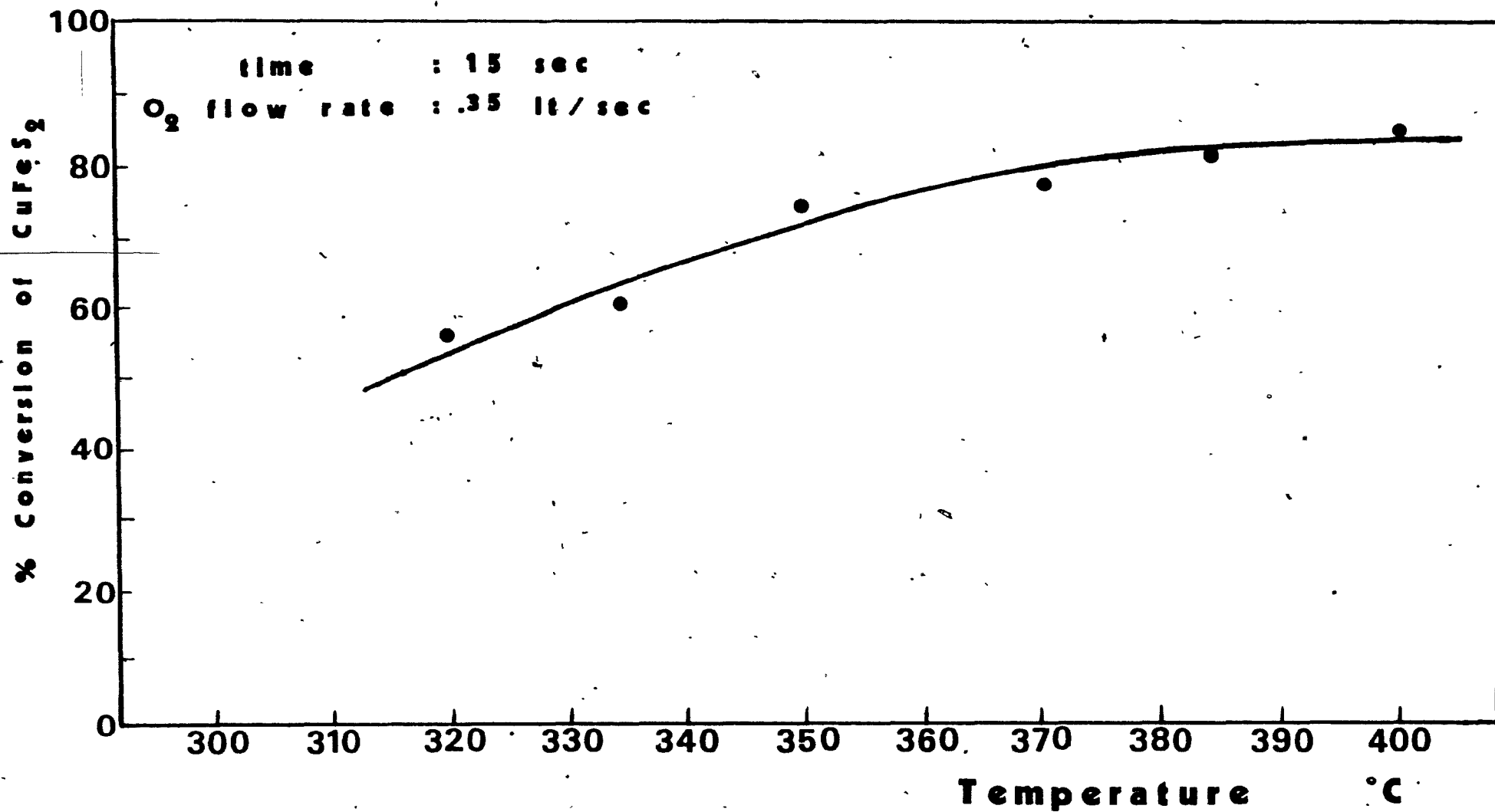


Figure 37. Roasting of CuFeS₂ in tube furnace. The conversion of CuFeS₂ vs. temperature.

of 320°C was selected for further experimentation in order to increase the percentage of chalcopyrite converted.

To study the effect of retention time, experiments with different retention times were carried out. The temperature was 320°C and oxygen flow rate 0.35 lt/s. Results are presented in figure 38. A time of 45s was selected as no further conversion appears to occur at longer times.

The effect of oxygen flow rate is presented in figure 39. The temperature was 320°C and the retention time 45 sec. Although there is not much difference between 0.30-0.35 lt/s, the best results were at 0.33 lt/s.

So far one could conclude that 75% of chalcopyrite is converted to magnetic product at the temperature of 320°C with a retention time of 45 seconds and an oxygen flow rate at 0.33 lt/s.

Oxygen is an expensive chemical product and probably the cost of this roasting would climb to unacceptable levels. So for the next set of experiments compressed air was used.

8.2.2 Roasting with air

The experiments were carried out the same way as

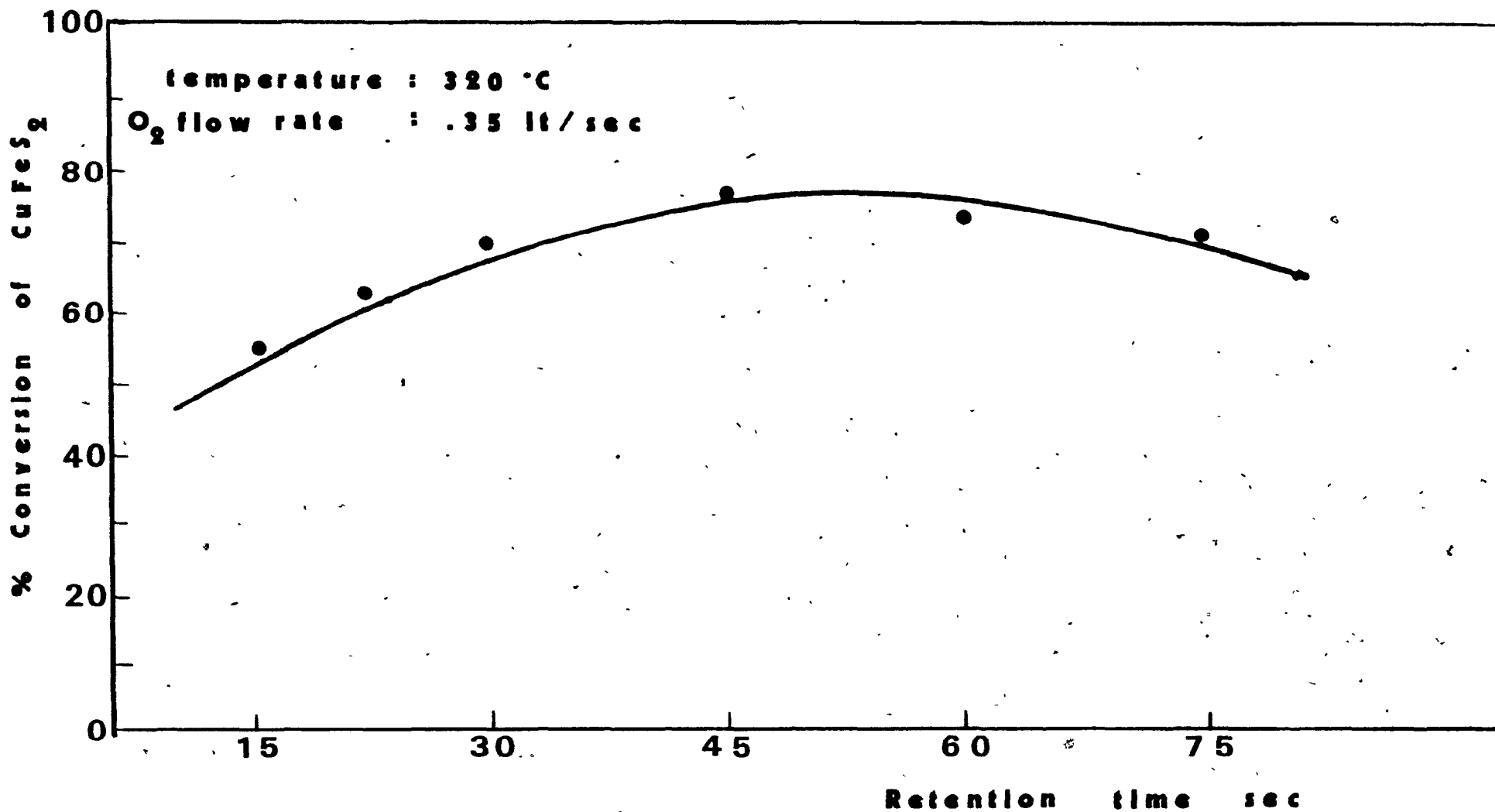


Figure 38. Roasting of CuFeS₂ in tube furnace. The conversion of CuFeS₂ vs. retention time.

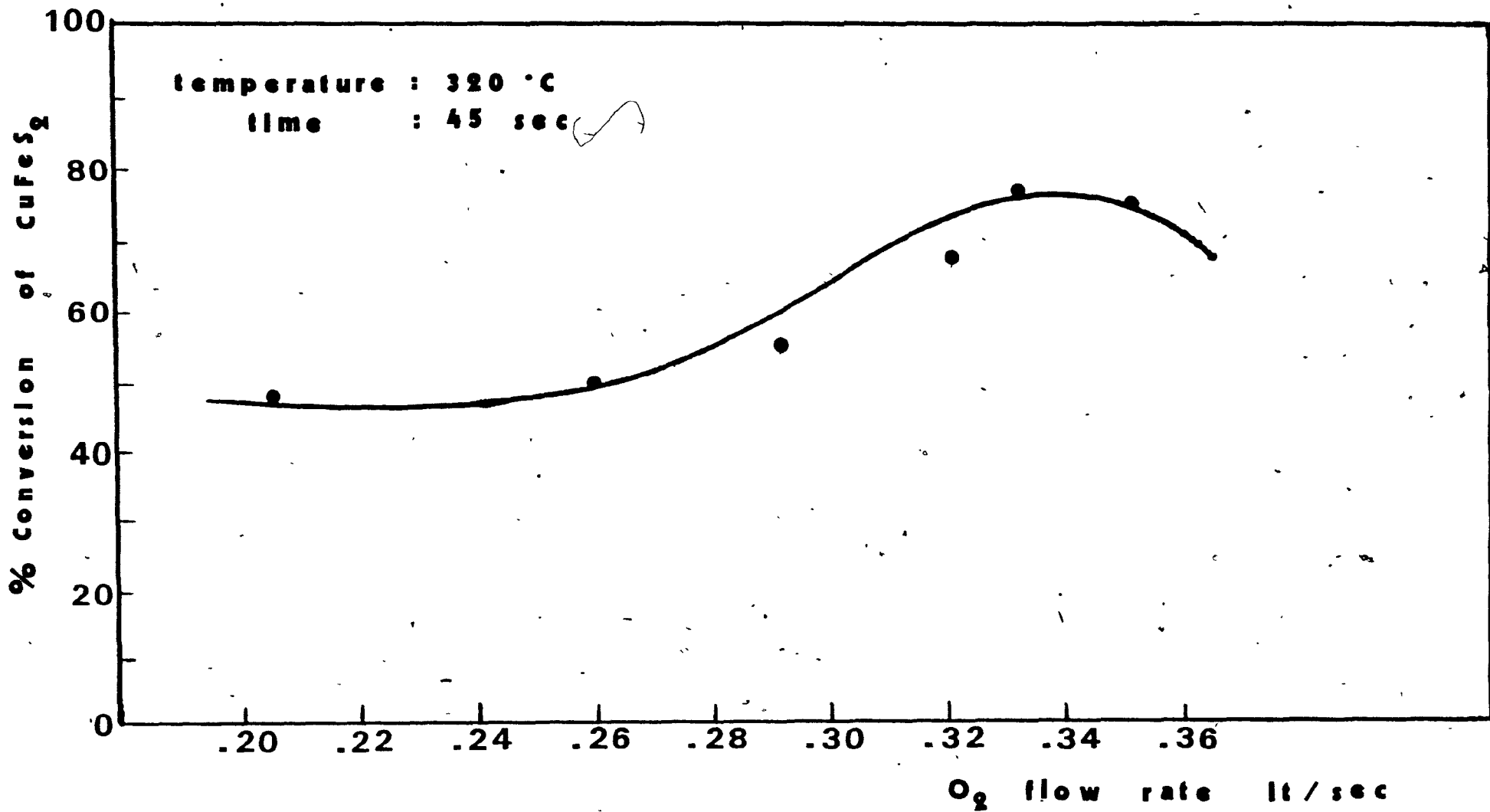


Figure 39. Roasting of CuFeS_2 in tube furnace. The conversion of CuFeS_2 vs. O_2 flow rate.

before but instead of oxygen compressed air was used.

Figure 40 presents the effect of temperature when the retention time is 45s and the air flow rate is 0.35 lt/s. A temperature of 700°C is needed for an acceptable conversion of 70%. However, the agglomeration effect almost disappeared.

Figure 41 presents the effect of retention time when temperature is 700°C and the air flow rate 0.35 lt/s. A conversion of 75% was achieved at 700°C with 30 seconds retention time and 0.35 lt/s air flow rate.

The oxidizing conditions are not as strong as before and chalcopyrite needs higher temperature to be converted to magnetic product.

8.3 Identification of the roasted products

The products of the roasting were identified by means of X-ray diffraction and microscope examination.

Figure 42 shows the X-ray diffraction pattern of the roasted chalcopyrite under the following conditions: temperature 320°C, retention time 45 sec. and oxygen flow rate 0.25 lt/s.

Mounted samples of roasted chalcopyrite were observed

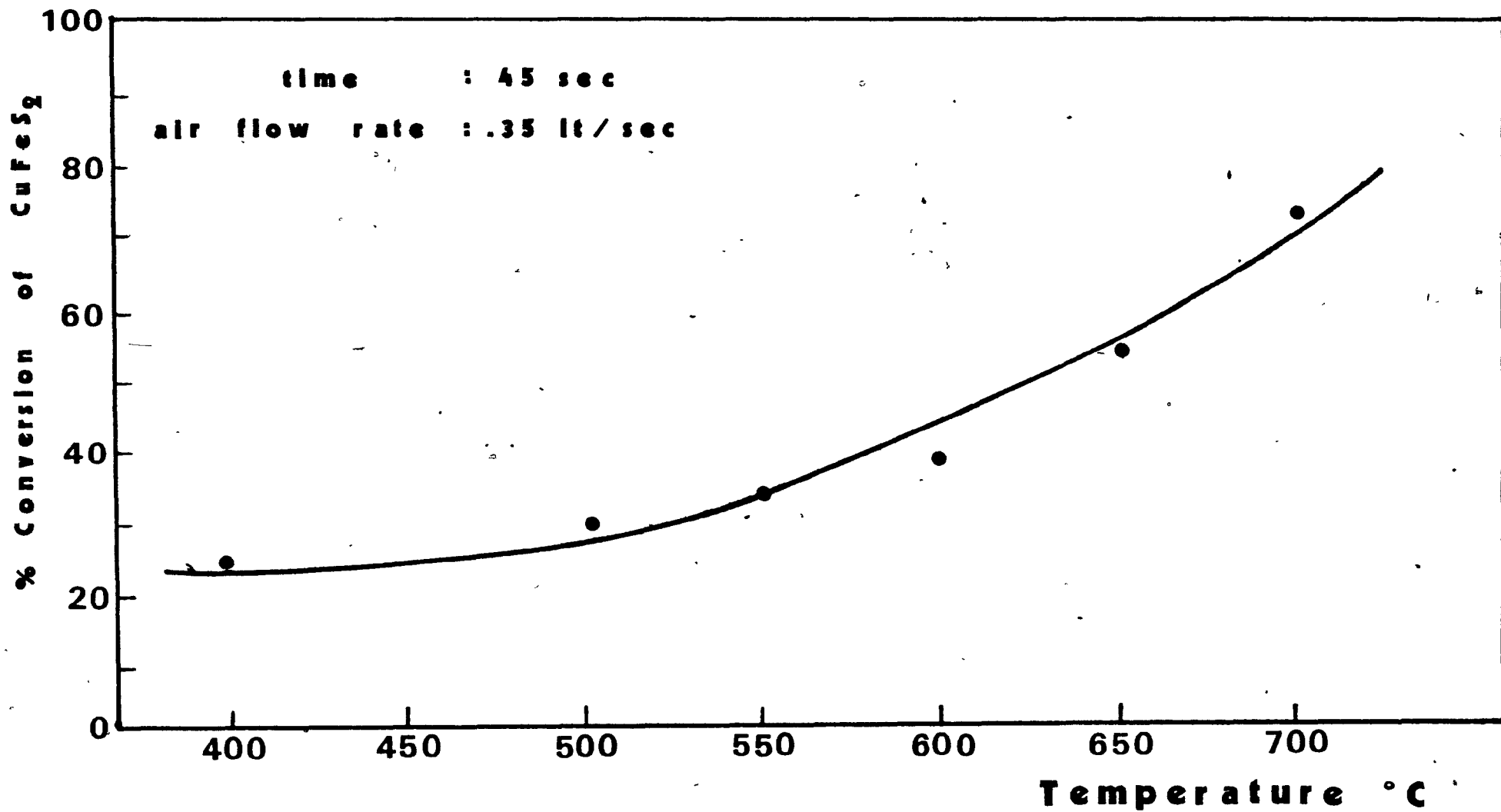


Figure 40. Roasting of CuFeS_2 in tube furnace. The conversion of CuFeS_2 vs. temperature.

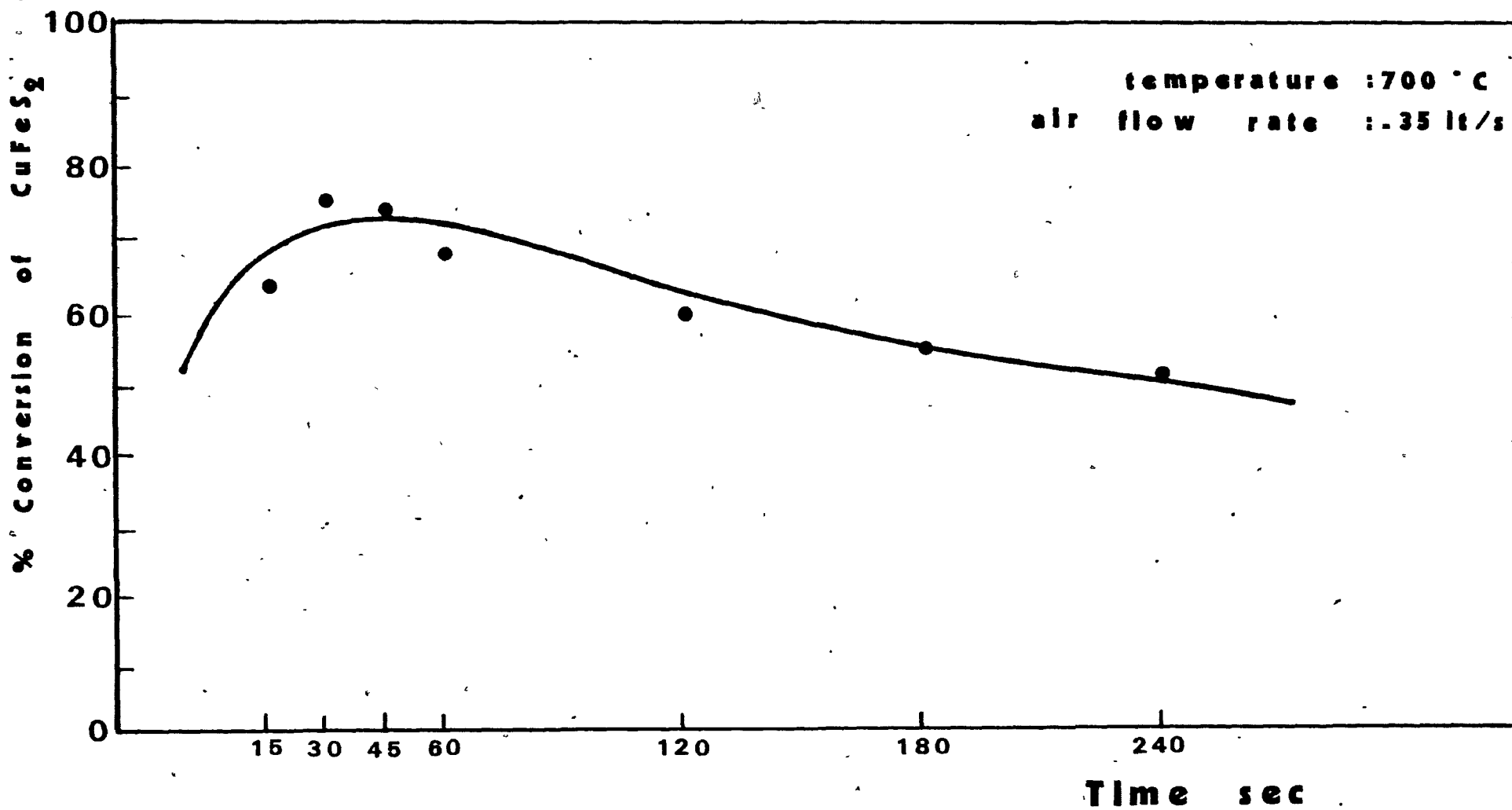


Figure 41. Roasting of CuFeS₂ in tube furnace. Conversion of CuFeS₂ vs. time.

FIGURE 42. X-ray diffraction pattern of chalcopyrite after roasting at 320°C, for 45 sec. with an oxygen flow rate of 0.25 lt/s.

92°

84°

$\text{CuO} \cdot \text{Fe}_2\text{O}_3$

PHILIPS PW1650/00

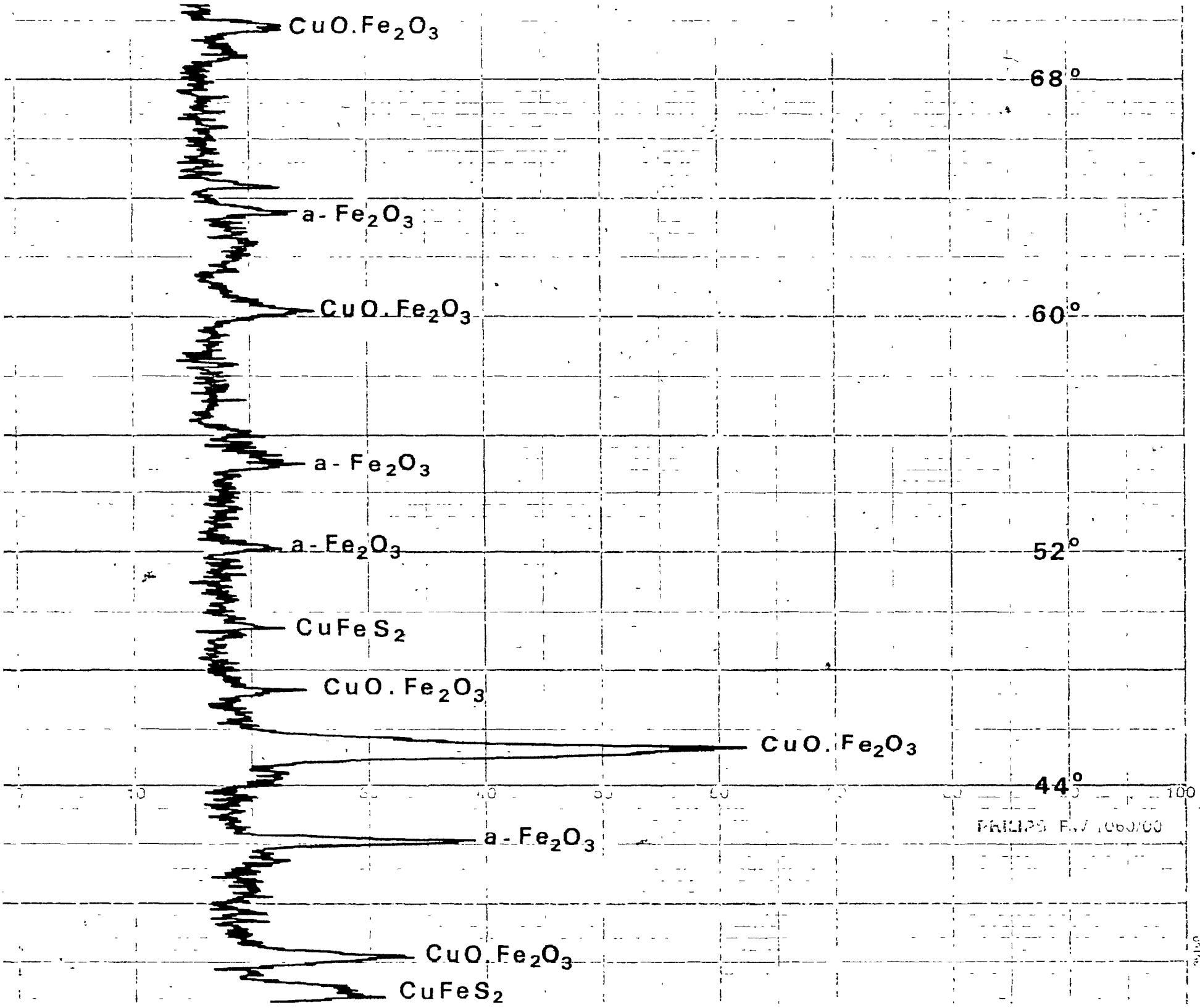
76°

CuFeS_2

$\text{CuO} \cdot \text{Fe}_2\text{O}_3$

68°

14

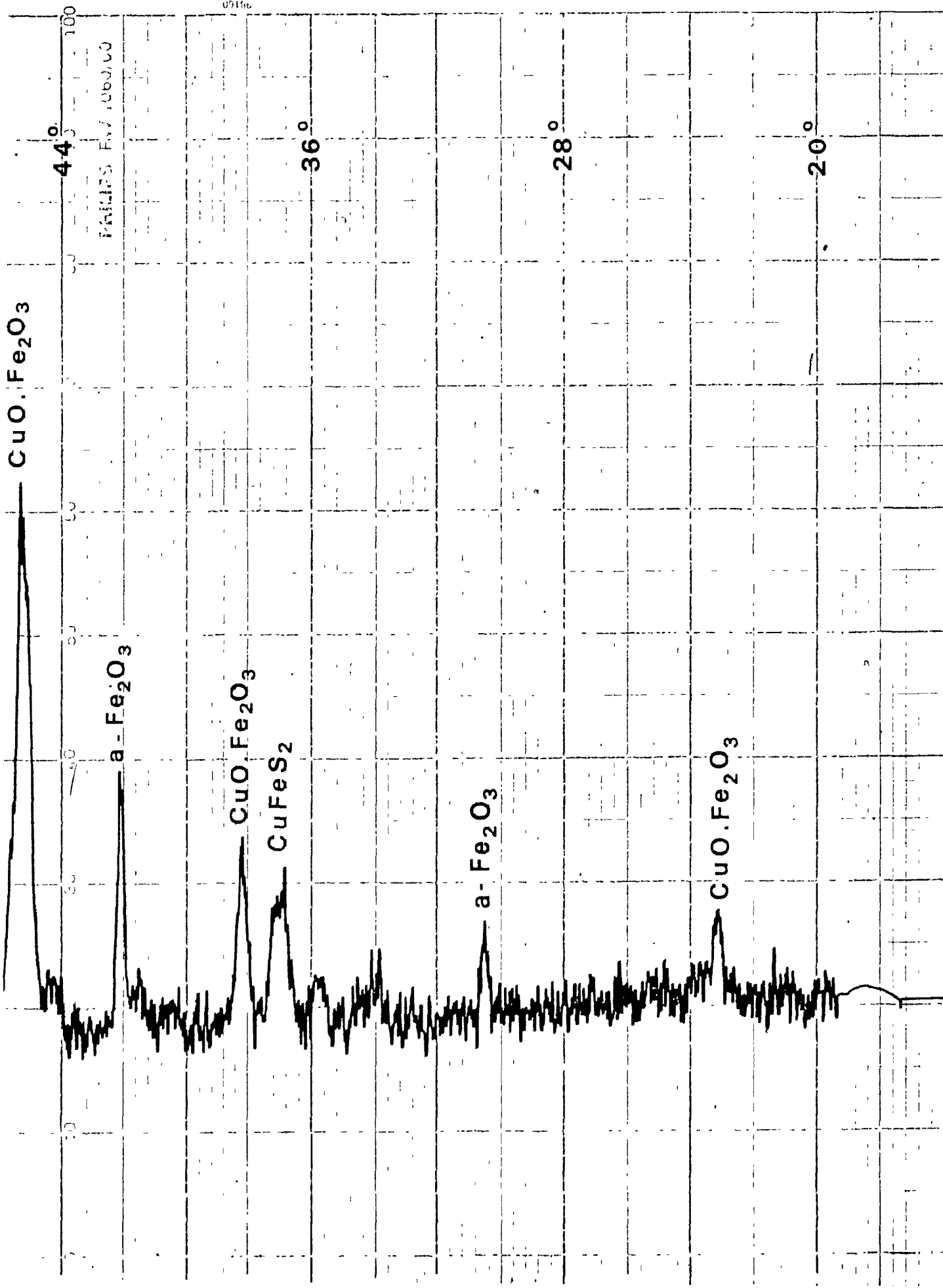


92

PHILIPS PW 1060/00

001100

573



44.3°

36.0°

28.0°

20.0°

CuO · Fe₂O₃

a-Fe₂O₃

CuO · Fe₂O₃

CuFeS₂

a-Fe₂O₃

CuO · Fe₂O₃

Intensity

100

50

50

50

0

100

50

50

50

0

100

50

50

50

0

100

50

50

50

0

100

50

50

50

0

100

50

50

50

0

100

50

50

50

0

100

50

50

50

0

100

50

50

50

0

100

50

50

50

0

100

50

50

50

0

100

50

50

50

0

100

50

50

50

0

100

50

50

50

0

100

50

50

50

0

100

50

50

50

0

100

50

50

50

0

100

50

50

50

0

100

50

50

50

0

100

50

50

50

0

100

50

50

50

0

100

50

50

50

0

100

50

50

50

0

100

50

50

50

0

100

50

50

50

0

100

50

50

50

0

100

50

50

50

0

100

50

50

50

0

100

50

50

50

0

100

50

50

50

0

100

50

50

50

0

100

50

50

50

0

100

50

50

50

0

100

50

50

50

0

100

50

50

50

0

100

50

50

50

0

100

50

50

50

0

100

50

50

50

0

100

50

50

50

0

100

50

50

50

0

100

50

50

50

0

100

50

50

50

0

100

50

50

50

0

100

50

50

50

0

100

50

50

50

0

100

50

50

50

0

100

50

50

50

0

100

50

50

50

0

100

50

50

50

0

100

50

50

50

0

100

50

50

50

0

100

50

50

50

0

100

50

50

50

0

100

50

50

50

0

100

50

50

50

0

100

50

50

50

0

100

50

50

50

0

100

50

50

50

0

100

50

50

50

0

100

50

50

50

0

100

50

50

50

0

100

50

50

50

0

100

50

50

50

0

100

50

50

50

0

100

50

50

50

0

100

50

50

50

0

100

50

50

50

0

100

50

50

50

0

100

50

50

50

0

100

50

50

50

0

100

50

50

<

using a Carl-Zeiss microscope with reflected light. Figures 43 and 44 show chalcopyrite roasted at 320°C, for 45s at an oxygen flow rate of 0.33 lt/s. The first microphotograph shows the feed to the Davis tube and the second one the Davis tube mags.

Figures 45 and 46 show chalcopyrite roasted at 700°C for 30s at an air flow rate of 0.35 lt/s. The first photograph again shows the feed to the Davis tube and the second one the Davis tube mags.

The oxidation of chalcopyrite takes place only on the surface of the particle producing a layer. However, this layer seems to be enough as it changes the overall susceptibility of the particles significantly.

8.4 Attempt at separation between chalcopyrite and galena

A synthetic mixture of chalcopyrite (60% wt, -37 μm) and galena (40% wt, - 37 μm) was prepared. The mixture was roasted in the presence of oxygen at 320°C for 45s, at an oxygen flow rate of 0.33 lt/s, as the best conditions found.

Before that galena was roasted on its own under the same conditions and the "agglomeration index" of the



Figure 43. Microphotograph of $-37\mu\text{m}$ particles of roasted CuFeS_2 at 320°C , for 45s at O_2 flow rate 0.33 lt/s. Magnification 440, reflected light under polarized conditions. C = chalcopyrite, P = pyrite, F = ferrite.



Figure 44. Microphotograph of $-37\mu\text{m}$ particles of Davis tube mags of roasted CuFeS_2 under the same conditions. Magnification 440 reflected light under polarized conditions. C = chalcopyrite, F = ferrite.



Figure 45. Microphotograph of $-37\mu\text{m}$ particles of roasted CuFeS_2 at 700°C , for 30s at air flow rate 0.33 lt/s. Magnification 440, reflected light under polarized conditions. C = chalcopyrite, F = ferrite, H = hematite.

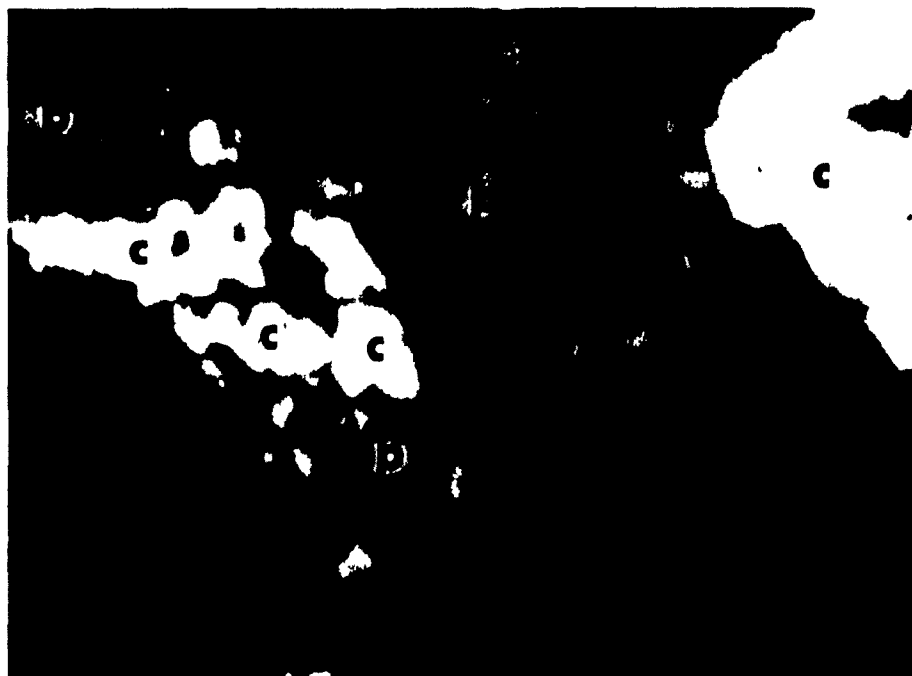


Figure 46. Microphotograph of $-37\mu\text{m}$ particles of Davis tube mags of roasted CuFeS_2 under the same conditions. Magnification 440, reflected light, polarized conditions. C = chalcopyrite, P = pyrite, F = ferrite, H = hematite.

material was determined in various temperatures. Some kind of sintering seems to take place around 400°C, as figure 47 shows. However, the product of roasting of the synthetic mixture was agglomerated as figures 48 and 49 show. It is then apparent that the two minerals cannot be separated by means of a physical method.

For the analysis of this result the REACTION program of the F.A.C.T. system was used. This program calculates changes in extensive thermodynamical functions. Printouts of the program for roasting in the presence of oxygen and for roasting in the presence of air, are presented in Appendix F. Both show that the reactions are exothermic as the change in enthalpies is lower than zero ($\Delta H < 0$) which means that heat is liberated. Therefore, the particles attain much higher temperature than is set by the furnace. In the temperature of 320°C the chalcopyrite starts to oxidize and the surface temperature increases apparently causing sintering with other chalcopyrite and galena grains.

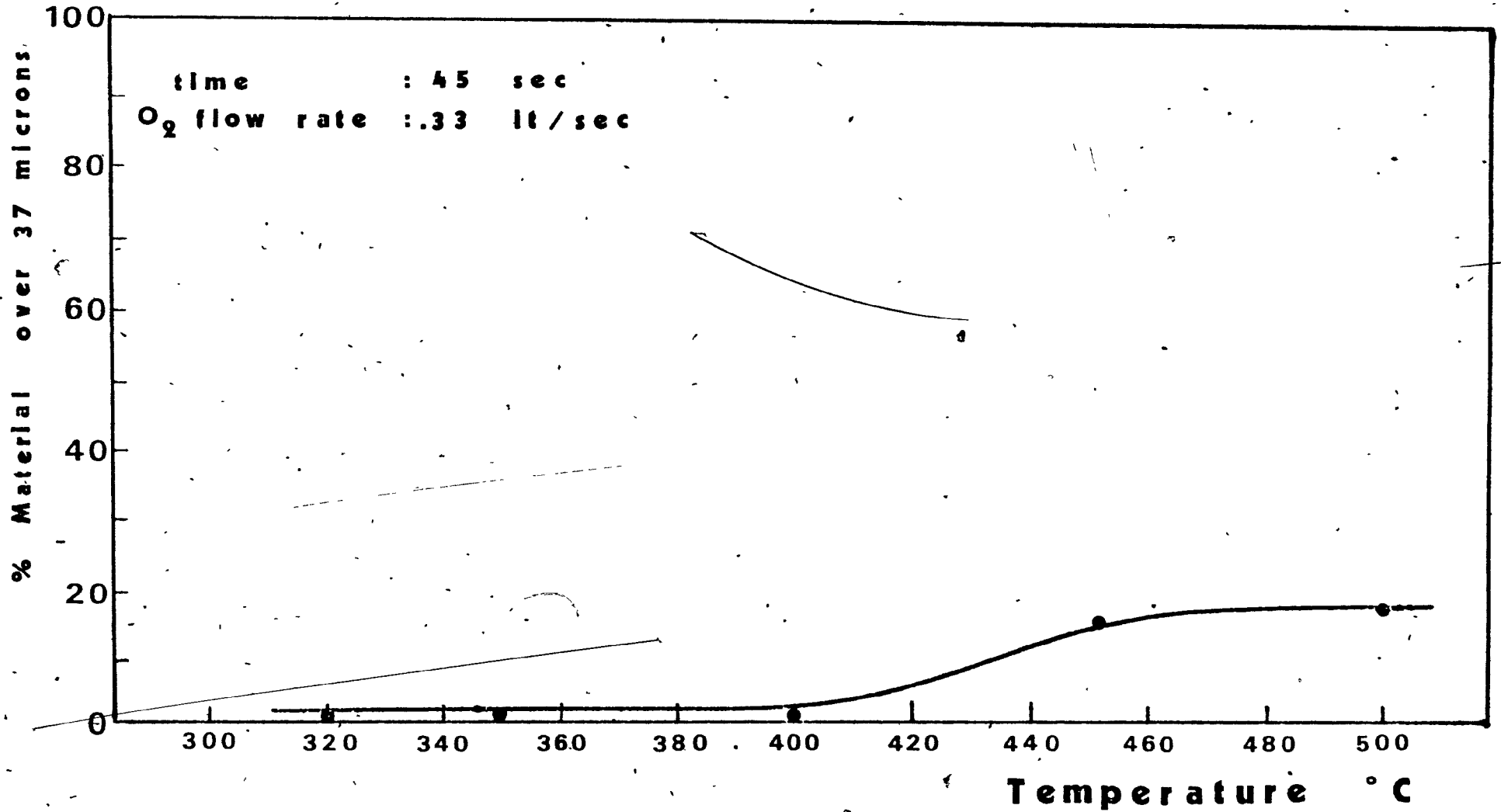


Figure 47. Roasting of PbS in tube furnace. "The agglomeration index" vs. temperature.

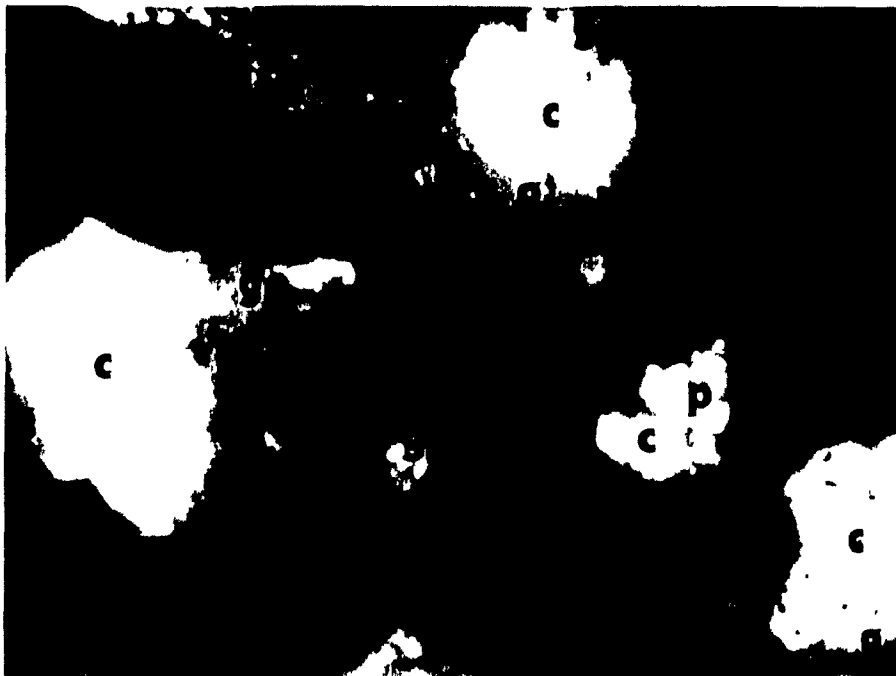


Figure 48. Microphotograph of $-37\mu\text{m}$ particles of sintered product of roasting of synthetic mixture at 320°C for 45s at O_2 flow rate 0.33 lt/s . Magnification 440, reflected light, polarized conditions. C = chalcopyrite, G = galena, H = hematite.

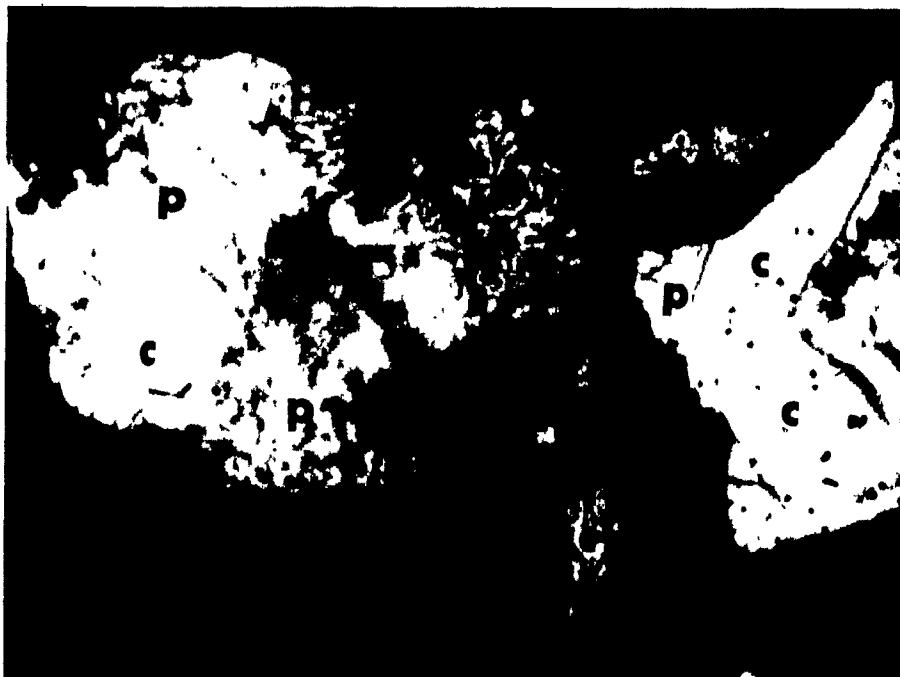


Figure 49. Microphotograph of $-37\mu\text{m}$ particles of sintered product of roasting of synthetic mixture under the same conditions. Magnification 440, reflected light, polarized conditions. C = chalcopyrite, G = galena, H = hematite, P = pyrite, F = ferrite.

9. HIGH GRADIENT MAGNETIC SEPARATION STUDY

9.1 Background

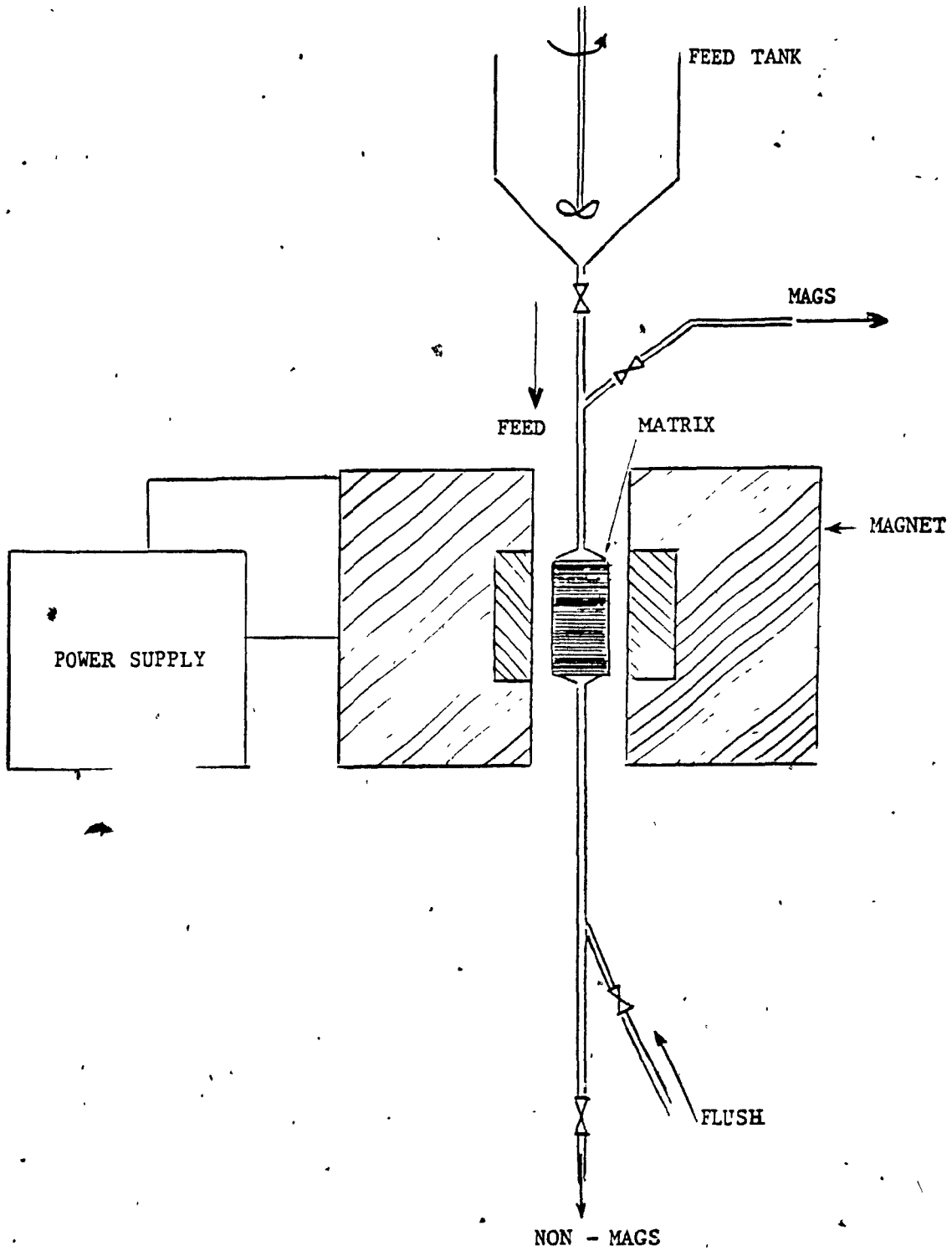
In High Gradient Magnetic Separation (HGMS) the magnetic trapping force is much greater than in any other magnetic device. These strong trapping forces are created by fine filamentary ferromagnetic matrices perturbing a strong background field and creating high field gradients. Because the force is large, fine and weakly magnetic particles can be captured by the matrix.

9.2 Equipment

The equipment used was an ERIEZ-MAGNETICS model. A, schematic diagram of the HGMS and the feed system is presented in figure 50. The separator consists basically of:

- a) A magnet and a power supply which provides fields up to 2 Tesla.
- b) A feed unit, which keeps the solids in suspension while they are fed into the system, and a flush used to flush out the magnetics trapped during the tests.

Fig. 50 Schematic diagram of HGMS.



c) A canister of 3.8cm in diameter and 10.2cm long to hold the matrix.

9.3 Experimental procedure

HGMS tests were carried out on both unroasted synthetic mixtures and roasted synthetic mixtures. The synthetic mixture consisted of 60% wt. of chalcopyrite (37 μm) and 40% wt. galena (-37 μm). The roasted synthetic mixture was prepared by slow heating at 320⁰C for 10 min., in a muffle furnace. The same fluid flow velocity in HGMS, of 5.3cm/s was used for both roasted and unroasted samples.

The goal of this study was to illustrate the effect of roasting on reducing the magnetic field required to trap the chalcopyrite.

9.4 The Recovery model for HGMS

This model developed by Nasset and Finch is described in paragraph 2.4.2. In order to predict the recovery, the particle parameters k and b must be known as well as the operating parameters.

Particle parameters

The particle volume susceptibility, " k " can be

measured from the magnetic profile developed on the Frantz separator. In the S.I. system the appropriate calculation is

$$k = \frac{2.5 \sin \theta \times 10^{-7} \rho_p}{I_{50}^2} \quad (\text{dimensionless}) \quad \text{Eq. 27}$$

The profile of the unroasted synthetic mixture is given in figure 17. The current I_{50} is taken as the current at which 50% reports to magnetics. From figure 16, $I_{50} = 0.995$ A and since $\theta = 20^\circ$ and $\rho_p = 4200 \text{ kg/m}^3$ then $k = 3.6 \times 10^{-4}$.

The profile of the roasted synthetic mixture is given in figure 18. Since $I_{50} = 0.015$ A, $\theta = 20^\circ$ and $\rho_p = 5.33 \text{ g/cm}^3 = 5330 \text{ Kg/m}^3$ then $k = 2.014$.

The particle radius b was determined from figure 51. These curves were obtained on a X-ray sedimentometer, the Sedigraph 5000D. This device employs a finely collimated X-ray beam to measure the change of particle concentration with time during settling in a sample cell. Curve 1 was obtained for the unroasted synthetic mixture and curve 2 for the roasted one. As particle radius the radius at which the cumulative mass percent equals 50 was selected. This radius for the unroasted and the roasted mixtures was 5 and 7 μm

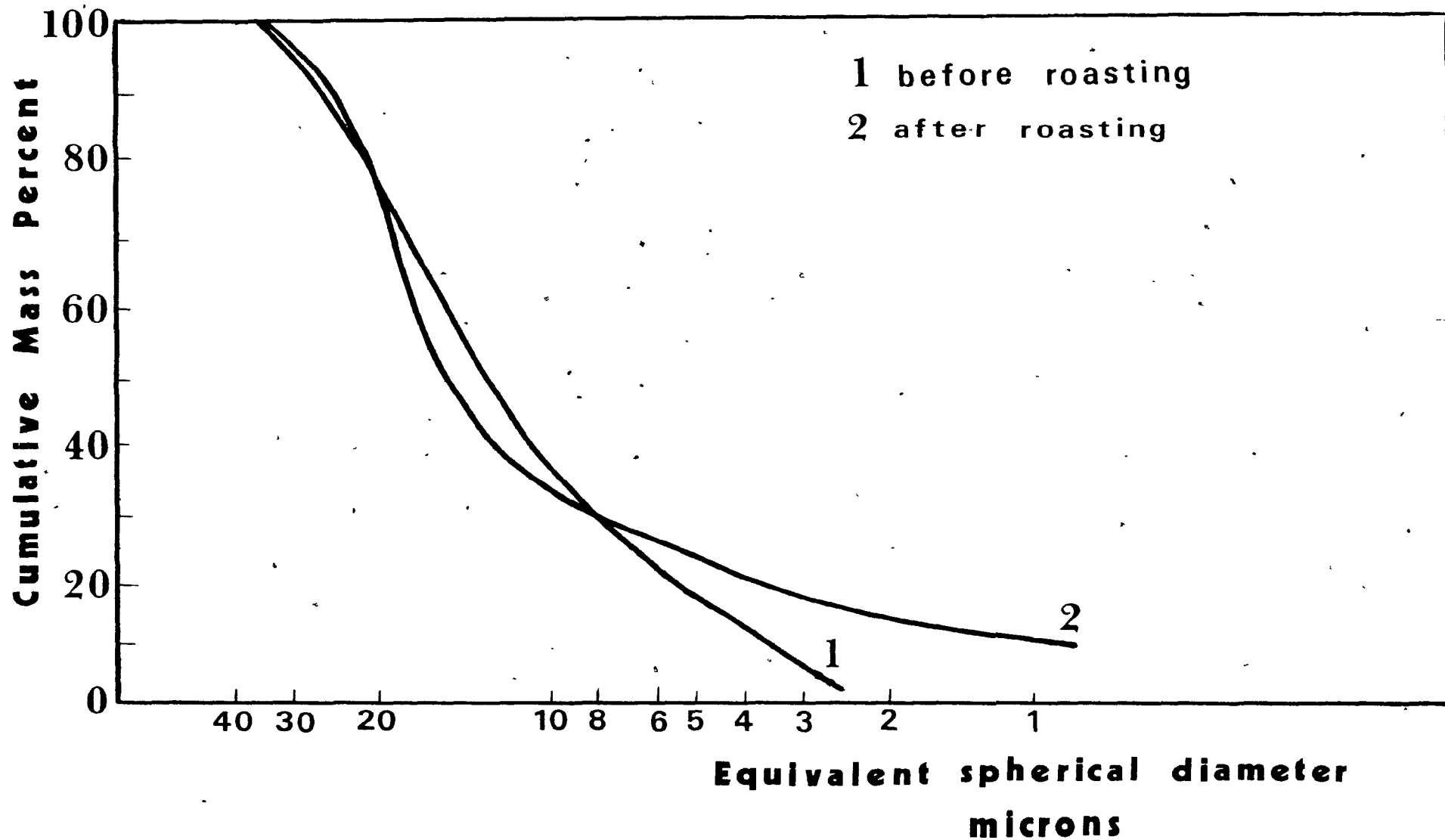


Figure 51. Size distribution of the synthetic mixture before and after roasting at 320°C, by slow heating, for 10 min.

respectively.

Operating parameters

As matrix expanded metal was used. The wire diameter was 0.9mm, so $\alpha = 0.000045m$. and 25g of metal were packed into the canister. The weight of each sample tested was 25g.

The mass of magnetics in the feed per unit of matrix was $L = 25 (0.60/25) = 0.60$ where 0.60 represents the 60% content of chalcopyrite in the feed. The flow velocity was selected to be 5.3cm/s. Once the above parameters had been selected it was only necessary to set the recovery and back calculate the required magnetic fields.

Tables 11 and 12 summarize the calculations for the unroasted and roasted synthetic mixtures. Recovery in both cases was set at 90%.

Table 11. Summary of calculations to estimate the required magnetic field. Unroasted synthetic mixture

$$L = 0.60$$

$$R = 90\%$$

$$R = (0.75 \frac{\gamma_m}{L}) \times 100$$

$$\gamma_m = 0.72$$

$$\rho_p = 4200 \text{ Kg/m}^3$$

$$\rho_w = 7750 \text{ Kg/m}^3$$

$$\epsilon = 0.7$$

$$\gamma_m = \frac{\epsilon}{4} \left| \left(\frac{N_L}{2.5} \right)^{0.8} - 1 \right| \frac{\rho_p}{\rho_w}$$

$$N_L = 36.8$$

$$b = 0.000005 \text{ m}$$

$$k = 3.627 \times 10^{-4}$$

$$\alpha = 0.000045 \text{ m}$$

$$\rho_f = 1000 \text{ Kg/m}^3$$

$$V_o = 5.32 \text{ cm/s} = 0.0532 \text{ m/s}$$

$$\eta = 0.001 \text{ Kg/m.s}$$

$$M_w = \mu_o H_o / 2\pi \times 10^{-7}$$

$$N_L = \frac{b \cdot k \cdot \mu_o \cdot H_o \cdot M_w}{V_o^{3/2} (\rho_f \cdot \eta \cdot \alpha)^{1/2}}$$

$$\mu_o H_o = B = 1.05 \text{ Tesla.}$$

Table 12. Summary of calculations to estimate the required magnetic field. Roasted synthetic mixture

$$\gamma_m = 0.72 \text{ (as before)}$$

$$\rho_p = 5330 \text{ Kg/m}^3$$

$$\rho_w = 7750 \text{ Kg/m}^3$$

$$\epsilon = 0.7$$

$$\gamma_m = \frac{\epsilon}{4} \left| \left(\frac{N_L}{2.5} \right)^{0.8} - 1 \right| \frac{\rho_p}{\rho_w}$$

$$N_L = 28.5$$

$$b = 0.000007\text{m}$$

$$k = 2.014$$

$$\alpha = 0.000045$$

$$\rho_f = 1000 \text{ Kg/m}^3$$

$$V_0 = 5.32\text{cm/s} = 0.0532\text{m/s}$$

$$\eta = 0.001 \text{ Kg/m.s}$$

$$M_w = \mu_0 H_0 / 2n \times 10^{-7}$$

$$N_L = \frac{b \cdot k \cdot \mu_0 \cdot H_0 \cdot M_w}{V_0^{3/2} \cdot (\rho_f \cdot \eta \cdot \alpha)^{1/2}}$$

$$\mu_0 H_0 = B = 1.02 \times 10^{-2} \text{ Tesla.}$$

9.5 Conditions of the tests

Having calculated the magnetic fields required, for a given flow velocity tests were organized around these fields. Because the field required for the roasted synthetic mixture is very low and cannot be produced accurately on the HGMS machine, the field of 0.228T was selected as the lowest operational field. The test conditions are summarized in table 13.

Table 13. Conditions of the HGMS tests

Series #	Run #	Sample (g)	Velocity (cm/s)	Field (T)
Unroasted				
1	1	25	5.3	1.776
	2	25	5.3	1.565
	3	25	5.3	1.431
	4	25	5.3	1.277
Roasted				
2	5	25	5.3	0.903
	6	25	5.3	0.688
	7	25	5.3	0.451
	8	25	5.3	0.228
Roasted				
3	9	25	9.7	0.228
	10	25	19.8	0.228

9.6 Results of test series 1 and 2

Runs of the test series 1 were carried out with an applied flow velocity of 5.3cm/s. Table 14 summarizes the results of runs 1,2,3 and 4.

The maximum operated field of 1.776 Tesla appears to be not enough for trapping most of the chalcopyrite as only 23.2% Cu report in the mags. However, the separation is very clean. The magnetic product contains 23.5% Cu and only 4%Pb.

Runs of the test series 2 were carried out with an applied flow velocity of 5.3cm/s. Table 15 summarizes the results of runs 5,6,7 and 8.

Much higher Cu recoveries (66%) are obtained at much lower fields (0.228T). This difference is illustrated in figure 52. However, unacceptably large Pb loss to the mags also occurs. This suggests either agglomeration of the material during roasting, or magnetic flocculation when exposed to the magnetic field. Further tests were conducted to determine which was responsible.

Figure 53 shows the copper grade-magnetic field

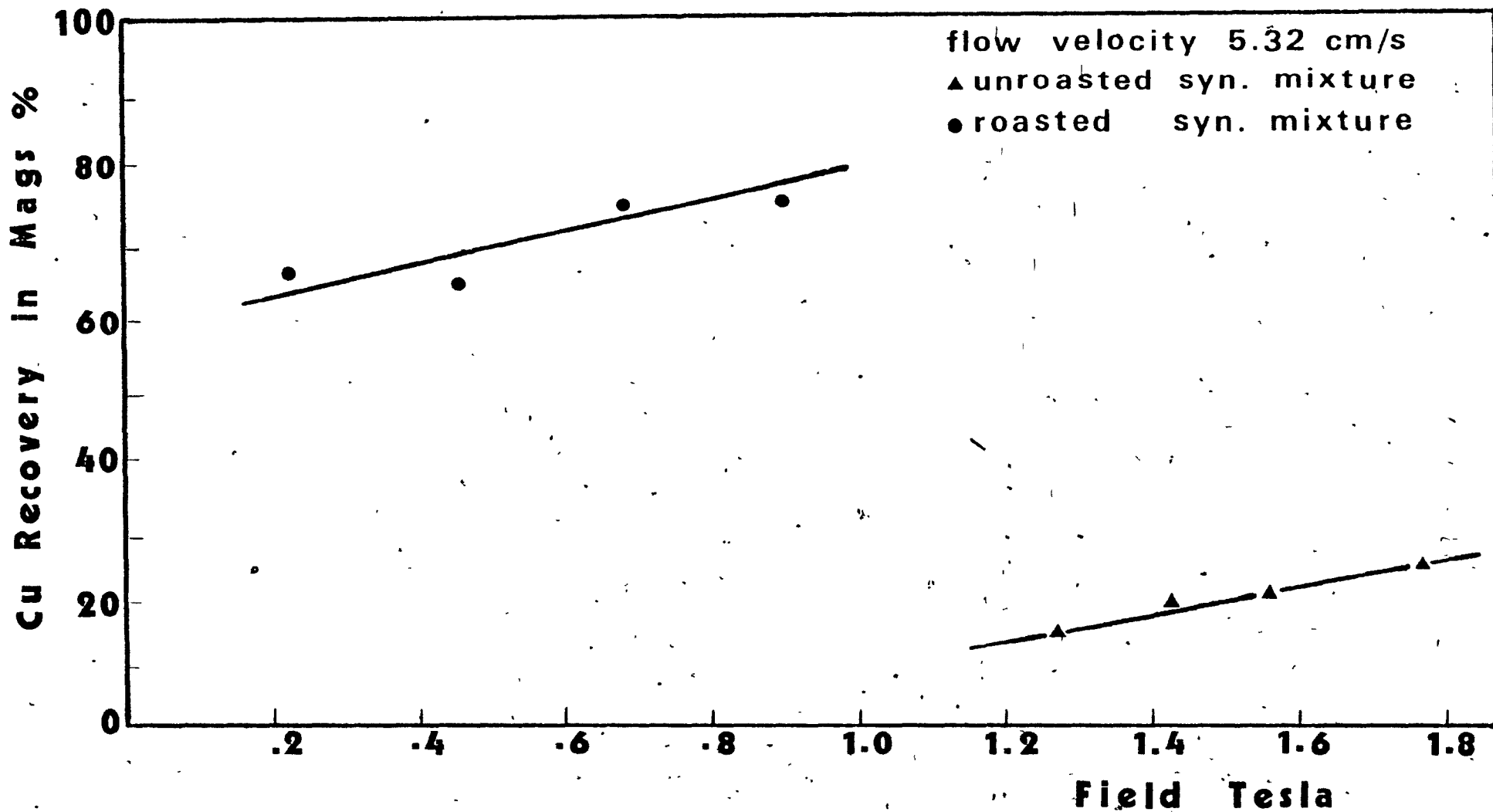


Figure 52. Copper Recovery in the magnetics vs. magnetic field, after HGMS on unroasted and roasted synthetic mixture.

Table 14. HGMS results of series 1

Run #	Product	wt (%)	Assay (%)		Distribution (%)	
			Cu	Pb	Cu	Pb
1	Mags	15	23.5	4	23.2	3.3
	Non-mags	85	13.7	30.5	76.8	97.7
		100.0			100.0	100.0
	Calculated feed Assay feed		15.2 17	26.5 27.5		
2	Mags	13.2	23.8	3.8	20	2
	Non-mags	86.8	14.5	30	80	98
		100.0			100.0	100.0
	Calculated feed Assay feed		15.7 17	26.5 27.5		
3	Mags	13	24.4	3.6	19.6	1.8
	Non-mags	87	15	29.5	80.4	98.2
		100.0			100.0	100.0
	Calculated feed Assay feed		16.2 17	26.1 27.5		
4	Mags	9.4	25.5	3.1	14	1.2
	Non-mags	90.6	16.3	25.8	86	98.8
		100.0			100.0	100.0
	Calculated feed Assay feed		17.1 17	23.6 27.5		

relationship when copper is considered in both mags and non-mags. Copper grades slightly decrease as the magnetic field increases.

Table 15. HGSM Results of series 2

Run #	Product	wt (%)	Assay (%)		Distribution (%)	
			Cu	Pb	Cu	Pb
5	Mags	67.3	10.8	23.7	74.8	61.8
	Non-mags	32.7	7.5	30.1	25.2	38.2
	Calculated feed	100.0			100.0	100.0
	Assay feed		9.7 11	25.8 24		
6	Mags	63.7	11.4	21.6	74	58.2
	Non-mags	36.3	7	27.2	26	41.8
	Calculated feed	100.0			100.0	100.0
	Assay feed		9.8 11	23.6 24		
7	Mags	61.7	11.8	20.6	64.6	45.2
	Non-mags	58.3	6.8	26.4	35.4	54.8
	Calculated feed	100.0			100.0	100.0
	Assay feed		11.2 11	28.1 24		
8	Mags	51.9	12.3	18	66.1	42.8
	Non-mags	48.1	6.8	26	33.9	57.2
	Calculated feed				100.0	100.0
	Assay feed		9.6 11	21.9 24		

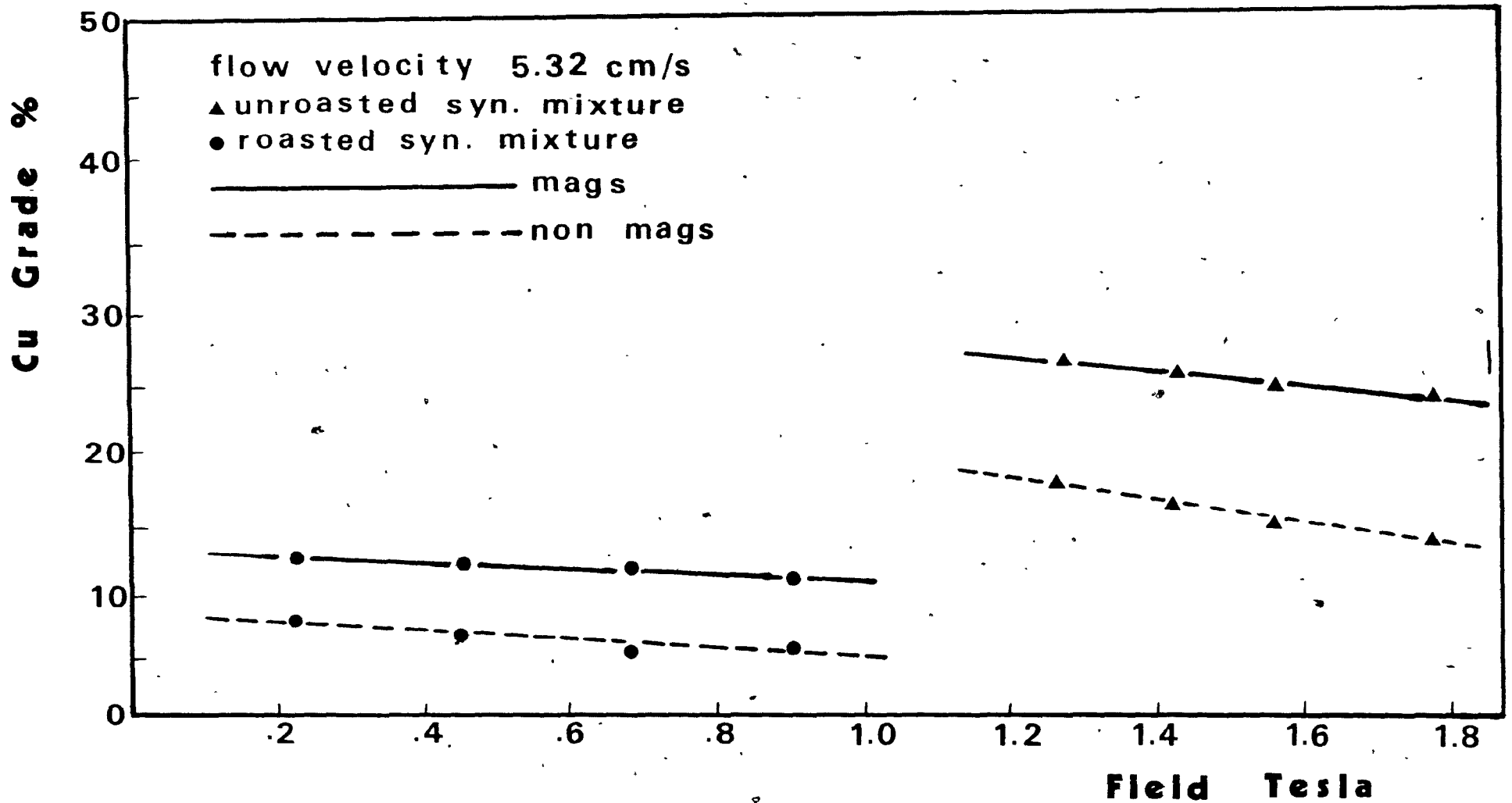


Figure 53. Copper grade in the magnetics and non-magnetics vs. magnetic field, after HGMS on unroasted and roasted synthetic mixture.

9.7 Magnetic flocculation or agglomeration?

In order to test whether magnetic flocculation or agglomeration caused the poor results obtained in the case of the roasted synthetic mixture, two tests were conducted.

In the first test 15g of chalcopyrite ($-37\mu\text{m}$) and 10g of galena ($-37\mu\text{m}$), (ratio: 15:10 = 60:40), were roasted separately under the same conditions (320°C , slow heating for 10 min.). The two calcines were thoroughly mixed and passed through the HGMS. The results are presented in table 16. Although, most of the copper is recovered in mags, about 31% of lead also reports to the mags. This test shows clearly that magnetic flocculation takes place as the feed to the separator cannot be agglomerated.

In the second test roasted synthetic mixture was passed through the Davis tube and the results are presented in table 17. Although only 53% of copper is recovered in mags, it is very clean with 27% Cu and 3.2% Pb. This result supports the fact that magnetic flocculation occurs during HGMS. Magnetic flocculation does not occur in Davis tube because of the lower magnetic field and the vigorous washing action that takes place.

Table 16. HGMS separation of roasted chalcopyrite and roasted galena

Field (T)	Flow velocity (cm/s)	Product	wt (%)	Assay (%)		Distribution (%)	
				Cu	Pb	Cu	Pb
0.228	5.3	Mags	46.4	13.8	16.3	67.7	31
		Non-mags	53.6	5.7	31.4	32.3	69
			100.0			100.0	100.0
		Calculated feed Assay feed		9.5	24.4	11	24

Table 17. Separation of roasted synthetic mixture on Davis tube

Flow velocity (cm/s)	Product	wt (%)	Assay (%)		Distribution (%)	
			Cu	Pb	Cu	Pb
0.6	Mags	22	27	3.2	53	3
	Non-Mags	78	6.7	31	47	97
		100.0			100.0	100.0
	Calculated feed Assay feed		11.2	24.9	11.2	24.5

9.8 Results of test series 3

Runs of the test series 3 were carried out with an applied magnetic field of 0.228 Tesla. Table 18 summarizes the results of runs 8, 9 and 10.

This series of tests was carried out in order to try to overcome the problem of magnetic flocculation, by

simply processing at higher flow velocities in the HGMS. The lowest magnetic field is limited by the equipment at 0.228 Tesla and the highest flow velocity at 19.8 cm/s.

The results generally improve as only 15% of Pb reports to the mags. However, the results suggest that an even lower operating magnetic field may be necessary to reduce the magnetic flocculation further or possibly a change in matrix design.

Table 18. HGMS Results of series 3

Run #	Product	wt (%)	Assay Cu	(%) Pb	Distribution Cu	(%) Pb
8	Mags	51.9	12.3	18	66.1	42.8
	Non-mags	48.1	6.8	26	33.9	57.2
		100.0			100.0	100.0
	Calculated feed Assay feed		9.6	21.9		24
9	Mags	32.7	14.5	17.4	51	23.7
	Non-mags	67.3	6.7	27.3	49	76.3
		100.0			100.0	100.0
	Calculated feed Assay feed		9.4	24.1		24.5
10	Mags	23	17.8	16.5	40	15
	Non-mags	77	8	28	60	85
		100.0			100.0	100.0
	Calculated feed Assay feed		10.3	25.3		24.5

9.9 HGMS of the B.M.S. sample

The B.M.S. sample was ground in a ball mill in order to increase the degree of liberation of galena. The grinding was wet, the fractional volume filling of the mill by powder was 0.05, the fractional volume filling by balls was 0.40 and the grinding time was 3 hours. Size analysis before grinding showed that the sample was closely sized with 80% of the sample was less than 29 μ m, and 30% less than 11 μ m. After grinding, 80% of the sample was less than 19 μ m but 30% was again less than 11 μ m. Particles of less than 10 μ m had undergone no size reduction.

The product of grinding was dried and then roasted in the muffle furnace at 320⁰C for 10 min. by slow heating. HGMS was then performed on the roasted product. Conditions and results of the HGMS are presented in the following tables 19 and 20. This series of tests was performed under the same conditions as series 3. The product in this case is more magnetic as the recoveries to mags are higher. However, the recovery of lead in the mags is higher than before (23% instead of 15%) suggesting that besides the problem of magnetic flocculation locking is still a major difficulty.

Table 19. Conditions of HGMS tests

Series #	Run #	Sample (g)	Velocity (cm/s)	Field (T)
		Roasted		
4	11	25	5.3	0.228
	12	25	9.7	0.228
	13	25	19.8	0.228

Table 20. HGMS Results of series 4

Run #	Product	wt (%)	Assay (%)		Distribution (%)	
			Cu	Pb	Cu	Pb
11	Mags	58.6	12.3	12	67.8	53.1
	Non-mags	41.4	8.3	15	32.2	46.9
		100.0			100.0	100.0
	Calculated feed Assay feed		10.7	13.2		
			11.8	13.6		
12	Mags	39.3	12.6	11	48.1	31.2
	Non-mags	60.7	8.8	15.7	51.9	68.8
		100.0			100.0	100.0
	Calculated feed Assay feed		10.3	13.8		
			11.8	13.6		
13	Mags	30.7	13.2	10.4	38.9	22.8
	Non-mags	69.3	9.2	15.6	61.1	77.2
		100.0			100.0	100.0
	Calculated feed Assay feed		10.4	14		
			11.8	13.6		

10. DISCUSSION

10.1 Roasting of chalcopyrite

Muffle furnace

Roasting of chalcopyrite for 6 hours at various temperatures was not successful in terms of the amount of ferrite obtained. However, it revealed that the ignition temperature of chalcopyrite was between 300 and 320°C which could be predicted to some extent from table 3 (paragraph 5.1). Products in temperatures between 320 and 500°C were mainly sulfates. Above 500°C copper ferrite is formed. Because of the long roasting time, equilibrium is established which allows the use of the F.A.C.T. system. The roasting products are in good agreement with those predicted thermodynamically.

Roasting of synthetic mixture at 320°C for 10 min. by slow heating gave appreciable amount of copper ferrite. Galena also reacted at this low temperature, which means that the actual temperature is much higher.

Roasting of B.M.S. samples at 320°C by different

heating methods for 10 min. showed that the method of heating is an important factor. Direct heating is more suitable for industrial roasting, however slow heating looked the most promising for separation. Why this happens is a point that needs further investigation.

Electron microprobe examination revealed that Fe:Cu ratio declines from 9 at the edge of the grains to about 0.9 at the center of the grains. The ratio of 0.9 is close to that for unroasted chalcopyrite suggesting that the core of the grains is unreacted. The S:Cu ratio increases from almost zero (no sulfur at the edge of the grains due to oxidation) to 0.9 at the center of the grains, again corresponding to chalcopyrite.

The ratio of susceptibilities of the roasted chalcopyrite mixture to the unroasted chalcopyrite is about 5,550:1.

Tube furnace

Roasting of chalcopyrite on its own under strongly oxidized conditions also gave an appreciable amount of copper ferrite. Roasting with oxygen at 320°C gave 75% conversion of chalcopyrite to a very magnetic form ($\text{CuO} \cdot \text{Fe}_2\text{O}_3$)

and Fe_2O_3) but the product was agglomerated. To achieve the same conversion using air the higher temperature of 700°C is needed, however, the product was not agglomerated.

The oxidation of chalcopyrite is an exothermic reaction. This means that heat is liberated and particles attain a much higher temperature.

The separation of roasted synthetic mixture using O_2 at 320°C did not work due to agglomeration. Because heat is liberated from the oxidation of chalcopyrite the temperature is actually much higher than 320°C , causing galena to be oxidized. Consequently the two minerals form agglomerates and cannot be separated by means of a physical method.

Agglomeration could possibly be avoided by roasting in a fluidized bed. This is also an interesting point which needs further investigation.

The method of separation of roasted chalcopyrite used in Algeria (26) described earlier was thought to be on the formation of Fe_2O_3 around chalcopyrite grains. What seems more likely to happen is the formation of $\text{CuO}\cdot\text{Fe}_2\text{O}_3$ as the results of this work have shown.

10.2 Magnetic separation of chalcopyrite-galena 124
mixtures

Separation on the Frantz separator

Since the Frantz separates according to magnetic susceptibility only and can achieve separation between minerals of very close magnetic susceptibility, its use gave several advantages:

- a) Mineralogical identification was made much easier by working with separate mineral fractions rather than with a wide range size.
- b) The magnetic profile obtained from Frantz allowed:
 - (i) Estimation of the potential of chalcopyrite separation from galena by HGMS.
 - (ii) Estimation of the magnetic susceptibility, with which it was possible to solve the HGMS model and select the magnetic field needed to trap chalcopyrite.

Separation of the synthetic mixture after roasting in the muffle furnace, at 250 mA gave a very clean non-magnetic galena concentrate (75% Pb, 1.2% Cu, 1.6% Fe). However

loss of lead in the mags was 26%. This galena is probably trapped by magnetic flocs.

Separation of the B.M.S. sample studied under various temperatures, methods of heating and retention times was not successful. Separation at 25 mA of the roast at 320°C by slow heating for 10 minutes gave unacceptable losses (58% Cu, 65% Fe) of copper and iron to the non-mags. Due to locking (55% of galena is locked with chalcopyrite), some chalcopyrite locked particles cannot be trapped.

Separation on HGMS

Since there are many parameters controlling the operation of HGMS, the use of the model in the investigation was helpful in selecting the initial test conditions.

One of the problems that could arise during operation is physical trapping by the matrix. This can happen not only when the particles are large compared to the wire diameter, but also when strongly magnetic materials are present in the feed and are not adequately flushed off the matrix and accumulate with repeated cycles. Particle size does not appear to be a factor here since the top size (35 μ m) is one thirtieth of the wire diameter. The matrix

was flushed thoroughly after each run.

HGMS of the unroasted synthetic mixture gave clean copper concentrates (25.5% Cu, 3.1% Pb) but very low copper recoveries (14%). After roasting the mixture has 5,550 times greater magnetic susceptibility. This enormous difference enables the use of very low fields. Figure 51 shows that recoveries are now higher (66%) obtained at much lower magnetic fields. However, due to magnetic flocculation large Pb loss (43%) to the mags occurs.

The problem of magnetic flocculation could be overcome by operating at even lower magnetic fields which were not attainable with the equipment used.

HGMS on the B.M.S. roasted sample was performed after grinding. The grinding was done to try to further liberate galena from chalcopyrite. Despite the long time, grinding proved to be inefficient for particles below 10 μ m and locking is still a major problem.

One interesting idea for further experimentation is to perform the HGMS on a dry system. This system would reduce the hydrodynamic drag force that is significant as the particles are very fine.

Separation on Davis tube

Davis tube provides a relatively weak magnetic field. Separation performed on the roasted synthetic mixture gave very clean copper concentrate (27% Cu, 3.2% Pb) and upgraded the galena concentrate to 31% Pb with 97% Pb recovery.

11. CONCLUSIONS

11.1 Roasting of chalcopyrite for 6 hours in a muffle furnace.

- Roasting produced copper ferrite at temperatures above 500°C.
- The amount of copper ferrite formed was very small (less than 10% wt.).
- There is agreement between the results obtained and those predicted thermodynamically.

11.2 Roasting of chalcopyrite-galena mixtures for 10 min. in a muffle furnace

- Method of heating appears to be an important factor.
- Roasting of the synthetic mixture by slow heating at 320°C for 10 min. produced a calcine whose separation on the Frantz gave a very clean galena concentrate (75% Pb, 1.2% Cu, 1.6% Fe).
- Roasting of the B.M.S. sample under the same conditions produced a calcine whose separation

on the Frantz at 25 mA was not successful due to the locking.

11.3 Roasting of chalcopyrite in a tube furnace

- Roasting of chalcopyrite with oxygen required very low temperatures and retention times but the product was agglomerated.
- 75% of chalcopyrite is converted to magnetic product at the temperature of 320⁰C with a retention time of 45s and an oxygen flow at 0.33 lt/s.
- Roasting of chalcopyrite with air required much higher temperatures (about 700⁰C), however the product was not agglomerated.
- 75% of chalcopyrite is converted to magnetic product at the temperature of 700⁰C with a retention time of 30s and an air flow rate of 0.35 lt/s.
- Roasting of synthetic mixture, due to the exothermic of the reaction of chalcopyrite gives sintered chalcopyrite-galena particles which cannot be separated.

11.4 HGMS Results

- HGMS on the unroasted synthetic mixture using a field of 1.776T and a flow velocity of 5.3 cm/s produced a Cu concentrate assaying 23.5% Cu and 4% Pb. However, Cu recovery is low (14%) suggesting the use of a higher field or lower flow velocity.
- HGMS on the roasted synthetic mixture using a field of 0.228T and a flow velocity of 5.3 cm/s improved the Cu recovery (66%), but an unacceptable loss of Pb to the mags occurs. Magnetic flocculation is responsible and the problem could be overcome by operating at even lower fields which were not available with the equipment in use.
- HGMS on the roasted B.M.S. sample after long time grinding suggests that besides magnetic flocculation, locking is still a major problem. B.M.S. sample is not suitable for roasting and magnetic separation.

11.5 Davis tube Results

- Separation of the roasted synthetic mixture

gave a very clean copper concentrate assaying 27% Cu and 3.2% Pb with a Cu recovery to mags of 53% and a lead concentrate assaying 31% Pb and 6.7% Cu with a Pb recovery to non-mags of 97%.

APPENDIX A - F.A.C.T. SYSTEM RESULTS

In the following tables the printouts of the program are presented for roasting 3g of CuFeS_2 in air (21% O_2). The second line describes the conditions of each reactant i.e. temperature in K, partial pressure in atm and state of the reactant (S=solid, L=liquid, G=gas). For the temperatures of 550, 500 and 450 $^\circ\text{C}$ the results were identical. Therefore, only the results of the temperatures of 685 and 550 $^\circ\text{C}$ are presented.

TABLE A-2. F.A.C.T. printout for heating of chalcopyrite at 550°C

XX

.0163CU+.0163FE+.0163S2+.2102+.79N2=
 (823.1,S) (823.1,S) (823.1,S) (823.1,G) (823.1,G)

0.948	(.833	N2	
	+	.149	O2	
	+	.155E-01	S*O3	
	+	.171E-02	S*O2 /	
	+	.295E-05	N*O	
	+	.596E-06	N*O2	
	+	.254E-09	N2O	
	+	.879E-13	O	
	+	.192E-13	N*O3	
	+	.124E-13	O3	
	+	.316E-16	N2O3	
	+	.270E-17	S*O	
	+	.153E-17	N2O4	
	+	.407E-21	N2O5	
	+	.260E-21	CU	
	+	.119E-26	N	
	+	.276E-29	N3	
	+	.150E-31	S	
	+	.762E-33	S*N	
	+	.660E-35	S2O	
	+	.772E-36	CU2	
	+	.152E-36	FE	
	+	.672E-42	S2	
	+	.193E-63	S3	
	+	.0	S7	
	+	.0	S6	
	+	.0	S5	
	+	.0	S4	
	+	.0	S8	
			(.823.0, 1.00	(,G)
	+	.0	(CU2O)*(FE2O3)	
			(.823.0, 1.00	(,S1)
	+	.0	(CU*O)*(FE2O3)	
			(.823.0, 1.00	(,S3)
	+	.163E-01	CU*S*O4	
			(.823.0, 1.00	(,S1)
	+	.815E-02	FE2O3	
			(.823.0, 1.00	(,S1)

APPENDIX - B. DAVIS TUBE CONCENTRATOR

The Davis tube concentrator is widely used as a rapid method for determining the magnetic (usually magnetite) content of ores either for the purpose of predicting the performance of direct current magnetic separators or as a means of controlling plant operation.

The apparatus consists of a powerful electromagnet with pointed poles and a long glass tube having facilities for introducing the sample and wash water. The tube is placed between the poles of the magnet and water flowing through it is agitated with short vertical strokes. Magnetic material is held between the poles, while gangue is washed out. When the wash water is clear the sample is transferred to a beaker, excess-water is decanted off and the residue is dried and weighted.

APPENDIX - C. X-RAY DIFFRACTION RESULTS

X-ray diffraction results of the products are presented in tables. Each table consists of a list of the d-spacing measured and a comparison with listed values.

Table C-1. UNHEATED CHALCOPYRITE SAMPLE

Measured values		Listed "d" values		
"d" spacing (Å)	Intensity	CuFeS ₂	FeS	Cu ₂ S
3.326	15			3.31
3.108	15			3.15
3.013	100	3.03 ⁽¹⁾		
2.693	40			2.718
2.628	25	2.64	2.617	
2.410	40			2.396 ⁽³⁾
2.201	40			1.987 ⁽¹⁾
1.901	40		1.909	1.908
1.859	75	1.852 ⁽²⁾		
1.842	75		1.845 ⁽³⁾	
1.627	50		1.644 ⁽²⁾	
1.586	60	1.590 ⁽³⁾		
1.567	40	1.572		
1.495	20	1.517		
1.441	20		1.425	

(1), (2) and (3) represent the main lines.

TABLE C-2. CHALCOPYRITE HEATED AT 300°C

Measured values		Listed "d" values		
"d" spacing (Å)	Intensity	CuFeS ₂	FeS	Cu ₂ S
3.260	10			3.27
3.137	20			3.15
3.042	15			3.05
3.011	100	3.03 ⁽¹⁾	2.869 ⁽¹⁾	
2.826	15	2.89		
2.786	10			2.755
2.691	20	2.60		
2.628	5		2.617	
2.407	60			2.396 ⁽³⁾
2.200	30		2.155	
1.897	10		1.909	
1.844	80	1.852 ⁽²⁾		
1.843	80		1.845	
1.629	10			1.632
1.569	15	1.572		

(1), (2) and (3) represent the main lines.

TABLE C-3. CHALCOPYRITE HEATED AT 320°C

Measured values		Listed "d" values		
"d" spacing (Å)	Intensity	CuSO ₄	CuFeS ₂	α-Fe ₂ O ₃
4.738	20		4.71 (4)	
4.180	20	4.187 (3)		
3.972	15	3.921		
3.691	25			3.66 (4)
3.545	75	3.549 (1)		
3.027	100		3.03 (1)	
2.694	60			2.69 (1)
2.615	75	2.616 (2)		
2.512	60			2.51 (3)
2.417	40	2.416		
2.213	30			2.201
2.083	10	2.093		2.070
1.969	10	1.963		
1.870	40		1.867	
1.851	40		1.852 (2)	
1.696	20			1.690 (2)
1.634	15			1.634

(1), (2), (3) and (4) represent the main lines.

TABLE C-4. CHALCOPYRITE HEATED AT 450°C

Measured values		Listed "d" values	
"d" spacing (Å)	Intensity	CuSO ₄	α-Fe ₂ O ₃
4.187	100	4.187 ⁽³⁾	
3.682	10		3.66 ⁽⁴⁾
3.557	100	3.549 ⁽¹⁾	
3.028	20	3.172	
2.701	80		2.603 ⁽³⁾
2.622	90	2.616 ⁽²⁾	
2.516	70		2.495 ⁽¹⁾
2.416	60	2.416	
2.310	15	2.321	
2.208	20		2.182
2.089	10		2.059
1.903	20		1.894
1.806	70	1.7749	
1.738	70		1.690 ⁽²⁾

(1), (2), (3) and (4) represent the main lines.

TABLE C-5. CHALCOPYRITE HEATED AT 500°C

Measured values		Listed "d" values		
"d" spacing (Å)	Intensity	CuFe ₂ O ₄ *	α-Fe ₂ O ₃	CuSO ₄
4.169	60			4.187 ⁽³⁾
3.688	40		3.66 ⁽⁴⁾	
3.541	80			3.541 ⁽¹⁾
2.745	100		2.69 ⁽¹⁾	
2.610	90	2.603 ⁽³⁾		
2.510	100	2.495 ⁽¹⁾		
2.413	55			2.416 ⁽⁴⁾
2.316	15		2.285	
2.201	50		2.201	
2.084	15		2.084	
1.979	70			1.971
1.775	40			1.7749
1.691	80		1.690 ⁽²⁾	
1.482	70	1.497 ⁽²⁾		
1.453	70	1.455 ⁽⁴⁾		
1.429	30			1.4298

* Crystallized in tetragonal system.

(1), (2), (3) and (4) represent main lines.

TABLE C-6. CHALCOPYRITE HEATED AT 550°C

Measured values		Listed "d" values		
"d" spacing (Å)	Intensity	$\alpha\text{-Fe}_2\text{O}_3$	$\text{CuFe}_2\text{O}_4^*$	$\text{Fe}_2(\text{SO}_4)_3$
5.941	80			5.98 ⁽²⁾
4.762	15		4.85 ⁽⁴⁾	
4.360	30			4.36 ⁽³⁾
4.114	40			4.13
3.499	35	3.66 ⁽⁴⁾		3.59 ⁽¹⁾
2.657	100	2.69 ⁽¹⁾		
2.579	45		2.603 ⁽³⁾	
2.489	100		2.495 ⁽¹⁾	
2.390	25		2.421	
2.232	25	2.285		
2.180	70		2.182	
1.817	80			1.824
1.756	15	1.746		
1.675	80	1.690 ⁽²⁾		
1.472	80		1.472 ⁽²⁾	
1.438	80	1.452	1.455	

* Crystallized in tetragonal system.

(1), (2), (3) and (4) represent the main lines.

TABLE C-7. CHALCOPYRITE HEATED AT 685°C

Measured values		Listed "d" values		
"d" spacing (Å)	Intensity	CuFe ₂ O ₄ *	CuFe ₂ O ₄ **	α-Fe ₂ O ₃
4.841	30	4.85 ⁽⁴⁾		
3.680	50			3.66 ⁽⁴⁾
3.006	60	2.995		
2.978	20		2.96 ⁽³⁾	
2.847	15			
2.691	90			2.69 ⁽¹⁾
2.581	70	2.603 ⁽³⁾		
2.514	100	2.495 ⁽¹⁾	2.517 ⁽¹⁾	
2.420	15	2.421	2.417	
2.321	55			2.285
2.205	60			2.201
2.059	25	2.059		
1.868	15			
1.844	65			1.838
1.692	80			1.690 ⁽²⁾
1.487	85	1.497 ⁽²⁾	1.479 ⁽²⁾	
1.451	80	1.455		

* Crystallized in tetragonal system.

**Crystallized in cubic system.

(1), (2), (3) and (4) represent the main lines.

APPENDIX-D. ESTIMATION OF DEGREE OF LIBERATION

The degree of liberation L as defined by Gaudin (36) is the percentage of mineral or phase occurring as free particles (A), in relation to the total of that mineral or phase occurring in the free (A) and locked forms (B). In the following record sheets the number B represents the parts per 20 parts of particle volume occupied by chalcopyrite or galena in the locked particle. B is calculated by summing all these values and dividing by 20. In other words, B represents the particle equivalents in volume of chalcopyrite and galena. Observations made under the microscope tend to overestimate the degree of liberation of the material being considered. Thus, to correct the error it is necessary to increase the number of particles actually observed to be locked by a locking factor. This locking factor is given as a function of the percentage of phase B in the total mineral surface (36, page 88, figure 50).

The degree of liberation in per cent ($L\%$) is given by the following expression:

$$\%L = \frac{A}{A+B} \times (100) \text{ where}$$

A, is the volume of free particles of chalcopyrite or galena.

B', is the particle equivalents in volume of chalcopyrite or galena, as locked grains corrected by the locking factor.

TABLE D-1. Record Sheet to measure degree of liberation(continued)

Volume of Locked Chalcopyrite

17-13-8-4-5-8-6-2-11-17-19-13-13-19-11-9

1-1-1-1-1-12-13-1-1-1-1-1-1-15-10-7-2-1

4-8-1-2-12-13-10-4-18-19-1-2-1-6-8-16-12

6-1-10-3-4-15-16-1-10-17-13-17-10-18-12-10-3

5-5-6-18-4-8-18-2-10-10-10-19-18-2-12-18

1-1-1-5-7-15-1-1-8-18-5-1-9-2-7-10-2-4-10

18-2-18-8-3-4-8-7-8-5-10-13-11-12-17-4-1

2-10-5-3-2-4-15-12-2-4-2-10-11-2-10-10-12-8

10-2-8-10-10-13-13-19-8-2-1-12-2-9-1-2-8

16-15-13-18-9-10-9-4-1-1-2-4-4-11-6-8-17

4-10-10-17-9-1-1-4-8-19-10-4-10-10-12-4

15-15-1-11-4-16-9-6-18-5-2-9-4-4-8-8-17-7

1-12-10-5-4-8-13

(214)

Table D-2. Record Sheet to measure degree of liberation

"L" of galena

Free galena

A=181

Locked galena

3-7-12-16-15-12-16-14-14-8-18-19-19-19-19
 19-19-7-9-1-2-19-19-19-19-19-5-17-10-13
 18-19-5-16-12-10-18-19-8-7-16-2-2-19-10-18
 19-14-12-7-8-14-19-10-17-9-5-4-19-10-3-7-10
 2-8-18-14-15-10-17-15-15-15-6-2-16-2-18-10-10
 1-19-2-18-8-2-16-16-19-10-19-19-7-13-9-19-19
 2-12-15-13-19-11-18-13-10-18-16-10-2-18-12-17
 15-16-12-13-12-15-10-7-9-8-3-4-19-18-10-15
 17-18-16-5-8-18-5-16-18-10-17-9-18-10-10-8-12
 18-18-18-12-10-7-1-12-17-18-19-1-4-16-8-18-11
 19-18-18-12-4-4-5-2-11-10-11-16-19-19-19-17-18
 2-8-16-2-9-14-3-16-10-3-11-19-19-16-12-1-16
 5-10-10-8-8-19-16-4-5-5-8-19-8-9-16-4-11-9
 14-2-15-13-18-11-16-16-12-12-3-13-19-8-15-10
 7-15-16-17-7

L% of Chalcopyrite

A=697 free particles

B=1,587/20=79 equivalent free particles

Per cent B = $79/214 = 37\%$

Locking factor = 1.25

$$L\% = \frac{697}{697 + 79 \times 1.25} = 88\%$$

L% of galena

A=181 free particles

B=2,845/20=142 equivalent free particles

Per cent B = $142/236 = 60\%$

Locking factor = 1.2

$$L\% = \frac{181}{181 + 142 \times 1.2} = 55\%$$

APPENDIX -E. FRANTZ ISODYNAMIC MAGNETIC SEPARATOR

The Frantz (figure 54) best known for its geological and mineralogical applications in achieving precise separation of minerals of different magnetic susceptibilities (34) has also been used to indicate the potential of a mineral mixture to be processed by magnetic methods (6,35).

The Frantz consists of an inclined chute which is placed between two long poles of a powerful electromagnet. The dry sample is fed down the chute parallel to the length of the pole pieces. The chute is also tilted to one side, so that the particles flow down one side of the chute when no magnetic field is applied. When current passes through the electromagnets, a magnetic field is produced between the pole pieces. The diverging shape of the pole creates a field gradient and causes a magnetic force to act on a paramagnetic particle in a direction opposite to the gravitational force.

This is illustrated in figure 55 (35), which shows a cross section of the chute and the pole pieces. A field gradient is produced in the positive X direction

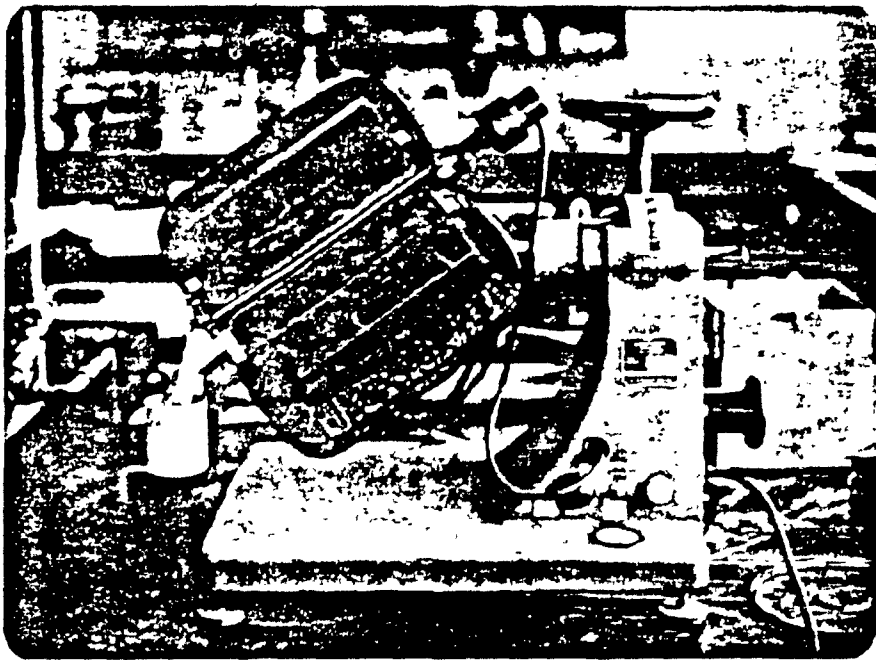
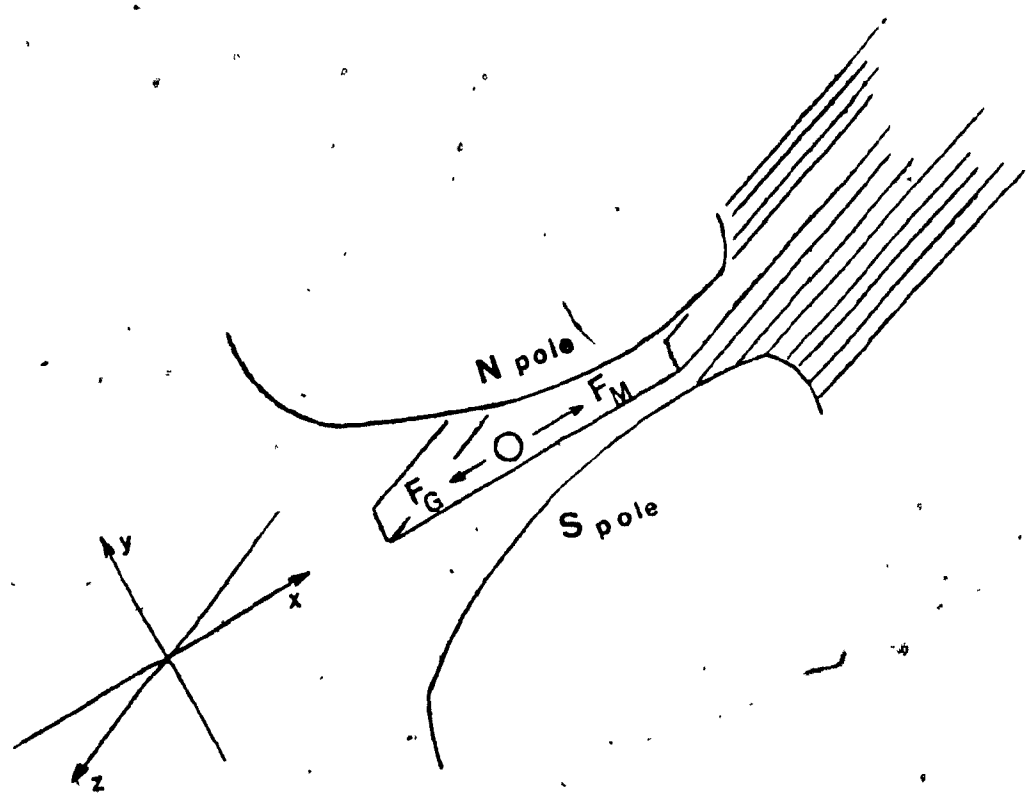


Fig. 54 Photograph of the Frantz Isodynamic Magnetic Separator.

Fig. 55 A force balance of a paramagnetic particle between the pole pieces of the Frantz separator.



producing a magnetic force (F_m) in opposition to the gravity force (F_g).

The main feature of the pole shape is that a constant product of field and field gradient (and thus a constant F_m) acts on a particle regardless of its position across the chute. The motion of the particles is then a result of the combined magnetic and gravitational forces.

Since F_m and F_g are both directly dependent on the cube of particle size, "b", the effect of particle size cancels and the separation is based only on the mass susceptibility of the particles. The Frantz makes very precise separations between particles of close susceptibility. Half-way down the chute a splitter divides the separated particles into magnetic and non-magnetic fractions.

The magnetic force is increased by increasing the current (I) through the electromagnet, and gravitational force is increased by increasing the side slope (θ).

APPENDIX - F. ELECTRON MICROPROBE RESULTS

CONCENTRATION %

Position of beam	WEIGHT				ATOM			
	Fe	S	Cu	O*	Fe	S	Cu	O*
1	43.949	0.059	4.831	51.161	19.37	0.05	1.87	78.71
2	26.257	0.172	6.597	66.973	9.87	0.11	2.18	87.84
3	11.615	4.019	17.182	67.183	4.33	2.61	5.63	87.43
4	22.480	12.315	17.024	48.181	9.90	9.45	6.59	74.06
5	36.54	4.552	9.988	48.921	16.31	3.54	3.92	76.23
6	30.528	32.377	36.183	0.911	25.04	46.26	26.09	2.61
7	31.195	32.671	35.166	0.968	25.49	46.50	25.25	2.76
8	31.259	33.102	34.469	1.169	25.35	46.76	24.57	3.31

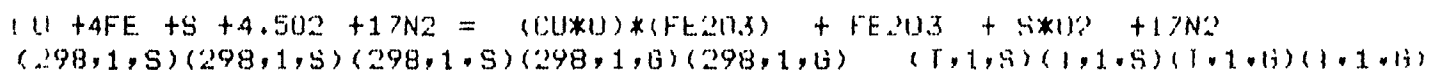
* O is not directly measured but inferred by difference.

APPENDIX-G. F.A.C.T. SYSTEM RESULTS

In the following tables the printouts of the REACTION program are presented for roasting CuFeS_2 with oxygen and with air. The second line describes the conditions of each reactant i.e. temperature in K, partial pressure in atm and state of the reactant (s=solid, l=liquid, g=gas). Calculations of the thermodynamical functions are presented for the temperatures of 320, 350, 450, 550 and 600°C.

TABLE G-2. F.A.C.T. printout for roasting of chalcopyrite
with air

XX



CALCULATIONS ARE BASED ON THE INDICATED NUMBER OF GRAM MOLES

 (I) DELTA H DELTA G DELTA V DELTA S DELTA U DELTA A
 (K) (CAL) (CAL) (L) (CAL/K) (CAL) (CAL)

	S	S1	S1	G	G	=	S2	S1	G	G
593	593.0	-439362.7	-741764.2	0.350E+03	-7.479	-447842.2	-750244.1			
623	623.0	-432819.4	-772906.2	0.394E+03	3.284	-442372.1	-782459.1			
723	723.0	-410228.7	-878955.2	0.542E+03	36.893	-423358.6	-892085.1			
823	823.0	-387376.0	-988173.2	0.690E+03	66.502	-404083.2	-1004830.1			
873	873.0	-376025.2	-1043842.2	0.764E+03	79.891	-394521.0	-1062338.0			

REREFENCES

1. Encyclopedia Britannica, 15th Ed. vol. 11, pp. 309-340.
2. Ouelette, P., and Farah, G.O., "Electrotechnology" vol. 1, (Edition P. Ouelette, J.A. King and P.N. Chereminisoff), Ann Arbor Science, 1978, pp. 351-525.
3. Oberteuffer, J.A. "Magnetic Separation: A Review of Principles, Devices and Applications", IEEE Transactions on Magnetics, Mag-10(2), June 1974, pp. 223-238.
4. Liu, Y.A., and Lin, C.J., "Assessment of Sulfur and Ash Removal from Coals by Magnetic Separation", IEEE Transactions on Magnetics, Mag-12(5), 1976, pp. 538-550.
5. Murray, H.H., "Beneficiation of Selected Industrial Minerals and Coal by High Intensity Magnetic Separation", IEEE Transactions on Magnetics Mag-12(5), 1976, pp. 498-502.
6. Dobby, G., Nasset, J.E., and Finch, J.A., "Mineral Recovery by High Gradient Magnetic Separation", Canadian Metallurgical Quarterly, vol. 18, no. 3, 1979, pp. 293-301.

7. Watson, J.H.P., "Magnetic Filtration", Journal of Applied Physics, vol. 44, 1973, pp. 4209-4215.
8. Nasset, J.E., and Finch, J.A., Fine Particles Processing, vol. 2, Edition, P. Somasundaran, A.I.M.E., 1980, pp. 1217-1242.
9. Finch, J.A., "Magnetic Separation", Mineral Processing Systems Seminar, McGill University, April 1981, p. 75.
10. Porter, C.R., and Goens, D.N., "Magnex Pilot Plant Evaluation - A Dry Chemical Process for the Removal of Pyrite and Ash from Coal," Trans. Am. Inst. Min. Engrs., vol. 266, 1979, pp. 175-180.
11. Meech, J.A., and Paterson, J.G., "Upgrading Chrysocolla Ores with Iron Pentacarbonyl", Trans. Inst. Min. Metall., Section C., vol. 89, 1980, pp. C152-C160.
12. Hwang, J.Y., Kellerud, G., Takayasu, M., Friedlaender, F.J., Purdue University Indiana, 3rd Joint Intermag-Magnetism and Magnetic Materials, Montreal Canada, July 1982.
13. Krukiewicz, R., and Laskowski, J., "Development of a Magnetizing Alkali Leaching Process for Concentration of Siderite Ores," 10th International Mineral Processing Congress, London 1973, pp. 391-410.
14. Khalafalla, S.W., "Magnetic Separation of the Second Kind: Magnetogravimetric, Magneto-hydrostatic and Magneto-hydrodynamic Separations," IEEE Transactions on Magnetics, vol. Mag-12(5), 1976, pp. 455-462.

15. Watson, J.H.P., "Wet HGMS Applied to the Removal of Tungsten from Tin Ores using Magnetic Fluids," IEEE Transactions on Magnetics, vol. Mag-16, no. 5, 1980, pp. 937-939.
16. Lin, C.J., et al., "Pilot Scale Studies of Sulfur and Ash Removal from Coals by High Gradient Magnetic Separation," IEEE Transactions on Magnetics, vol. Mag-12(5), 1976, p. 513.
17. Maxwell, E., Kelland, D.R., and Akoto, I.Y., "High Gradient Magnetic Separation of Mineral Particulates from Solvent Refined Coal," IEEE Transactions on Magnetics, vol. Mag-12(5), 1976, p. 507.
18. Habashi, Fathi, "Chalcopyrite. Its Chemistry and Metallurgy," McGraw Hill, 1978, pp. 45-62.
19. Volsky, V., and Sergievskaya, E., "Theory of Metallurgical Processes", Mir Publishers, Moscow 1971, from reference 18.
20. Tafel, V., and Greylich E., "Über die Vorgänge bei der Röstung von Chalcopyrit," Met. Erz, 21, 1924, pp. 517-520, from reference 18.
21. Meunier, L., and Vanderpoorten, H., "Les Réactions de Grillage de la Chalcopyrite," Métallurgie, 1, 1956, pp. 31-35, from reference 18.
22. Margulis, E.V., and Ponomarev, V.D., "Investigation of the Chemical Mechanism of the Oxidation of Chalcopyrite," Zh. Prikl, Khim, 35, 1962, pp.970-979, from reference 18.

23. Lenchev, A., and Bumazhnov, F., "Chemistry of Thermal Decomposition of Chalcopyrite to Bornite", God. Sofii Univ. Khim. Fak., 66, 1975, pp. 441-453.
24. Maurel, C., "Types of Réactions d'Oxidation Observées au cours d'Analyse Thermique Différentielle, dans l'Air, de Minéraux Sulfurés et Arseniés de Fe, Co, Ni, Cu, Zn, Ag et Pb," Bull. Soc. Franc. Min. Crist., 87(3), 1964, pp. 377-385, from reference 18.
25. Razouk, R.I., et al., "Roasting of Copper Sulfides part II. Natural Copper Sulfides (Covellite and Chalcopyrite)," J. Appl. Chem. (London), 15, 1965, pp. 191-196, from reference 18.
26. Salze, A.M., "Note sur la Séparation Electromagnétique des Blendes et des Chalcopyrites à Ain Barbar, Algérie," Revue d'Industrie Minérale, vol. 351, 1923, pp. 373-376.
27. Dean, R.S., and Davis, C.W., "Magnetic Concentration of Ores," Trans. Am. Inst. Min. and Met. Engrs., vol. 112, 1934, pp. 509-537.
28. Smit, J., and Wijn, H.P.J., "Ferrites, Physical Properties of Ferrimagnetic Oxides in Relation to their Technical Applications," John Wiley and Sons, 1959, pp. 136-176.

29. Smit, J., "Magnetic Properties of Materials," McGraw Hill, Inter-University Electronics Series, vol. 13, 1971, pp. 20-42.
30. Standley, K.J., "Oxide Magnetic Materials," Clarendon Press, 1962, pp. 35-73.
31. Wagner, C., Über der Mechanismus der Bildung von Ionenverbindungen höherer Ordnung (Doppelsalze, Spinelle, Silicate)," Z. Phys. Chem., B34, 1936, pp. 309-316, from reference 29.
32. Zener, C., "Imperfection in nearly Perfect Crystals," Wiley, New York, 1952, from reference 29.
33. Reference 8, page 295.
34. Hess, H.H., "Notes on Operation of Frantz Isodynamic Magnetic Separator," S.G. Frantz Co.
35. Dobby, G.S., "High Gradient Magnetic Capture of Mineral Particles," M. Eng. Thesis, McGill University, 1977, p.52.
36. Gaudin, A.M., "Principles of Mineral Dressing," McGraw Hill, 1939, Chapter 4, pp. 70-89.